CHAPTER-III

Mixed ligand molybdenum complexes of 2-pivaloylamino-6-acetonyl-isoxanthopterin (H_2L^2) with selected nitrogen – sulphur donors as the ancillary ligands

Abstract

The new compounds were synthesized through a redox reaction between $Na_2MoO_4.2H_2O$ and 2-pivaloylamino-6-acetonylisoxanthopterin (H_2L^2) in presence of one of the ancillary ligands shown below. They have been characterized by elemental analysis, electrospray ionization mass spectrometry, different spectroscopic methods and cyclic voltammetry (CV). Their optimized geometry (with lowest steric energy) have been obtained by molecular mechanics (MM2) method; the optimized bond lengths and bond angles data tally with the literature x-ray structural data [17,19]. The kinetic aspects of their reactions with $Me_3N\rightarrow O$ have been studied. The negative $\Delta S^{\neq}$ values are consistent with an associative mechanism for these processes. One of the products of these reactions have been isolated and characterized to be a di-μ-oxo binuclear Mo(V) complex [compound **(6)]**, indicating oxygen atom transfer nature of this reaction. ^{1}H NMR, fluorescence spectra and CV data throw light on the redox "non-innocent" behavior of the pterin ligand (H_2L^2) here.

Introduction

The 6-substituted pterin-containing molybdenum and tungsten enzymes, apart from a couple of exceptions, e.g., the acetylene hydratase, catalyze formal hydroxylation (Equation 1) and the net oxygen atom transfer (OAT) reaction (Equation 2), to and from a variety of biologically important substrates and the oxygen atom is ultimately derived from water[13, 27a, 27b,52].

$$RH + H_2O = ROH + 2H^+ + 2e^- \quad (1)$$

$$X + H_2O = XO + 2H^+ + 2e^- \quad (2)$$

Recent X-ray crystallographic studies on such enzymes have provided fresh challenges to the synthetic chemist to replicate the functional and structural features of such enzymes [52-56]; at least development of coordination chemistry of pterin ligands would provide bench-mark data regarding their spectroscopic, electrochemical, oxygen atom transfer activity properties and their correlation with the electronic structures of the metal (Mo or W) – pterin compex compounds [34, 27b, 77-81]. The metal centre as well as the pterin ligand, can exist in more than one oxidation states and their assignments in new coordination compounds along with their electronic structures, is an involved task [34, 70]. Nevertheless, such data will be complementary

for the study of functional aspects of the enzyme catalytic centers and correlation of their spectroscopic data with electronic structures[1a, 1c-e, 1g,12, 63, 64,71, 72].

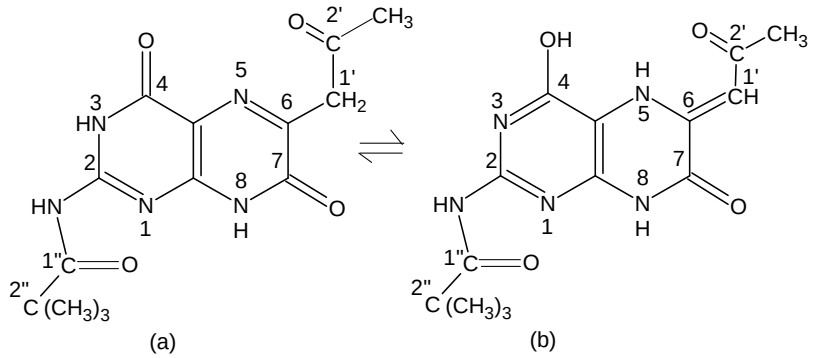

Scheme (III-1): Structural formulae of the two tautomeric forms of the free of pterin ligand (H_2L^2)

As part of our continued interest in this direction [4], we report here the studies on new molybdenum compounds of 2-pivaloylamino-6-acetonyl-isoxanthopterin [H_2L^2] [Scheme(III-1)] and their reactivity towards a typical enzyme substrate like trimethylamine N-oxide [82 – 84] and that of analogue like PPh_3. The 7-oxo group of the pterin ligand [H_2L^2] corresponds to the pyran ring oxygen atom of 'molybdopterin', as revealed through x-ray structural work[77, 78, 85].

The ancillary ligands used here are as follows (abbreviation used given in the parenthesis)[Scheme (III-2)].

Experimental

Materials

Reagent grade chemicals were used as received. Pivalic anhydride, trimethylamine N-oxide and $Na_2MoO_4.2H_2O$ were obtained from Fluka, Switzerland, Aldrich, U.S.A. and J. Baker, U.S.A. respectively. Different solvents were purified following literature procedures [2]. Silica gel for flash chromatography (230 – 400 mesh) (dried at 453K for 6h before use), Silica gel (GF_{254}) for TLC and spectroscopic grade DMF for cyclic voltammetric (CV) measurements are purchased from SRL, Mumbai. 6-acetonylisoxanthopterin was obtained by published procedure [4, 24, 76]. It was used for the reaction with pivalic anhydride as described in the next section. All the solvents were distilled under dinitrogen atmosphere.

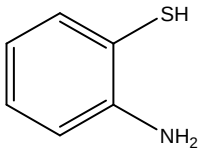

2-Aminothiophenol [H (atp), C_6H_7NS, F.W. 125.19]

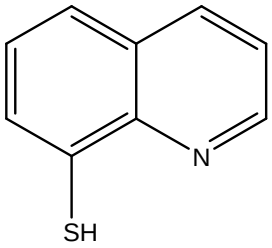

Thiooxine [H(thiox), C_9H_7NS, F.W. 161.22]

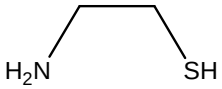

2-Aminoethanethiol [H(aet), C_2H_7NS, F.W. 77.15]

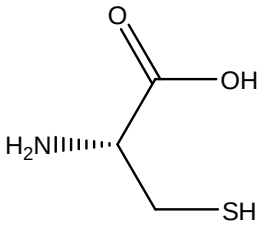

L-cysteine [H_2(cys), $C_3H_7NO_2S$, F.W. 121.16].

Scheme (III-2)

Method

All synthetic steps are carried out under dinitrogen atmosphere using Schlenk procedure [Fig. (III-1)] and red lamps/subdued light [3]. All heating operations including boiling under reflux, are carried out on a paraffin oil bath. Flash chromatography (silica gel 230 – 400 mesh) [Fig. (III-2)][42,43] was performed under dinitrogen flow as well. For the above steps dinitrogen was purified by BTS column. Column dimensions for the flash chromatographic purification of the pivalated pterin ligand and the corresponding molybdenum (IV) compounds are 2.5 m ID x70 cm and 1.2 cm ID x 50 cm respectively; in

each case the overall column length included a 250-200 ml bulb at the top. The above systems provided with 500-600 mg of the pivalated pterin ligand and 40-50 mg of corresponding complex respectively, in the pure form per batch operation. Most of the instrumental measurements have been published earlier [4]. FTIR spectra (KBr) were recorded on a Shimadzu FTIR-8300 spectrophotometer. Fluorescence spectra were recorded on an Elico (SL 174) spectrofluorometer. ^{1}H NMR spectra are recorded using a Bruker, Avance 300 MHz NMR spectrometer.

Synthesis of the complexes

The precautions [e.g., controlled heating in a paraffin oil bath under dinitrogen atmosphere in the dark, flash chromatography (silica gel 230 – 400 mesh) under dinitrogen atmosphere, etc] taken during synthesis of these compounds, are essential for getting them in the pure condition. Presence of the pivaloyl substituent in these compounds provides them with optimum solubility in common solvents like CH_2Cl_2, $C_2H_4Cl_2$, CH_3OH, DMF and DMSO, thereby facilitating their ease of handling and purification process.

2-pivaloylamino-6-acetonylisoxantho pterin (H_2L^2)

The desired ligand was prepared by boiling under reflux a mixture of 6-acetonylisoxanthopterin (0.71g, 3.0 mmol) [4, 24, 76] and pivalic anhydride (8 cm^3, 40 mmol) in controlled conditions (2h, dinitrogen atmosphere, darkness, paraffin oil bath) [5]. The reaction mixture was evaporated in a rotary evaporator (363K, 15 mmHg) and the deep brown crude product was purified by flash chromatography (silica gel 230 – 400 mesh) using CH_2Cl_2-MeOH (9:1 v/v) as eluant, evaporated again and dried in vacuo; yield 90%. Its purity was checked through TLC. The product gave a positive 2, 4-DNP test and decomposed without melting above 573K (Found C, 53.7; H, 6.4; N, 19.9. $C_{14}H_{17}N_5O_4$ (319.3) calcd. : C, 52.7; H, 5.4; N, 21.9%). UV-VIS [MeOH, λ_{max}/nm (log ε)]: 221(4.36), 294(4.10), 319.4sh (3.99), 356(4.10).

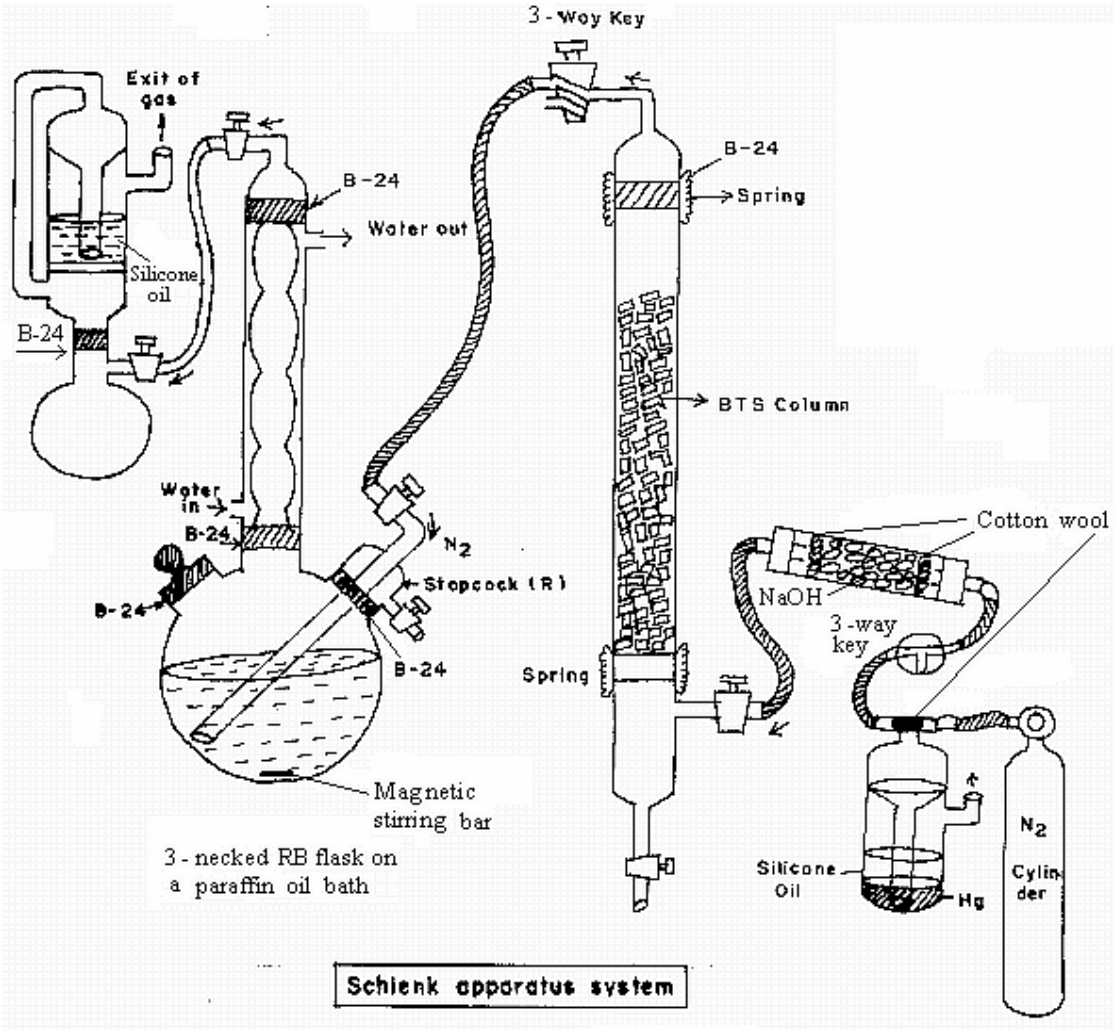

Fig.(III-1): The Schlenk system used in this study is depicted here schematically. The BTS column (2.5 cm ID x 70 cm) could be regenerated periodically by passing H_2 gas at 155° C for the requisite time period, leading to the colour change (dark grey → shining black) of the BTS catalyst. The 250 ml 3-necked flask is initially filled with N_2 gas by the evacuation – purging cycles (at least 4) using the stopcock (R) and then a steady flow of N_2 gas is maintained, with the gas escaping through the silicone oil bubbler at the left hand side [42,43].

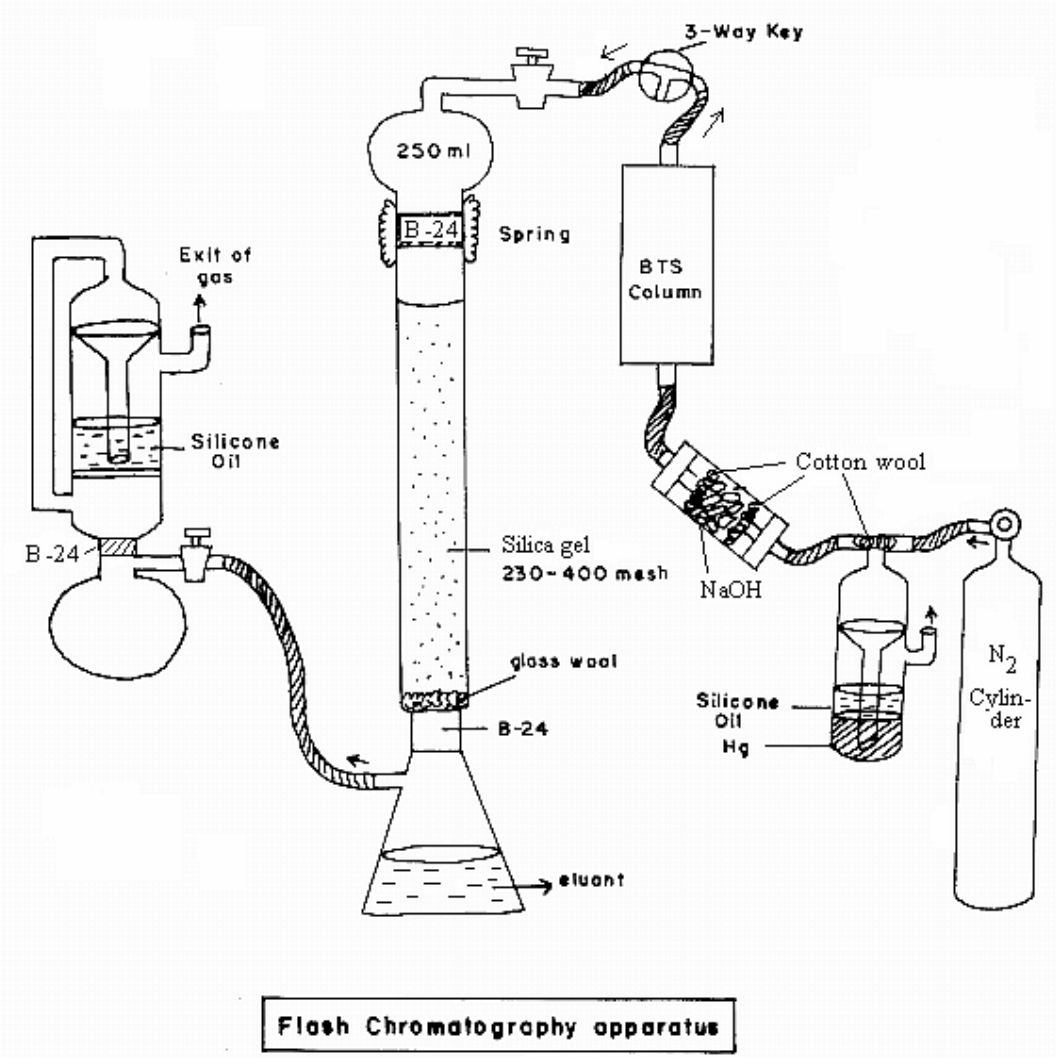

Fig.(III-2): The flash chromatography system used in this study is shown here schematically. Column dimensions for the flash chromatographic purification of the pivalated pterin ligand and the corresponding metal complexes were 2.5 cm ID x 70 cm and 1.2 cm ID x 50 cm respectively; in each case the overall column length included a 250-200 ml bulb at the top of the column. These systems provided with 500-600 mg of the pivalated pterin ligand and 40-50 mg of the corresponding complex respectively, in the pure form per batch operation. The silica gel (230-400 mesh) was dried at 453 K for 6 h before use [2b, 42].

$[Mo^{IV}(L^2)_2.(CH_3OH)_2]$ (1)

To a methanolic solution (100 mL) of 2-pivaloylamino-6-acetonylisoxanthopterin (H_2L^2, 0.3 g, 0.94 mmol) 5 mL aqueous solution of $Na_2MoO_4.2H_2O$ (0.113 g, 0.47 mmol) was added, pH of the solution was adjusted to 5.4 by the addition the 1:3 HCl and boiled under reflux (paraffin oil bath) for 6h at 345K under darkness and dinitrogen atmosphere. A dark brown product was obtained through removal of the solvent in a rotary evaporator and it was subjected to flash chromatography (silica gel 230-400 mesh) for purification using CH_2Cl_2:CH_3OH (95:5 v/v) as eluant, the final dark brown product was recovered through evaporation of solvent in a rotary evaporator and dried in vacuo over P_4O_{10} .Yield was 65%. Its purity was cheeked through TLC (UV Lamp). (Found C, 45.96; H, 4.4; N, 18.5 %; $MoC_{30}H_{38}N_{10}O_{10}$ (762.59) calcd. C, 45.34; H, 4.82; N, 17.63 %) UV-VIS (CH_3OH) [λ_{max}/nm (log ε) 280 (4.58), 346 (4.69), 376sh (4.58), 415 (4.48) and 450sh (4.21)]. The compound is fluorescent. Schematic structure of compound **(1)** is shown in Scheme (III-3).

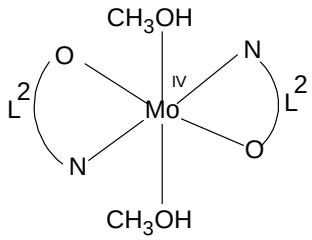

Scheme (III-3)

$[Mo^{IV}(atp)_2L^2].CH_3OH$ (2)

An aqueous solution (5 mL) of $Na_2MoO_4.2H_2O$ (0.095 g, 0.39 mmol) was mixed with a 100 mL of methanolic solution of 2-pivaloylamino-6- acetonyl-isoxanthopterin (H_2L^2, 0.25 g, 0.78 mmol) in a round bottom flask and purged with dry dinitrogen gas. Then pH of the solution was adjusted to 5.34 by 1.3 HCl. The mixture was boiled under dinitrogen gas and darkness on paraffin oil bath for 6h. Methanol was evaporated in a rotary evaporator and the residual compound was dried over P_4O_{10} for 24h. Next it was redissolved in CH_3OH followed by the addition of 2-amino thiophenol [H(atp), 0.049 g, 0.39 mmol] to it. The reaction mixture was stirred for 2h at 313K under darkness and dinitrogen atmosphere. Again CH_3OH was removed by a rotary evaporator. The crude product was purified through flash chromatography (silica gel 230-400 mesh) using CH_2Cl_2:CH_3OH (98:2 v/v)as eluant. The final snuff red colored compound was recovered by evaporation of the solvent in the rotary evaporator and dried over P_4O_{10} in vacuo. Purity was checked through TLC (UV lamp).

Yield was 60%. (Found C, 46.80; H, 4.1; N, 14.4 %: $MoC_{27}H_{31}N_7S_2O_5$ (693.65) calcd, C, 46.71; H, 4.47; N, 14.13 %.) UV-VIS (CH_3OH) [λ_{max}/nm (log ε): 347(4.84), 373.5sh (4.63), 414.5 (4.54), 446.5 sh (4.33)]. Schematic structure of compound **(2)** is shown in Scheme (III-4).

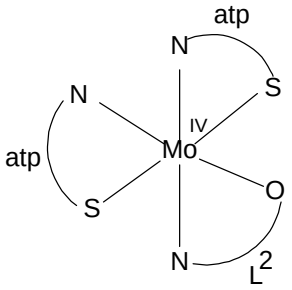

Scheme (III-4)

$[Mo^{IV}(thiox)_2\ L^2].CH_3OH$ (3)

To a methanolic solution (100 mL) of 2-Pivaloylamino-6-acetonylisoxanthopterin (H_2L^2, 0.25g, 0.78 mmol) in a three necked flask, an aqueous solution (5 mL) of $Na_2MoO_4.2H_2O$ (0.094 g. 0.39 mmol) was added and pH was adjusted to 5.23 by adding 1:3 HCl. After purging with dry dinitrogen gas, it was boiled under reflux at 345K on a paraffin oil bath under dinitrogen atmosphere and darkness for 6h. Then it was dried using a rotary evaporator and kept overnight over P_4O_{10} in vacuo. After redissolving the product in CH_3OH (100 mL), thiooxine [H(thiox), 0.063 g. 0.39 mmol] was added to it. After stirring the mixture at 313K for half an hour in dinitrogen atmosphere, a few drops of methanolic solution of anhydrous sodium acetated was added; stirring was started and continued for 1.5h at 313K under dinitrogen atmosphere and darkness. The compound was dried in a rotary evaporator. It was subjected to flash chromatography (silica gel 230-400 mesh) for purification using CH_2Cl_2:CH_3OH (98:2 v/v) as eluant. The yellow brown compound was recovered after evaporating the solvent in a rotary evaporator and finally dried in vaccuo over P_4O_{10}. Yield was 70%. Purity was checked by TLC (UV lamp). (Found C, 51.80; H. 4.02, N, 13.04 %; $MoC_{33}H_{31}\ N_7O_5S_2$ (765.71) calcd. C, 51.76; H, 4.08; N, 12.80 %). UV-VIS (CH_3OH) [λ_{max}/nm (log ε): 220 (4.93), 239 (5.51), 332 (4.55), 348 (4.56), 410 (4.26), 445sh (4.01)]. Schematic structure of compound **(3)** is shown in Scheme (III-5).

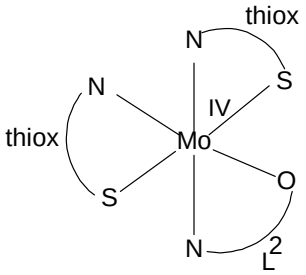

Scheme (III-5)

$[Mo^{IV}(aet)_2\ L^2]$. CH_3OH (4)

To an aqueous solution (5 mL) of $Na_2MoO_4.2H_2O$ (0.094 g. 0.39 mmol), a methanolic solution (100 mL) of 2-pivaloylamino-6-acetonylisoxanthopterin (0.25 g, 0.78 mmol) was added in a three necked flask and pH was immediately adjusted to 5.5 by 1.3 HCl. It was purged with dry nitrogen and boiled under reflux (oil bath) for 6h at 345K under darkness and dinitrogen atmosphere. It was dried in a rotary evaporator. Next after redissolving this product in methanol, 2-aminoethanethiol [H_2(aet), 0.047 g, 0.61 mmol] was added to it and pH was adjusted to 6.05 by a methanolic solution of anhydrous sodium acetate. Then the above mixture was warmed to 300K and stirred for 2h under darkness and dinitrogen atmosphere. The product thus obtained was dried in a rotary evaporator. The final product was obtained as shining dark brown microcrystals by flash chromatography (silica gel 230-400 mesh) using CH_2Cl_2:CH_3OH (95:5 v/v) as eluant and removal of the solvent in a rotary evaporator. It was dried over P_4O_{10} in vacuo. Yield was 75%. Purity was checked by TLC (UV lamp). (Found C, 38.3; H, 5.0; N, 16.25; $MoC_{19}H_{31}N_7O_5S_2$ (597.57) calcd, C, 38.19; H, 5.20; N, 16.41). UV-VIS (CH_3OH) [λ_{max} /nm (log ε) 218 (4.40), 269sh (3.96), 309 (3.86), 347 (4.08), 377sh (3.89), 414sh (3.87), 442sh (3.66)]. Schematic structure of compound **(4)** is shown in Scheme (III-6).

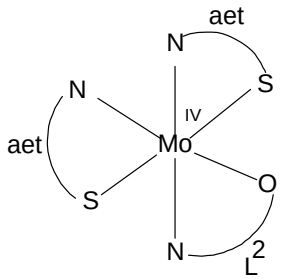

Scheme (III-6)

$(PPh_4)_2$ $[Mo^{IV}(cys)_2L^2].CH_3OH$ (5)

To a solution of $Na_2MoO_4.2H_2O$ (0.095 g, 0.4 mmol) in H_2O (5 mL), a solution of the pterin ligand (H_2L^2) (0.25 g, 0.78 mmol) in CH_3OH (50 mL) was added, pH of reaction mixture was adjusted to 5.2 by the addition of 1:3 HCl and then the solution was boiled (paraffin oil bath) under reflux for 6h in the dark and dinitrogen atmosphere. The dark coloured solution was evaporated in a rotary evaporator and the reddish-brown product was redissolved in CH_3OH (50 mL); L-cysteine (0.05 g, 0.41 mmol) was dissolved in CH_3OH (20 mL) by the addition of requisite amount of anhydrous sodium acetate and warming. The two above-mentioned solutions were mixed together, Ph_4PBr (0.43 g, 1.03 mmol) was added, the pH of the solution was adjusted to 6.0 using 1:3 HCl and stirred at room temperature (300K) for 2h. The reaction mixture was evaporated and purified by flash chromatography (silica gel 230 – 400 mesh) under dinitrogen flow; a mixture of C_6H_6 and CH_2Cl_2 (1:1 v/v) was used (three times) for removing excess of Ph_4PBr. The desired compound was eluted as a reddish fraction by a mixture of CH_2Cl_2:CH_3OH (9:1 v/v). On evaporating this fraction (rotary evaporator), compound **(5)** was obtained as reddish brown micro crystals; it was dried in vacuo over P_4O_{10}. Purity was checked by TLC (UV lamp). Yield was 70%. [Found: C, 60.45; H, 5.0; N, 7.5% $MoC_{69}H_{69}N_7O_9S_2P_2$ (1361.62) calcd. C, 60.83; H, 5.10; N, 7.20 %]. UV-VIS (CH_3OH) [λ_{max}/nm (log ε): 254 (4.48), 268 (4.57), 275sh (4.54), 347 (4.46), 416 sh (4.19), 456sh (9.77)]. Schematic structure of compound **(5)** is shown in Scheme (III-7).

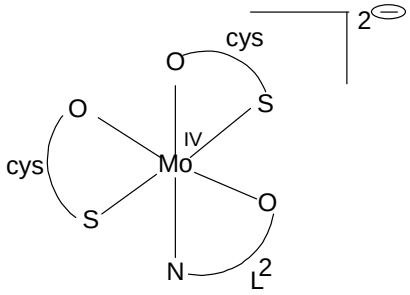

Scheme (III-7)

$(PPh_4)_2[L^2(cys)\ Mo^V\text{-}\mu(O_2)\text{-}MoV(cys)\ L^2].CH_3OH$ (6)

This is a product of the reaction between compound **(5)** and $Me_3N{\rightarrow}O$ (according to Equation (III-1 and 2). Equimolar solutions of the compound **(5)** (0.25 g, 0.19 mmol) in CH_3OH and $Me_3N{\rightarrow}O$ (0.014 g, 0.19 mmol) were mixed and stirred at 300K for overnight under dinitrogen atmosphere and darkness. A dark brown solution thus obtained was dried in a rotary evaporator and purified through flash chromatography (silica gel 230-400 mesh),

using CH_2Cl_2: CH_3OH (97:3 v/v) as eluant. Finally the solution was removed using a rotary evaporator and the dark brown product dried in vacuo over P_4O_{10}. Yield was 80%. Purity was checked by TLC (UV lamp). [Found C, 55.30; H, 4.56; N, 9.60 %; $Mo_2C_{83}H_{84}O_{15}N_{12}S_2P_2$ (1807.60) calcd. C, 55.15 ; H, 4.68; N, 9.30 %.]. UV-VIS (CH_3OH) λ_{max}/nm (log (ε): 252sh (4.20), 270 (4.26), 308sh (3.70), 350 (4.10), 410sh (3.80)]. Schematic structure of compound **(6)** as well as the probable reaction pathway are shown in Scheme (III-8).

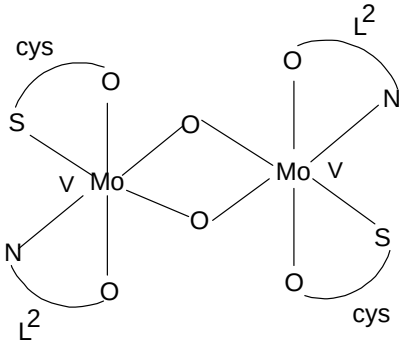

(a)

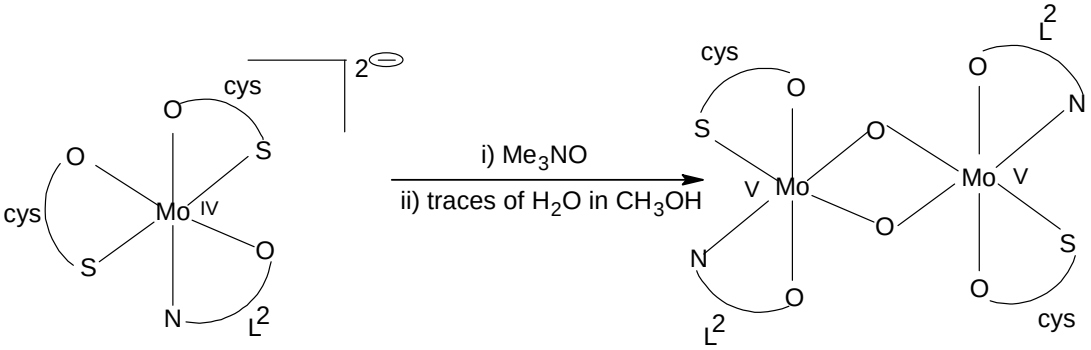

(b)

Scheme (III-8): (a) The schematic structure of compound **(6); (b)** the reaction path way of formation of **(6)**; Equation (III-1 and 2).

Results and Discussion

ESIMS data

Electrospray ionization mass spectra (ESIMS) involving soft ionization technique, has proved to be a valuable tool for characterizing compounds of different classes including inorganic and coordinating compounds [11]. As usual, the assignment of molecular formula

(or any definite fragment originating from it) is confirmed by the experimental value of m/z (most abundant isotopic mass) as well as matching between the experimental and calculated (simulated) isotopic distribution profile [11,18]. For the organic compounds containing O, F, P, and I the relative intensities of M, M+1 and M+2 isotopic peaks are of great value in recognizing the molecular ion (M^+) peak or any well-defined fragment confirming it. Sometimes, isotope peaks may be more intense than calculated value because of ion-molecular interactions that vary with sample concentration or with the class of compounds involved, e.g., the transfer of a hydrogen atom from the excess of the compound to the molecular ion in some cases [11]. An M-1 peak is common and occasionally an M-2 peak (loss of H_2) or even rare M-3 peak (from alcohols) is reasonable [11]. Absence of molecular ions (or an extremely weak M^+ peak is characteristic of highly branched molecules, alcohols, molecules with long alkyl chains, aryl ketons and benzyl compounds [11].

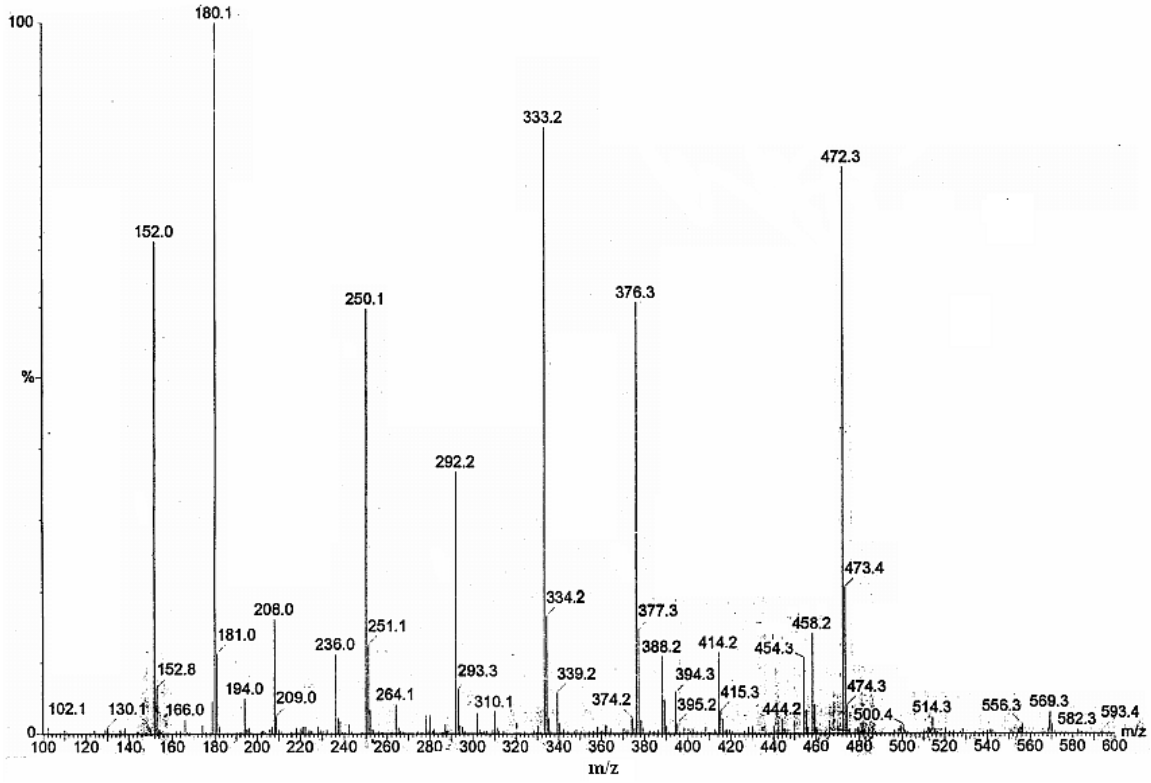

Fig. (III-3): ESIMS data of (H_2L^2) over the region m/z = 100-600.

The molecular formula of the ligand (H_2L^2) was verified through its ESIMS data [Fig. (III-3 to 6)]. The molecular ion peak [$H_2L^2 + H^+$] or $[C_{14}H_{18}N_5O_4]^+$ of the ligand appeared as a weak signal (1.6%) at m/z = 320.3, where H_2L^2 = 319.3 ($C_{14}H_{17}N_5O_4$). Some of the prominent ESIMS peaks (m/z) observed for this compound can be assigned to the fragments

stated below; the isotopic distribution pattern agreed with the theoretically predicted pattern, calculated using a computer program [18]. These peaks are $[H_2L^2 - HCN]^+$ or $[C_{13}H_{16}N_4O_4]^+$ at 292.2 (37.5%); $[H_2L^2 - HCN - CH_2CO]^+$ or $[C_{11}H_{14}N_4O_3]^+$ at 250.1 (60.6%). Assignment for peak at m/z 180.1 is shown in Fig. (III-6).

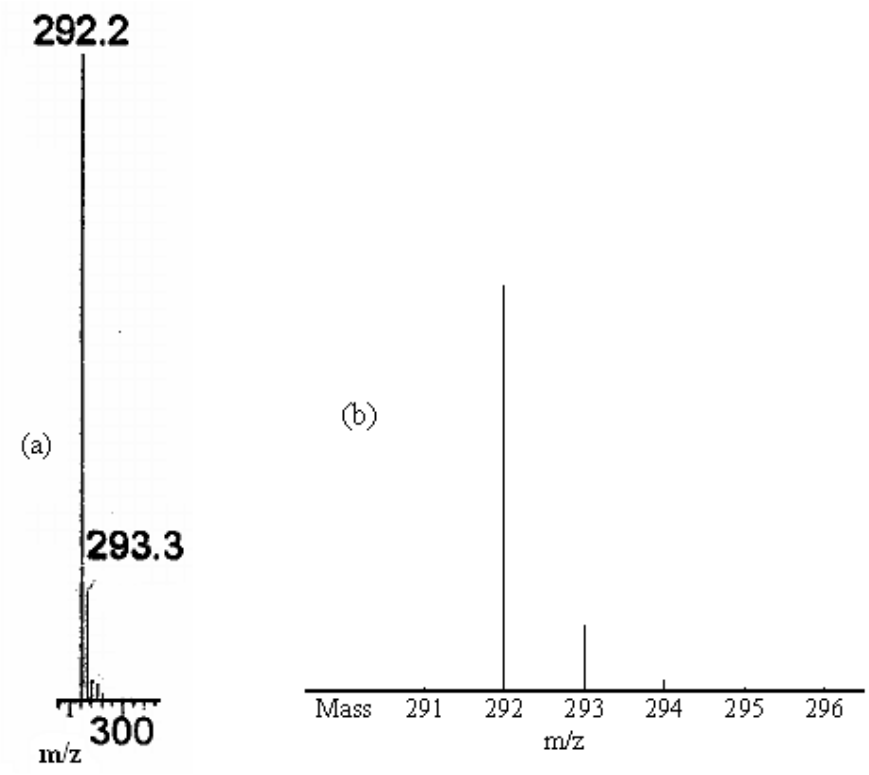

Fig. (III-4): (a) ESIMS data (m/Z = 292.2) of (H_2L^2) corresponding to the fragment $[M - HCN]^+$; (b) the calculated isotope pattern, [$M = C_{14}H_{17}N_5O_4$, MW = 319].

For compound **(1)** the ESIMS data at the m/z (= 727) region [Fig. (III-7)] corresponds essentially to the desolvated species, $[M-3H]^+$ or $[MoC_{28}H_{27}N_{10}O_8]^+$ where M represents the desolvated species. Fig. (III-7a) corresponds to the experimental isotopic distribution pattern and Fig. (III-7b) to that of the calculated isotope distribution pattern [18], thereby supporting the above assignment as well as the chemical composition of the parent molecule in conjunction with elemental analysis and other physicochemical data. This peak also confirms the architectural stability of the compound **(1)**, with the pterin residues possessing several branched chains.

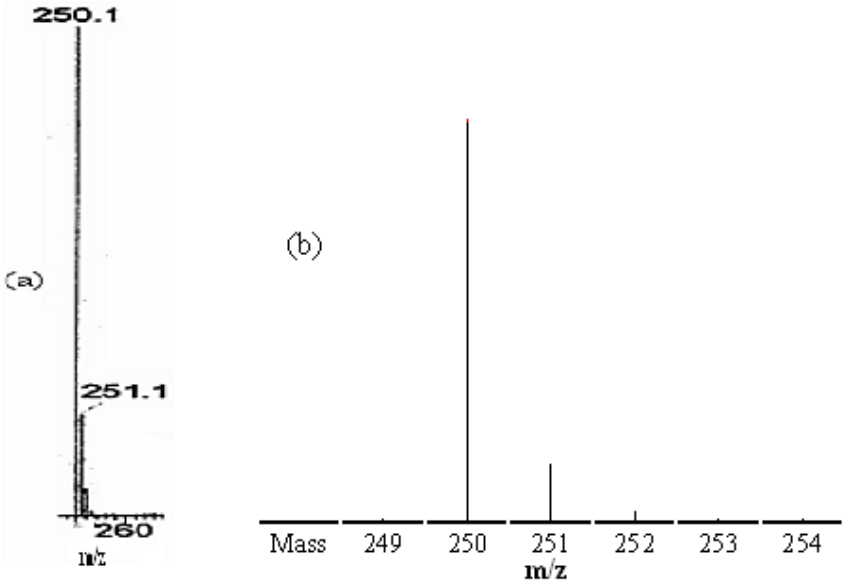

Fig. (III-5): (a) ESIMS data (m/z = 250.1) of (H_2L^2) corresponding to the fragment $[M - HCN - CH_2CO]^+$; (b) the calculated isotope pattern, [M = $C_{14}H_{17}N_5O_4$, MW = 319].

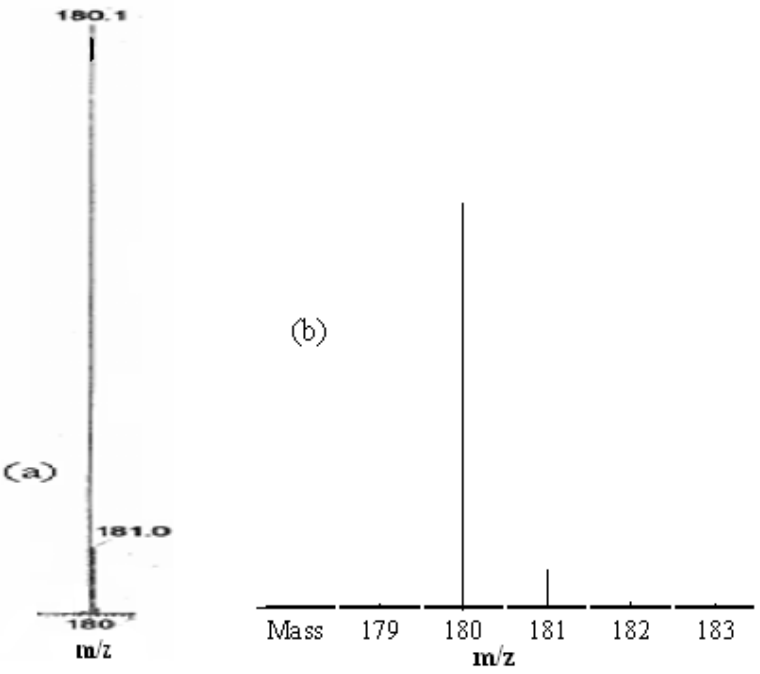

Fig. (III-6): (a) ESIMS data (m/z = 180.1) of (H_2L^2) corresponding to the fragment $[M + 2H - CH_2COCH_2 - (CH_3)_3CCO]^+$; (b) the calculated isotope pattern, [M = $C_{14}H_{17}N_5O_4$, MW = 319].

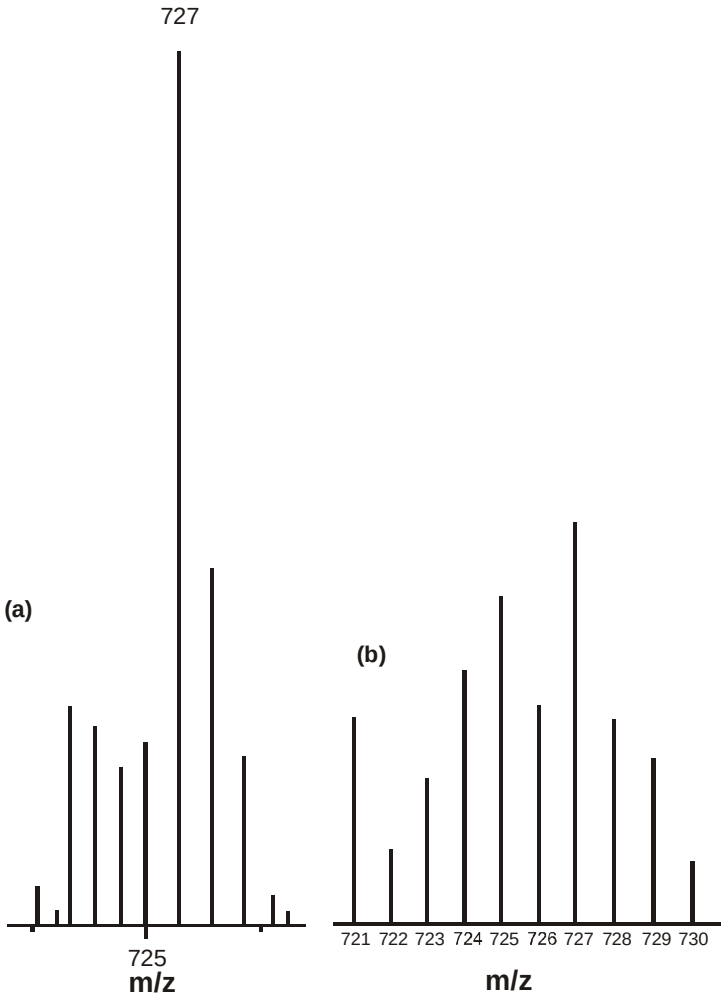

Fig. (III-7): (a) ESIMS data of the compound **(1)** at the m/z(=727) region corresponding to the fragment $[M\text{-}3H]^+$ or $[MoC_{28}H_{27}N_{10}O_8]^+$ where M represents the desolvated species of this compound and (b) the calculated isotope pattern.

In the ESIMS data of compound **(2)** a significant peak is observed at m/z 658 [Fig. (III-8a)] which can be demonstrated as $[M\text{-}3H]^+$ or $[MoC_{26}H_{24}N_7S_2O_4]^+$, where M represents the desolvated species. This peak indicates the compactness of the coordination core and architectural stability of the compound. The above conclusion is further supported by the simulation of isotope distribution pattern [Fig. (III-8b)] [18]. The slight dissimilarity in intensity between the two distribution patterns is due to the ion molecular interaction during the mass spectral process [11].

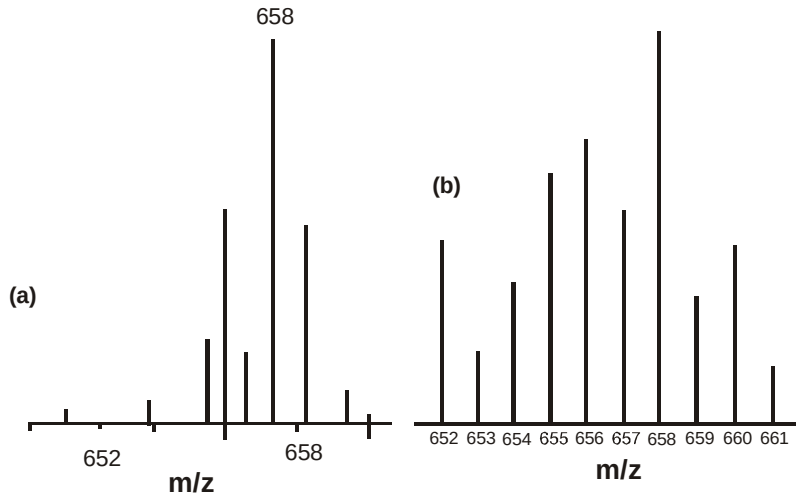

Fig. (III-8): (a) ESIMS data of the compound **(2)** at the m/z(=658) region corresponding to the fragment $[M\text{-}3H]^+$ or $[MoC_{26}H_{24}N_7S_2O_4]^+$and (b) the calculated isotope pattern.

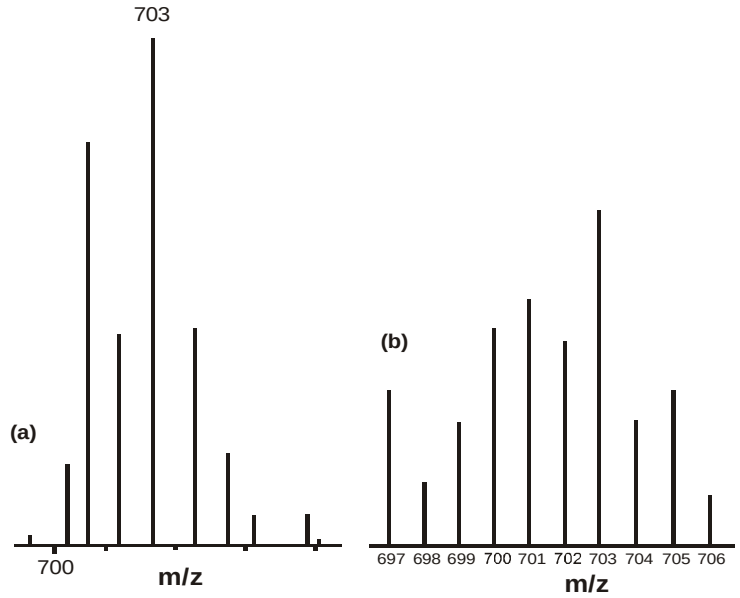

Fig. (III-9): (a) ESIMS data of the compound **(3)** at the m/z(=703) region corresponding to the fragment $[M\text{-}2CH_3]^+$ or $[MoC_{30}H_{21}N_7O_4S_2]^+$and (b) the calculated isotope pattern.

The ESIMS data of the compound **(3)** at m/z(=703) region (most abundant isotopic mass) is shown in the Fig. (III-9a). This is the peak nearest to molecular ion peak and can be represented as $[M - 2CH_3]^+$ or $[MoC_{30}H_{21}N_7O_4S_2]^+$, where M represents desolvated species. The confirmation of the molecular formula is done by simulated isotope distribution pattern

Fig. (III-9b) [18]. The difference in intensity between the two distribution patterns is due to the ion molecular interaction during the mass spectral process [11].

In case of compound **(4)** the ESIMS spectra of the desolvated molecular ion peak (most abundant isotopic mass) is obtained as $[M - 2H]^+$ or $[MoC_{18}H_{25}N_7O_4S_2]^+$at m/z (=563.4) region, as in Fig. (III-10a), where M represents the desolvated species. A satisfactory matching is observed when a simulation of this peak is done [Fig. (III-10b)] [18].

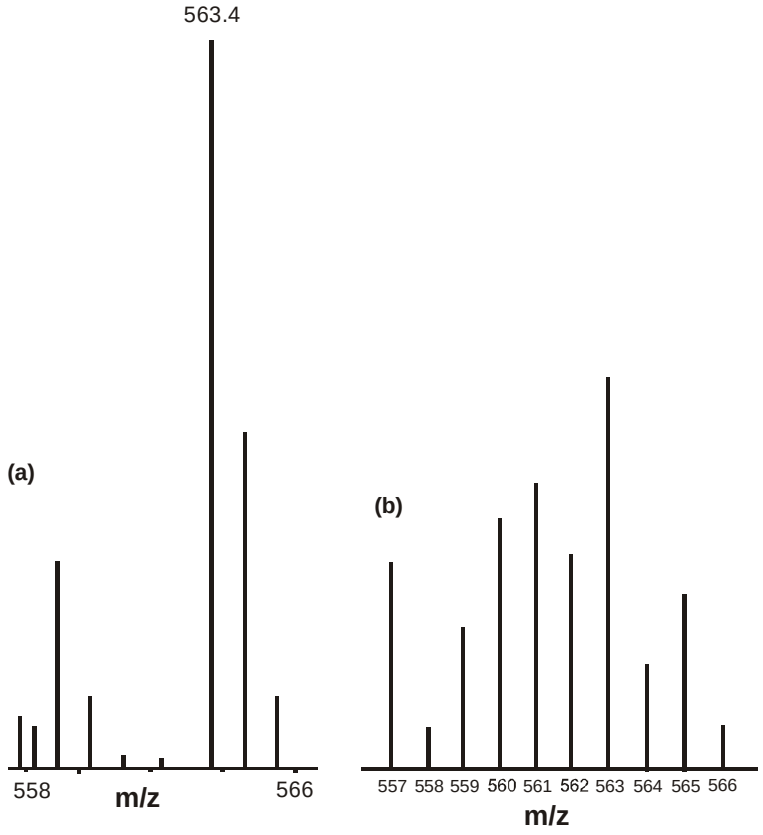

Fig. (III-10): (a) ESIMS data of the compound **(4)** at the m/z(=563.4) region corresponding to the fragment $[M-2H]^+$ or $[MoC_{18}H_{25}N_7O_4S_2]^+$ and (b) the calculated isotope pattern.

Fig. (III-11a) (ESIMS data of compound **(5)** shows the characteristic isotope pattern in the region m/z(= 989) corresponding to the fragment $[M-(H + PPh_4)]^+$ or $[MoC_{44}H_{44}N_7O_8S_2P]^+$ where M is the desolvated species of compound **(5)**. The m/z value (most abundant isotopic mass) and the isotopic distribution profile agreed with the corresponding theoretical value [Fig. (III-11b)] [18], thereby supporting the chemical composition of this complex, in conjunction with the elemental analysis and different

physicochemical data. The slight difference in intensity between the experimental and calculated peaks is due to ion-molecule interaction, e.g., the transfer of a hydrogen atom from the excess of the compound to the molecular ion [11]. The mass spectral data also verified the mononuclear nature and the architectural stability of compound **(5)** containing the pterin ligand residue [$(L^2)^{2-}$] with two major substitutents at the 2- and 6- positions of the pterin ring (Scheme (III-1).

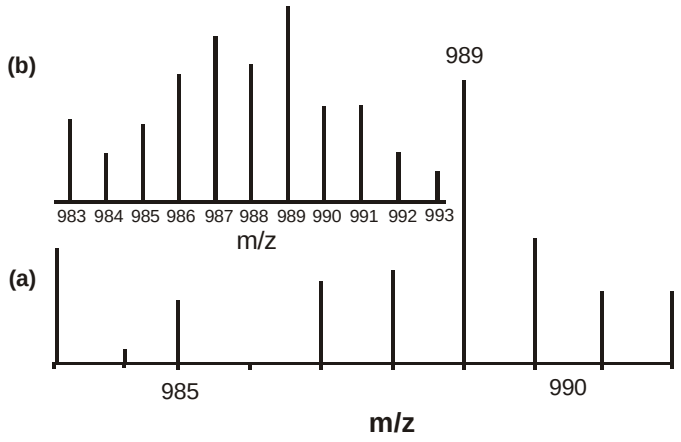

Fig. (III-11): (a) ESIMS data of the compound **(5)** at the m/z(=989) region corresponding to the fragment $[M-(H + PPh_4)]^+$ or $[MoC_{44}H_{44}N_7O_8S_2P]^+$and (b) the calculated isotope pattern.

The molecular formulation of compound **(6)** as a binuclear complex, is supported by ESIMS data where a peak is found at m/z (= 1098) region [Fig. (III-12a)] which may be assigned as $[(M + 2H) - 2PPh_4]^+$ or $[Mo_2C_{34}H_{42}N_{12}O_{14}S_2]^+$ where M represents the desolvated species. The isotope distribution pattern (most abundant isotopic mass) obtained experimentally matched with the theoretically calculated one, as represented in Fig. (III-12b) [18]. This indicates the architectural stability of the core.

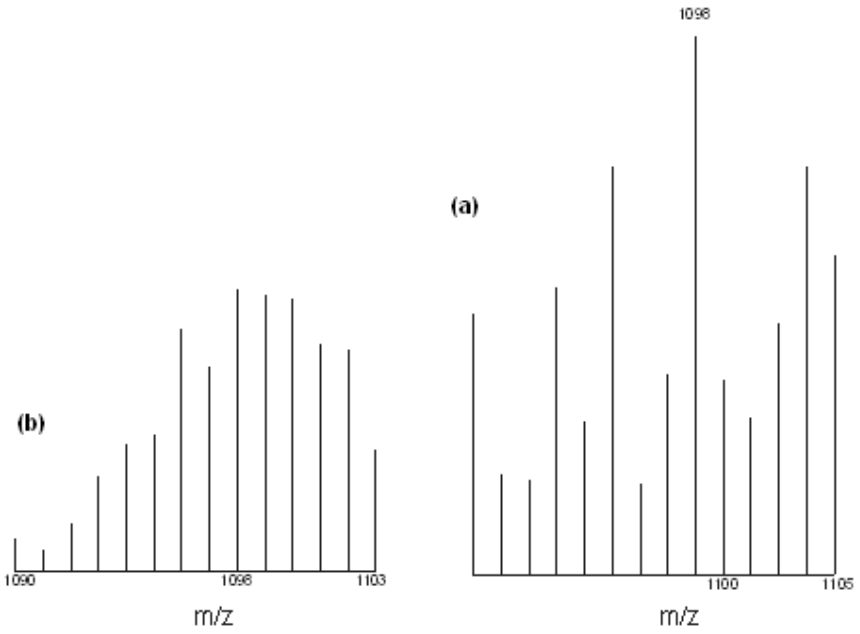

Fig. (III-12): (a) ESMS data of the compound **(6)** at the m/z(=1098) region corresponding to the fragment $[(M+2H) - 2PPh_4]^+$ or $[Mo_2C_{34}H_{42}N_{12}O_{14}S_2]^+$and (b) the calculated isotope pattern.

Table (III-1): The prominent ESIMS peaks (m/z) observed for compounds (**1**) to (**6**) along with their assignments, as par Fig. (III-3) to (III-12).

Compound	m/z	Assigned fragmentation peak observed in the ESIMS data*
(H_2L^2)	292.2	$[M - HCN]^+$;
(1)	727	$[M-3H]^+$
(2)	658	$[M-3H]^+$
(3)	703	$[M-2CH_3]^+$
(4)	563.4	$[M-2H]^+$
(5)	989	$[M-(H + PPh_4)]^+$
(6)	1098	$[(M + 2H) - 2PPh_4]^+$

*M represents the desolvated species

The above formulations of the compounds were further confirmed by measuring the Λ_M (ohm^{-1} cm^2 mol^{-1}) in methanol (using ca. 1 x 10^{-3} mol solution of the complexes). For the

compound **(1)** to **(5)** Λ_M values obtained are with in the range of 10 -15 ohm^{-1} cm^2 mol^{-1}, which are consistent with the non-electrolytic nature of these compounds [21]. On the other hand for the compound **(6)**, Λ_M value was ca. 150 ohm^{-1} cm^2 mol^{-1} confirming the 2:1 nature of the compound [21].

IR spectroscopy

On comparing the IR spectra of free ligand (H_2L^2) with that of compound **(1)** [Fig.(III-13)], it is observed that the in plane δ(O-H) and δ(O-H) + ν(C-O) modes of vibrations of the free ligand at 1363.6 and 1329 cm^{-1} respectively, are absent in the complex; a new band appears in the complex at 1255.6 cm^{-1} due to ν(C-O) mode of vibration resulting from deprotonation of OH(4) group [11]. In case of compounds **2**, **3**, **4**, **5** and **6** [Fig. (III-14) to Fig. (III-18)], this band appears at 1253.6, 1253, 1261.4, 1261.6 and 1255.6 cm^{-1} respectively [11]. The IR bands in the region around 1589 – 1500 cm^{-1} due to ν(C=C) and ν(C=N) vibrations of the ligand (H_2L^2) are modified in the complexes due to electronic redistribution associated with deprotonation and coordination (vide Schemes (III-1) and (III-9). No distinct band due to the ν(Mo=O_t) mode in the range 980-880 cm^{-1} and ν(Mo-O_b-Mo) mode in the region 800-750 cm^{-1} could be identified for the compound **1**, **2**, **3**, **4** and **5**, this is in agreement with their formulations. The compound **(6)** does not absorb in the region 980-880 cm^{-1} (indicating the absence of Mo=O_t bond) but absorbs at 802 cm^{-1} with moderate intensity (indicating the presence of Mo-O_b-Mo bond) [22]. The coordination modes of the pterin ligand in all the above compounds are the same and as par Scheme (III-9).

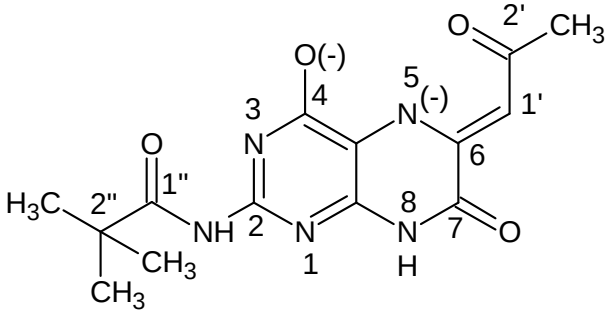

Scheme (III-9)

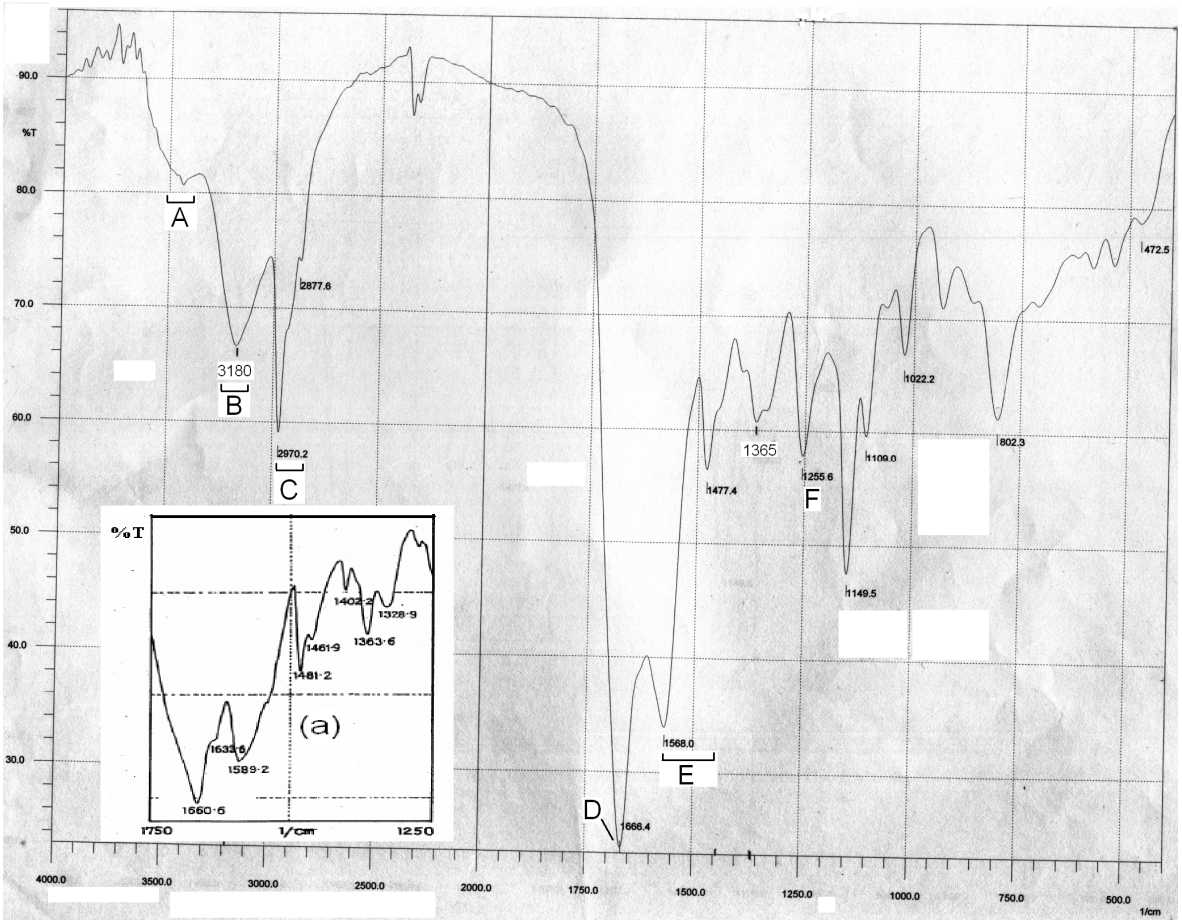

Fig.(III-13): (a) FTIR spectrum (KBr) of H_2L^2 (in set)
FTIR spectrum (KBr) of compound **(1)**

A: the broad O-H stretching vibration of the CH_3OH

B: the broad N-H stretching vibration, hydrogen bonded, 3180 cm^{-1}.

C: the C-H stretching vibrations, 2966, 2873 cm^{-1}.

D: the C=O stretching vibrations of the (C=O) (1′) and (C=O) (2′) groups, 1664.5 cm^{-1}.

E: the C···C and C···N ring stretching vibrations of the pterin ligand and C_6H_5 (2') group, 1654, 1618, 1560, 1541, 1481 cm^{-1}.

F: the ν (C-O) mode of the O(4) phenoxide group, 1255.6 cm^{-1}.

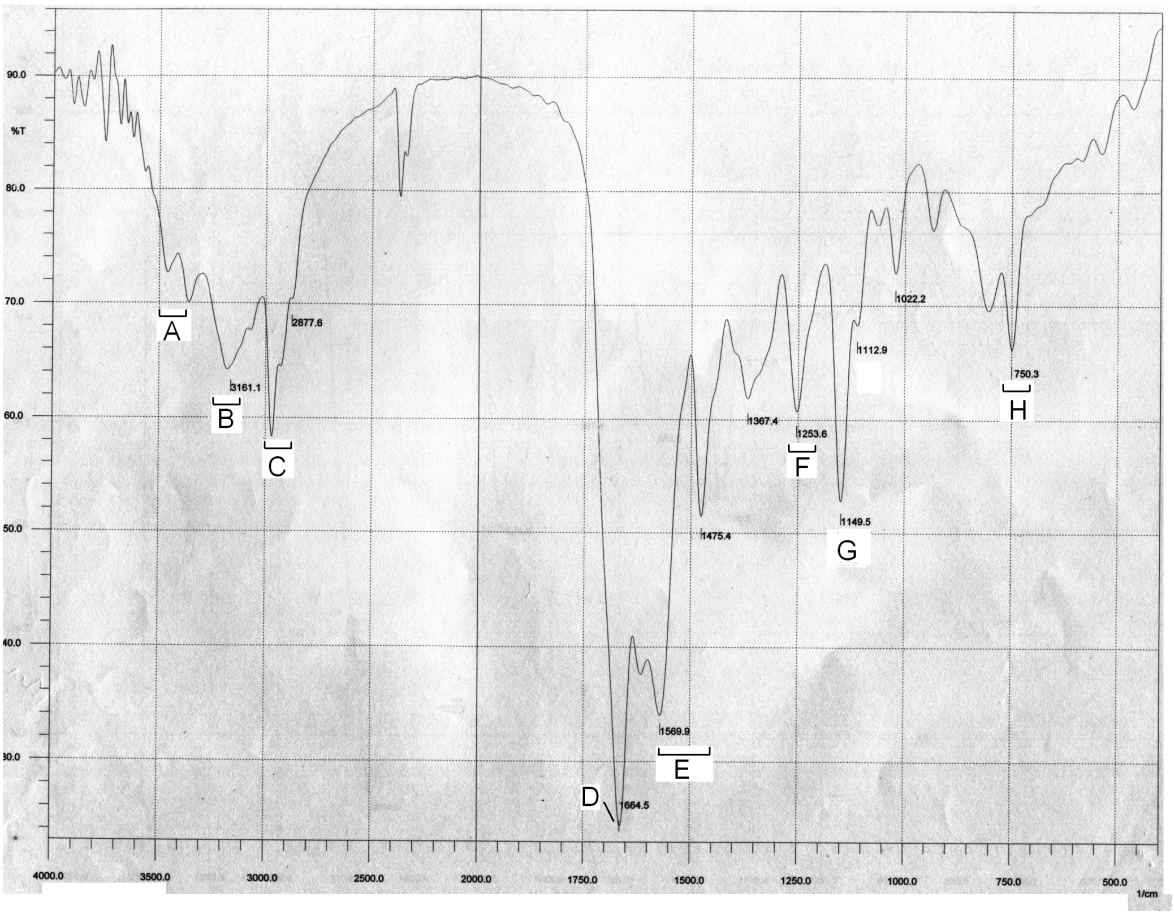

Fig.(III-14): FTIR spectrum (KBr) of compound **(2)**

A: the broad O-H stretching vibration, hydrogen bonded (CH_3OH), 3400 cm^{-1}.

B: the broad N-H stretching vibration, hydrogen bonded, 3161 cm^{-1}.

C: the C-H stretching vibrations 2967, 2877 cm^{-1}.

D: the C=O stretching vibrations of the (C=O) (1″) and (C=O) (2′) groups, 1664 cm^{-1}.

E: the C⋯C and C⋯N ring stretching vibrations of the pterin 1569, 1475 cm^{-1}.

F: the ν (C-O) mode of the O(4) phenoxide group, 1253 cm^{-1}.

G: the ν (C-N) + δ (NH_2) vibrations of the $(atp)^{1-}$ residue, a broad band over the region 1200-1159 cm^{-1} [11].

H: : the out-of-plane C-H (aromatic) bending vibrations, 750 cm^{-1}.

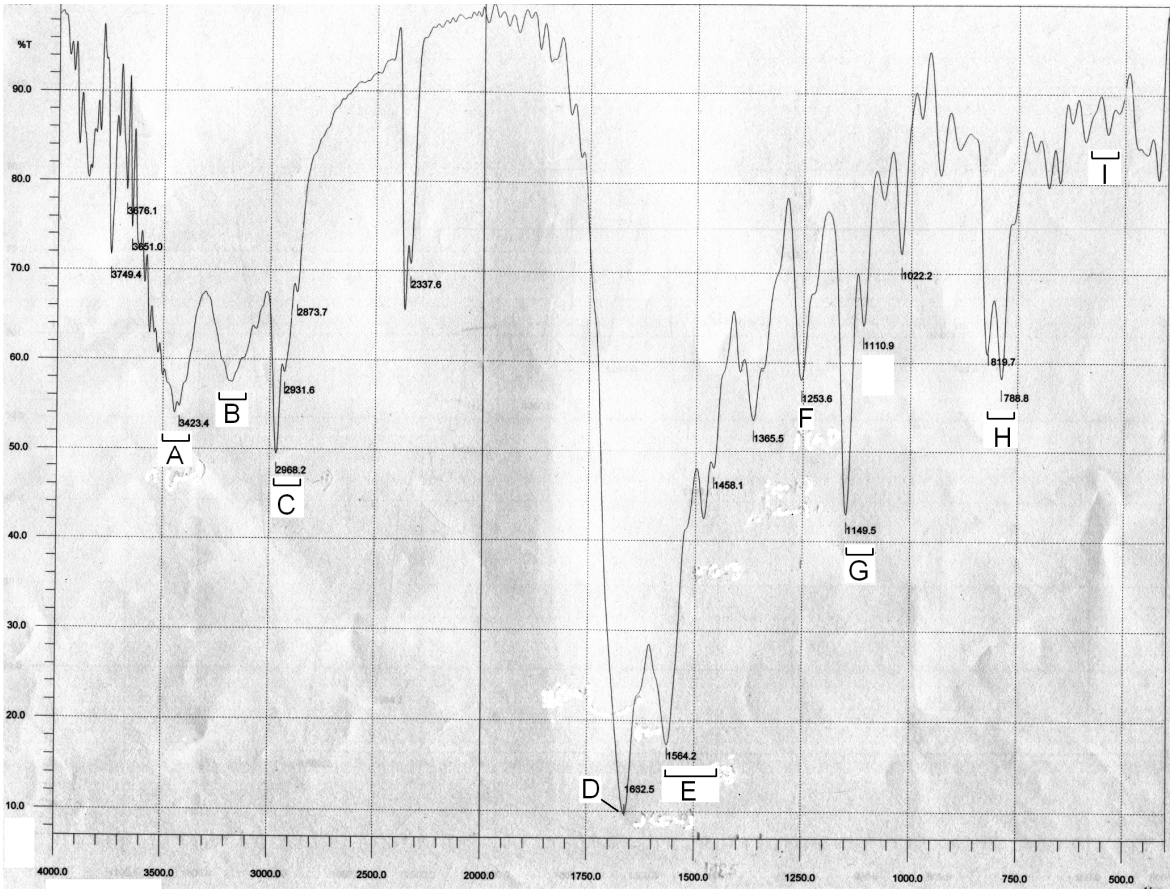

Fig.(III-15): FTIR spectrum (KBr) of compound **(3)**

A: the broad O-H stretching vibration, hydrogen bonded (CH_3OH), 3423 cm^{-1}.

B: the broad N-H stretching vibration, hydrogen bonded, 3150 cm^{-1}.

C: the C-H stretching vibrations 2968, 2631, 2873 cm^{-1}.

D: the C=O stretching vibrations of the (C=O) (1″) and (C=O) (2′) groups, 1662 cm^{-1}.

E: the C⋯C and C⋯N ring stretching vibrations of the pterin, $(thiox)^{1-}$ 1564, 1458 cm^{-1}.

F: the ν (C-O) mode of the O(4) phenoxide group, 1253 cm^{-1}.

G: the ν (C-N) + δ (NH_2) vibrations , a broad band over the region 1200-1159 cm^{-1} [11].

H: the out-of-plane C-H (aromatic) bending vibrations, 788 cm^{-1}.

I: the ν (C-S) mode related to the $(thiox)^{1-}$ residue, 500-600 cm^{-1},

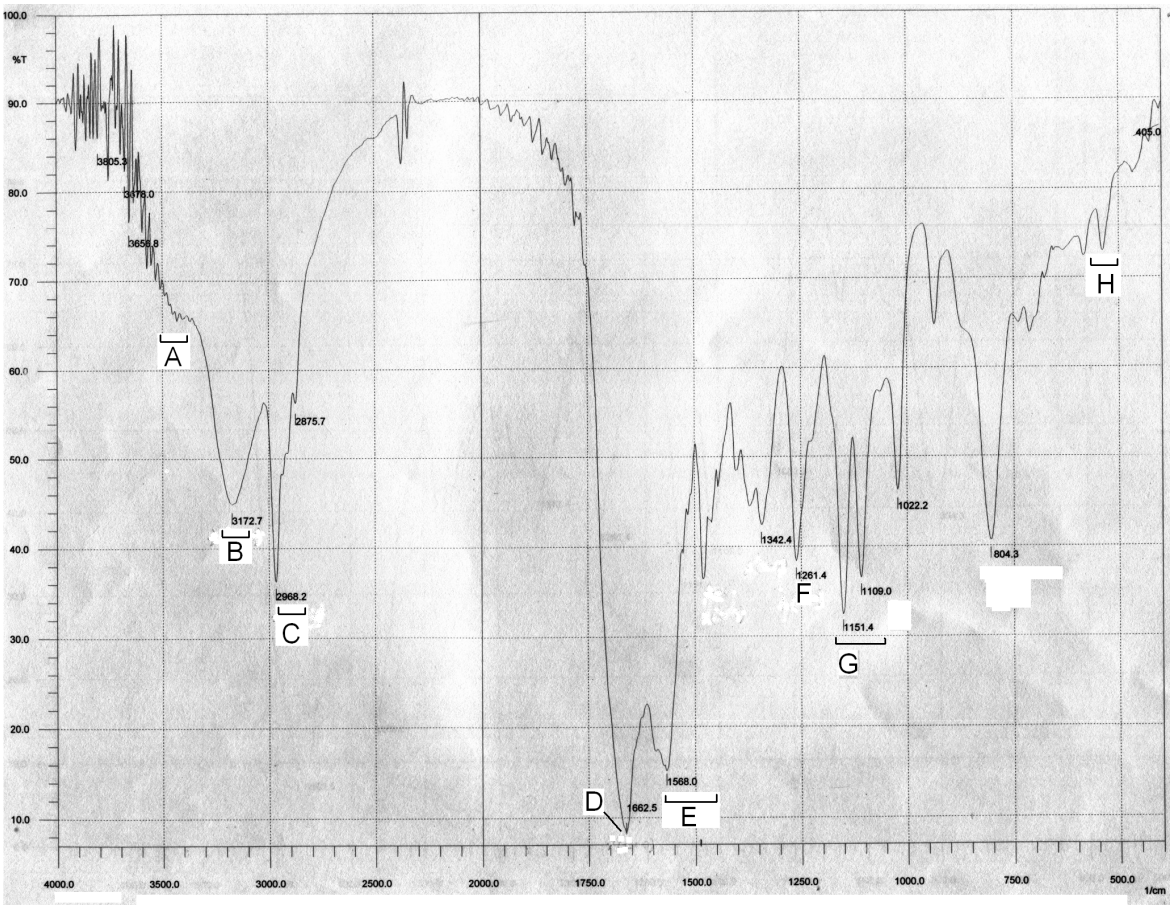

Fig.(III-16): FTIR spectrum (KBr) of compound **(4)**

A: the broad O-H stretching vibration, hydrogen bonded (CH_3OH), 3423 cm^{-1}.

B: the broad N-H stretching vibration, hydrogen bonded, 3172 cm^{-1}.

C: the C-H stretching vibrations 2968, 2875 cm^{-1}.

D: the C=O stretching vibrations of the (C=O) (1″) and (C=O) (2′) groups, 1662 cm^{-1}.

E: the C⋯C and C⋯N ring stretching vibrations of the pterin, $(aet)^{1-}$ 1568, 1458 cm^{-1}.

F: the ν (C-O) mode of the O(4) phenoxide group, 1261 cm^{-1}.

G: the ν (C-N) + δ (NH_2) vibrations , a broad band over the region 1200-1159 cm^{-1} [11].

H: the ν (C-S) mode related to the $(aet)^{1-}$ residue, 500-600 cm^{-1}.

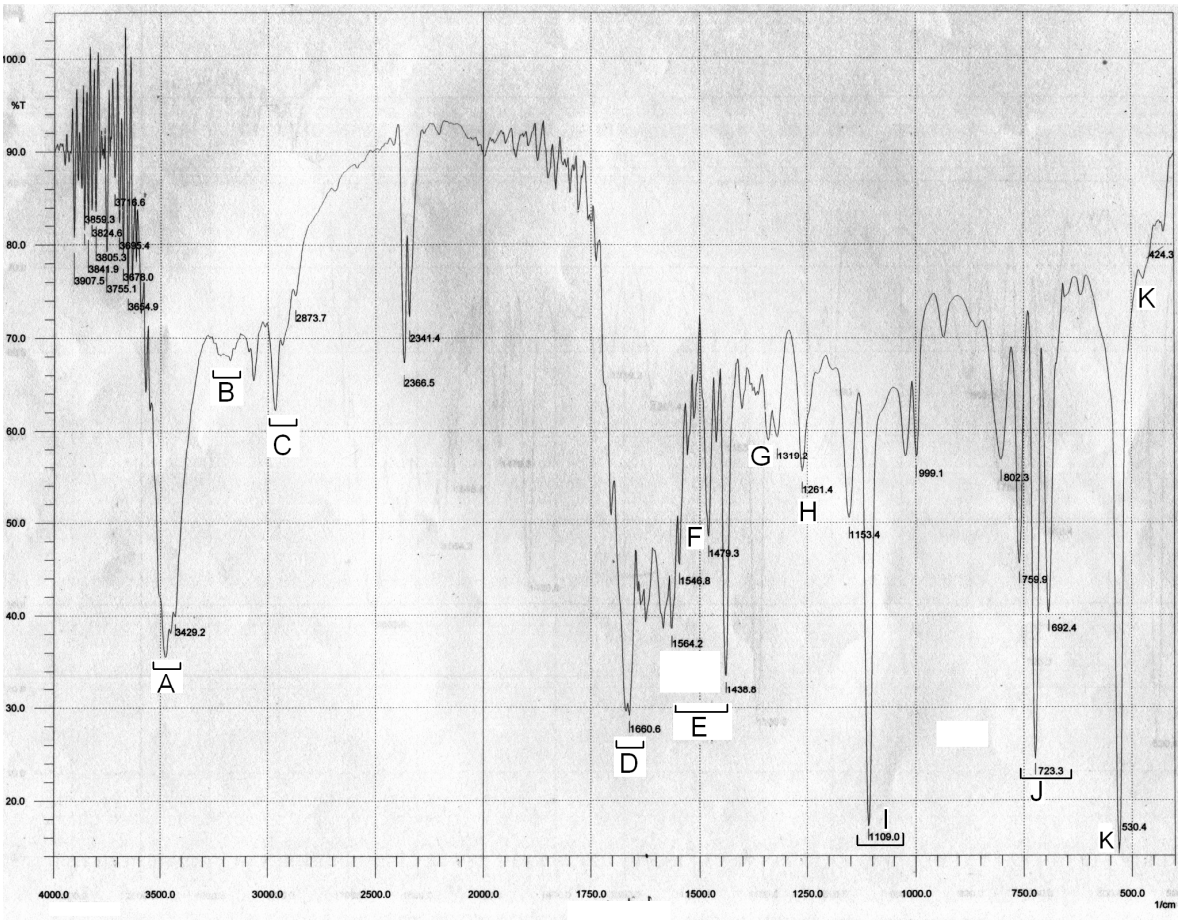

Fig.(III-17): FTIR spectrum (KBr) of **(5)**

A: the broad O-H stretching vibration, hydrogen bonded (CH_3OH), 3467, 3429 cm^{-1}.

B: the broad N-H stretching vibration, hydrogen bonded, 3154 cm^{-1}.

C: the C-H stretching vibration, 2964 cm^{-1}.

D: the C=O stretching vibrations of the (C=O) (1″) and (C=O) (2′) groups, 1660 cm^{-1}.

E: the C⋯C and C⋯N ring stretching vibrations of the pterin, 1564, 1546, 1436 cm^{-1}.

F: the antisymmetric stretching vibrations ν_{as} (CO_2^-) of cysteine residues, 1479 cm^{-1}.

G: the symmetric stretching vibrations ν_s (CO_2^-) of cysteine residues, 1319 cm^{-1} [11d].

H: the ν (C-O) mode of the O(4) phenoxide group, 1261 cm^{-1}.

I : the ν (C-N) + δ (NH_2) vibrations , a broad band over the region 1200-1159 cm^{-1} [11].

J : the out-of-plane C-H (aromatic) bending vibrations.

K: the out-of-plane C⋯C (aromatic, Ph_4P^+) bending vibrations, 530.4cm^{-1}.

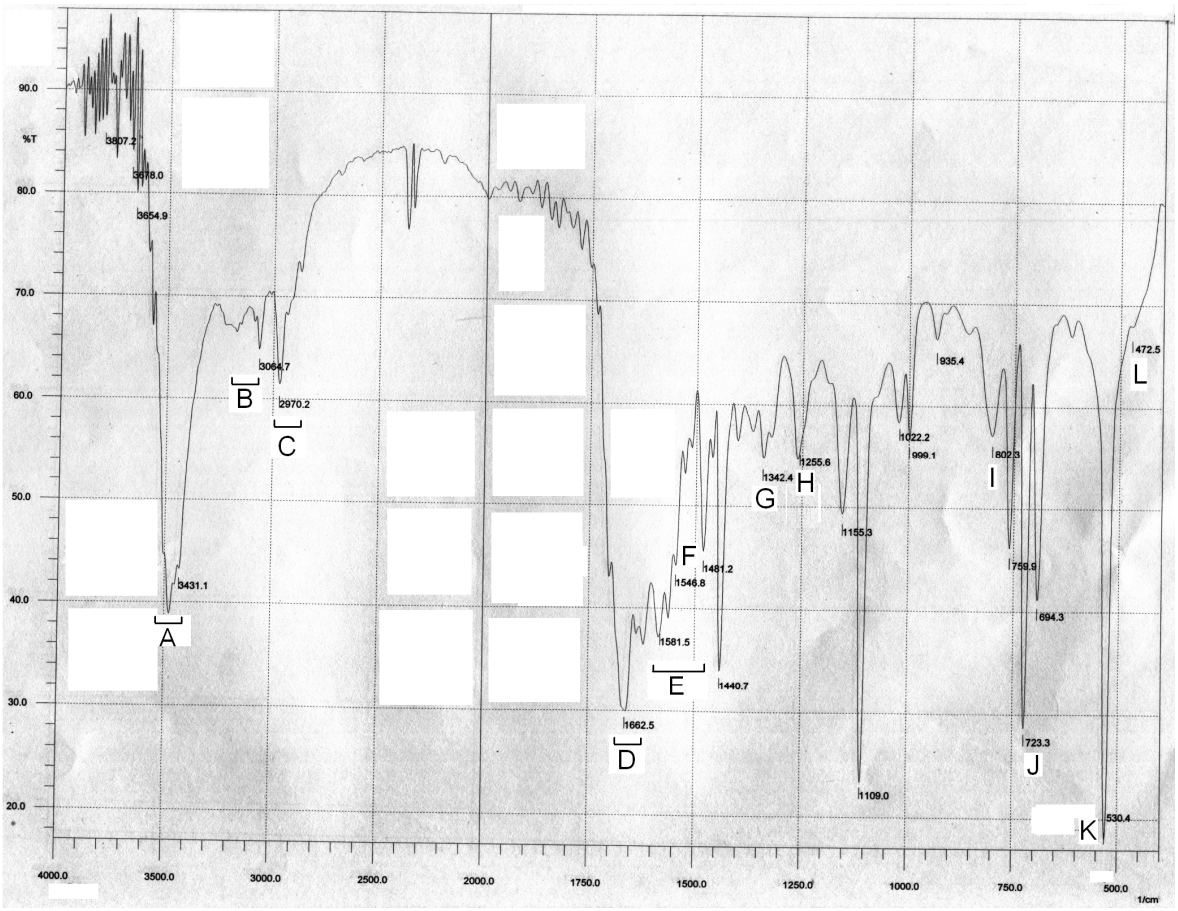

Fig.(III-18): FTIR spectrum (KBr) of (**6**)

A: the broad O-H stretching vibration, hydrogen bonded (CH_3OH), 3467, 3429 cm^{-1}.

B: the broad N-H stretching vibration, hydrogen bonded, 3154 cm^{-1}.

C: the C-H stretching vibration, 2964 cm^{-1}.

D: the C=O stretching vibrations of the (C=O) (1″) and (C=O) (2′) groups, 1688 cm^{-1}.

E: the C⋯C and C⋯N ring stretching vibrations of the pterin, phenyl rings, Ph_4P^+ cation, 1600, 1585, 1544, 1436 cm^{-1}.

F: the antisymmetric stretching vibrations ν_{as} (CO_2^-) of cysteine residues, 1483 cm^{-1}.

G: the symmetric stretching vibrations ν_s (CO_2^-) of cysteine residues, 1340 cm^{-1} [11d].

H: the ν (C-O) mode of the O(4) phenoxide group, 1261 cm^{-1}.

I: the ν (Mo-O_b-Mo) mode related to the (μ-O) group, 802 cm^{-1}.

J: the out-of-plane C-H (aromatic, Ph_4P^+) bending vibrations, 723 cm^{-1}.

K: the out-of-plane C⋯C (aromatic, Ph_4P^+) bending vibrations, 530.4cm^{-1}.

L: the ν (N-C-C-S) mode of the cysteine residues, 470 cm^{-1}.

^{1}H-NMR spectroscopy

The ^{1}H-NMR data in CD_3OD of (H_2L^2) have been assigned on the basis of several expanded spectra, the corresponding ^{1}H-^{1}H COSY data and protonic integration values [11(b), 47,48]. For (H_2L^2) [Scheme(III-1)], the NH(2), NH(8) and NH(3) signals (each broad, singlet) appear at δ7.10, δ10.61 and δ12.42, respectively. CH_3(3′) signal (triplet, J = 4.8 Hz) appears at δ1.29. CH_2(1′) signal is assigned at δ3.63 (octet; J_1 = 7.2 Hz, J_2 = 3.6 Hz); 2D NMR data indicate that its multiplicity arises from spin-spin interactions with both CH_3(3′) and NH(2) groups. The three methyl groups of the t-butyl residue (2″) are non-equivalent on the ^{1}H NMR time scale: two of them appear at δ1.195 (multiplet; J_1 = 3.9 Hz, J_2 = 2.4 Hz, J_3 = 0.9 Hz) and the other one could be located at δ1.17 (multiplet; J_1 = 9.1 Hz, J_2 = 2.9 Hz). The 2D NMR spectra (^{1}H – ^{1}H COSY) of (H_2L^2) shown in Fig. (III-19).

Most of the ^{1}H-NMR signals of (H_2L^2) [Scheme (III-1)] including that of the NH(2) group, have been assigned on the basis of the ^{1}H -^{1}H COSY data [Fig. (III-20a)] ; they indicate predominance of the vinylogous amide tautomer [Scheme (III-1b)]. The NH proton signals (weak broad / singlet) of the pterin ring are not connected by any cross peaks and they are located [Fig. (III-20b)] on the basis of literature data [57(b),48,4c,58] as well as their change over during the metal coordination process. For (H_2L^2) the CH_3(2′) (δ 1.097) and CH(1′) (δ 6.15) signals (each a sharp singlet) could be read off from the ^{1}H -^{1}H COSY spectrum [Fig. (III-20a)]; the same is true for the three CH_3(2″) (δ 1.24, 6H, double doublet ; δ 1.15, 3H, doublet) and NH(2) (δ 4.30) signals. The last signal is practically invisible in the 1D spectrum.

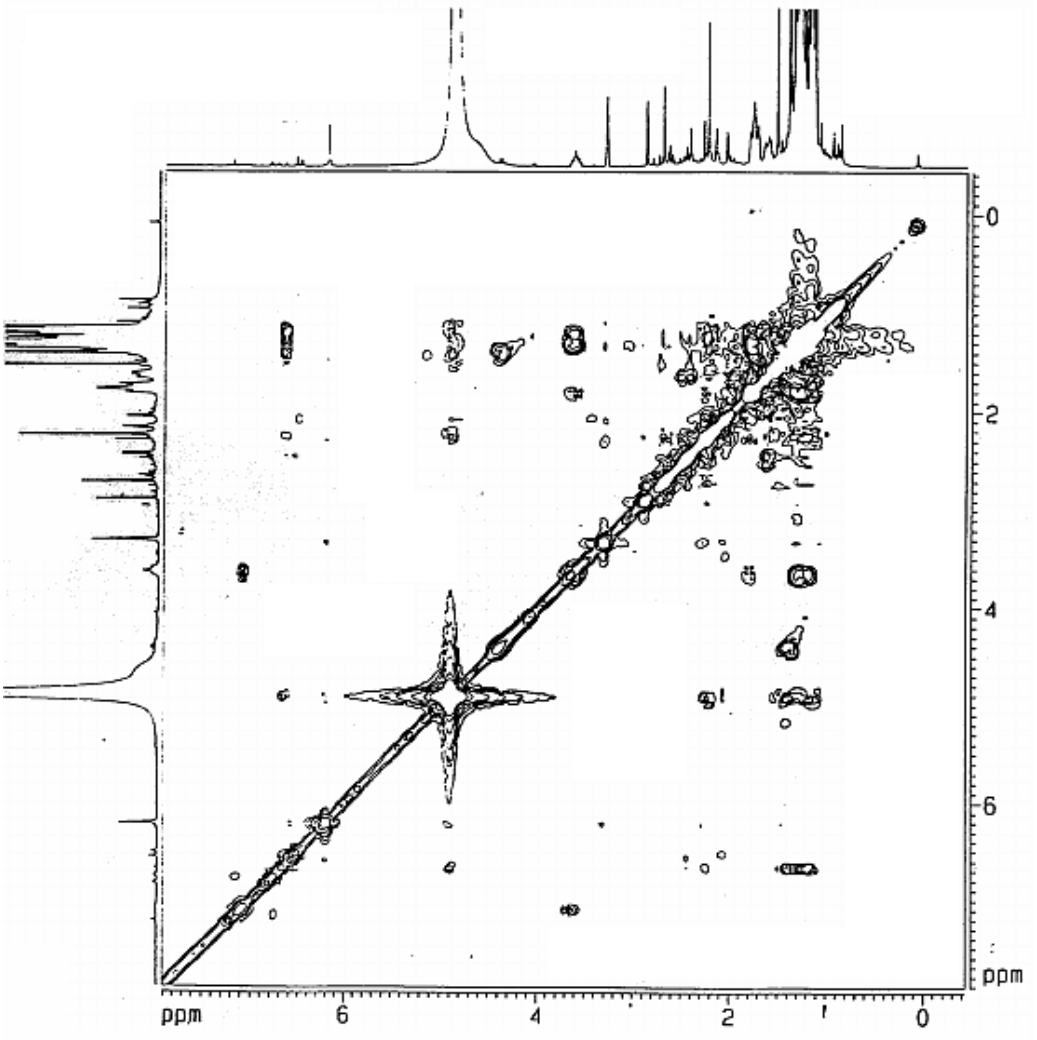

Fig. (III-19): ^{1}H-^{1}H COSY data (symmetrized) of (H_2L^2) in CD_3OD over the region 8.0 to -0.5. Its basic interpretation is indicated in the text.

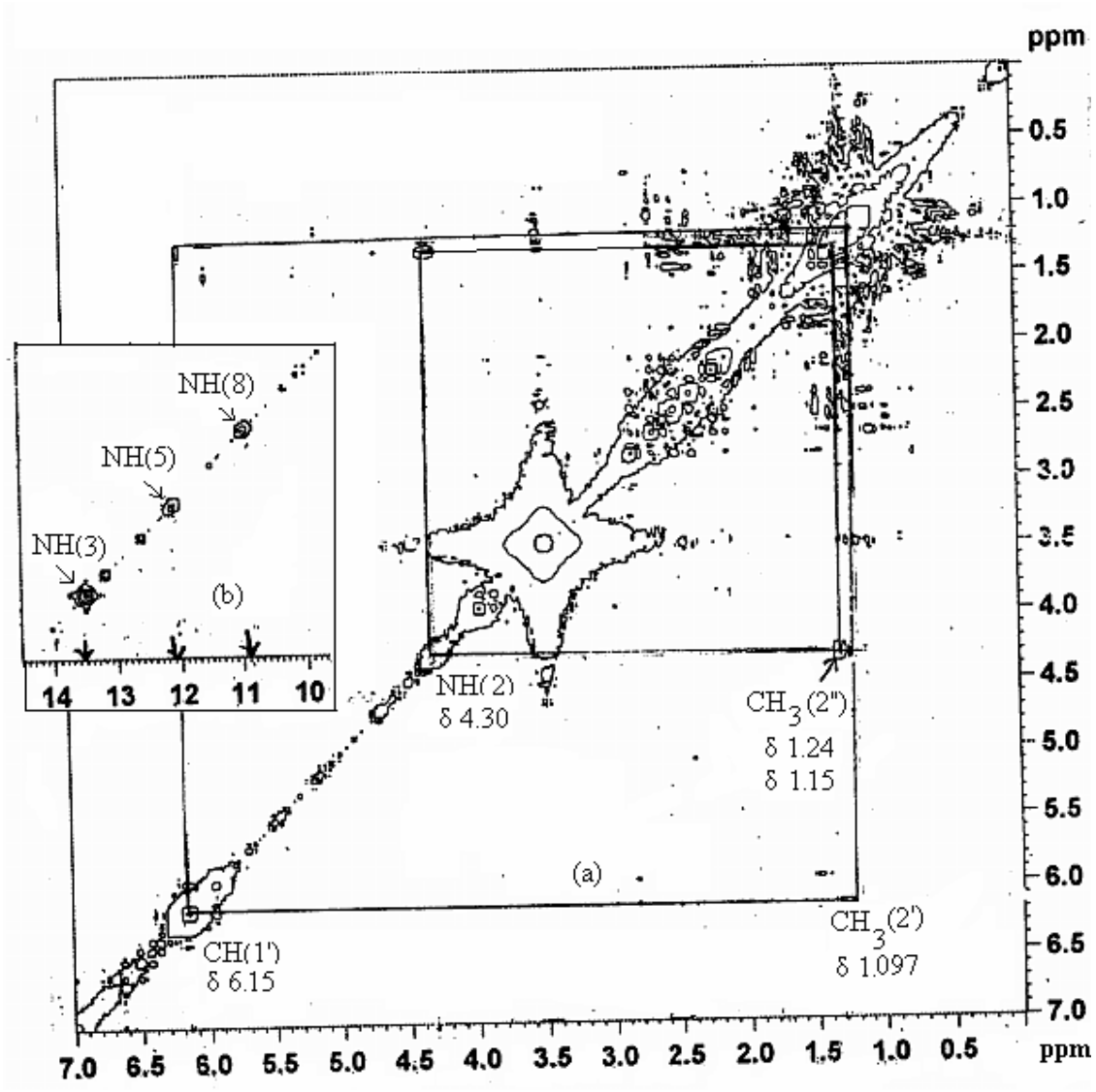

Fig. (III-20): (a) ^{1}H-^{1}H COSY data (symmetrized) of (H_2L^2) in DMSO-d_6 over the region δ7.0-0.0; (b) different NH signals of (H_2L^2) are located here (vide text for details)

The 1-D and 2-D NMR data of compound **(1)** are presented in Fig. (III-21) and Fig. (III-22) respectively. The CH(1′), NH(2), CH_3(2′) [Scheme (III-1)] and CH_3(2″) signals could be assigned at δ6.23(ss), δ4.04(s), δ1.445 respectively [Fig. (III-21) and Fig. (III-22)]. The NH(8) signal appears at δ12.40(wb); the OH(CH_3OH) signal is located at δ13.60. A perusal of Table (III-2) indicates that the CH(1′) and CH_3(2′) signals undergo minor change from their free ligand position upon coordination to the [Mo(IV)] centre in the relevant

complexes; non-participation of the 6-carbonyl group in the metal coordination process may be inferred from the chemical shift values of the CH(1′) signal.

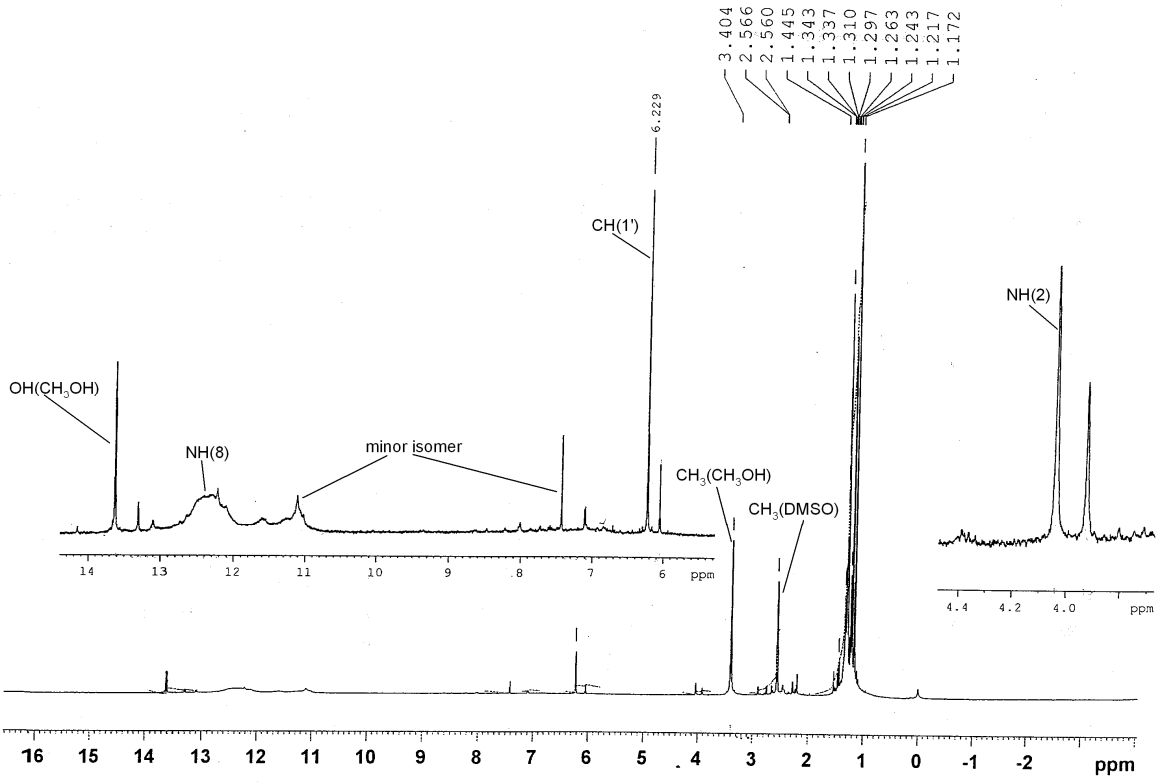

Fig.(III-21): ^{1}H NMR data of compound (**1**) in DMSO-d_6 over the region δ16.0-0.0(vide text for details).

The strong deshielding of the NH(8) signal is due to participation of the O(4) atom in the coordination process, leading to electron density withdrawal from NH(8) position in accordance with the Joule's hypothesis [5b]. The O(4) atom along with the N(5) atom confers bidented pterin ligand coordination in this case. The pivotal role of the N(5) atom in the metal coordination has been established x-ray structurally [50]. The latter aspect highlights redox non-innoent nature of the pterin ligand residue. Besides this the NH(3) and NH(5) signals of the free ligand (H_2L^2) are absent here indicating their deprotonation during the metal coordination process. Taking into account the two CH_3OH molecules and overall coordination number of six is achieved here as indicated in Scheme (III-3). This NMR spectrum is characterized by a small amount of an additional isomer as indicated by the ^{1}H-NMR signal at δ3.39, δ6.05, δ7.45 and δ11.1 respectively.

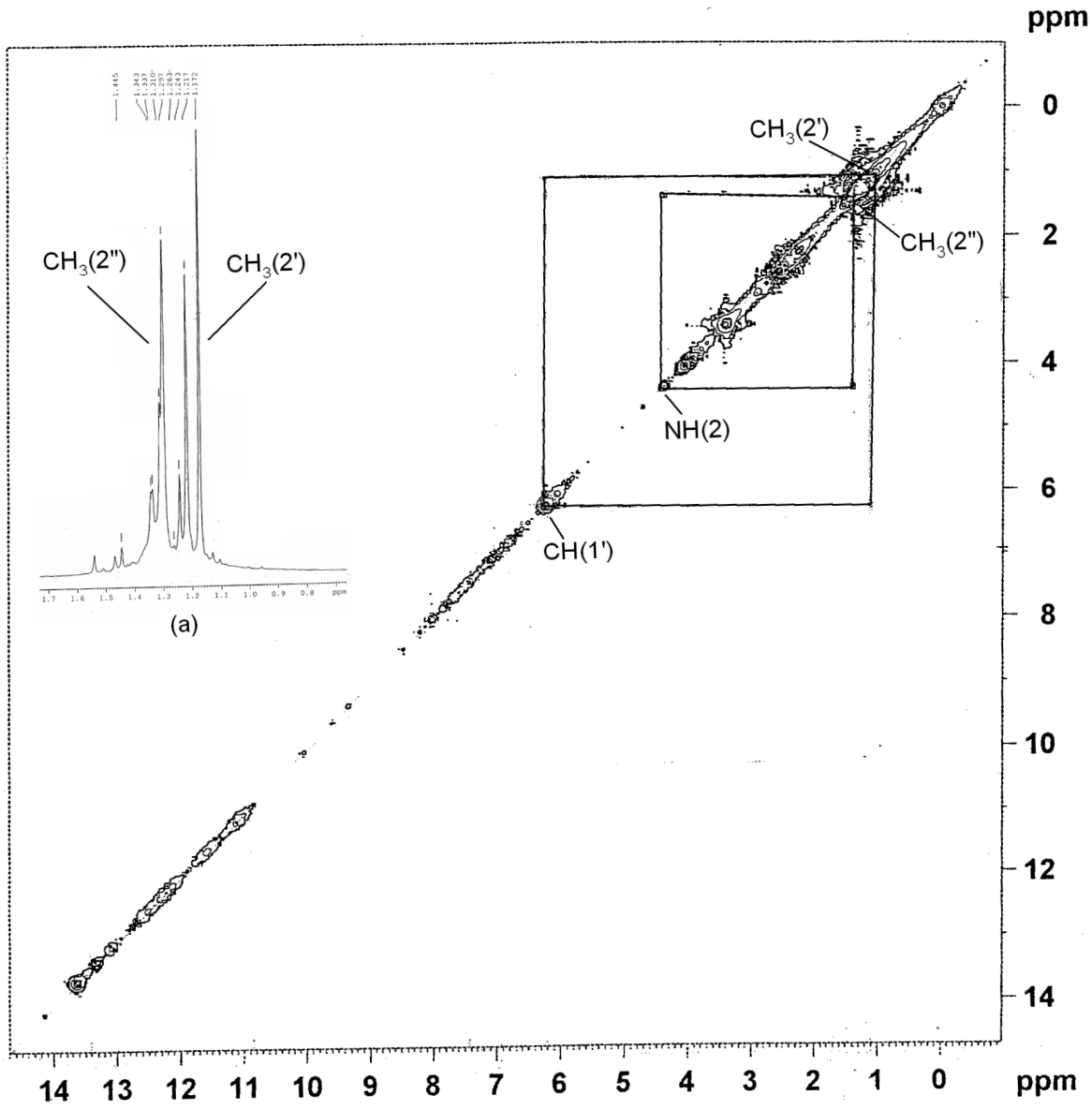

Fig.(III-22): ^{1}H-^{1}H COSY data (symmetrized) of compound (**1**) in DMSO-d_6 over the region δ14.0-0.0; (a) different $CH_3(2')$ and $CH_3(2'')$signals of (**1**) are located here (vide text for details).

Fig.(III-23) to Fig. (III-26) shows the ^{1}H-NMR data of the ancillary ligand 2-aminothiophenol, H(atp) [Scheme (III-2)]. Assignments some of the relevant signals are indicated in the above figures.

Fig.(III-27) to Fig.(III-29) represent the 1D and 2D NMR data of compound **(2)**.The 1-D and 2-D NMR data of compound **(2)** help to assign the relevant proton signals. For

example, the CH(1′) signal is assigned at δ6.27. The aromatic proton signals of the $(atp)^{1-}$ residue are spread over the region δ6.4- δ7.3 [Fig. (III-28)]. Besides this 2-D NMR data help the NH(2) and CH_3(2″) signals at δ4.35 and δ1.30 respectively. The doublet centered around δ1.26 could be assigned to CH_3(1′) signal. Besides this the NH(8) and OH(CH_3OH) could be located at δ12.40 and δ13.72 respectively. As usual the contributions from a minor isomer could be located at δ11.2, δ6.09 and δ1.19. The relevant Δ values of Table (III-2) for **(2)** indicate the bidentate nature of the pterin ligand, coordinating with Mo(IV) centre through O(4) and N(5) atom. Considering the two $(atp)^{1-}$ residues an hexacoordinated Mo(IV) complex could be visualized as in Scheme (III-4).

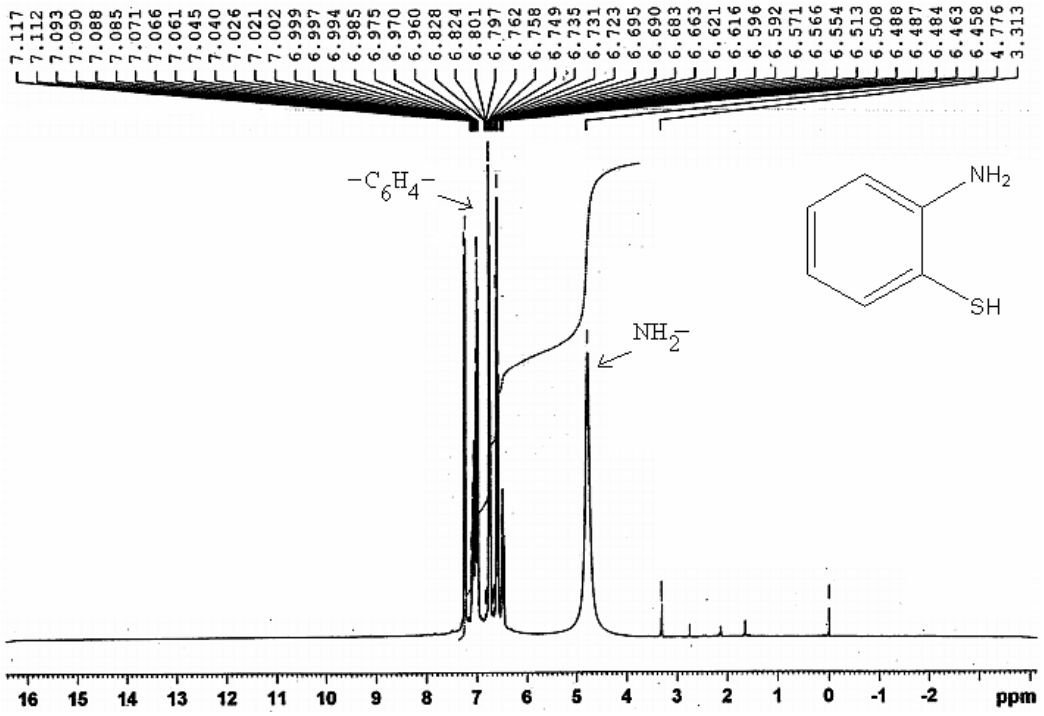

Fig.(III-23): ^{1}H NMR data of 2-aminothiophenol in CD_3OD vs. TMS, over the region δ, 16.0-00.

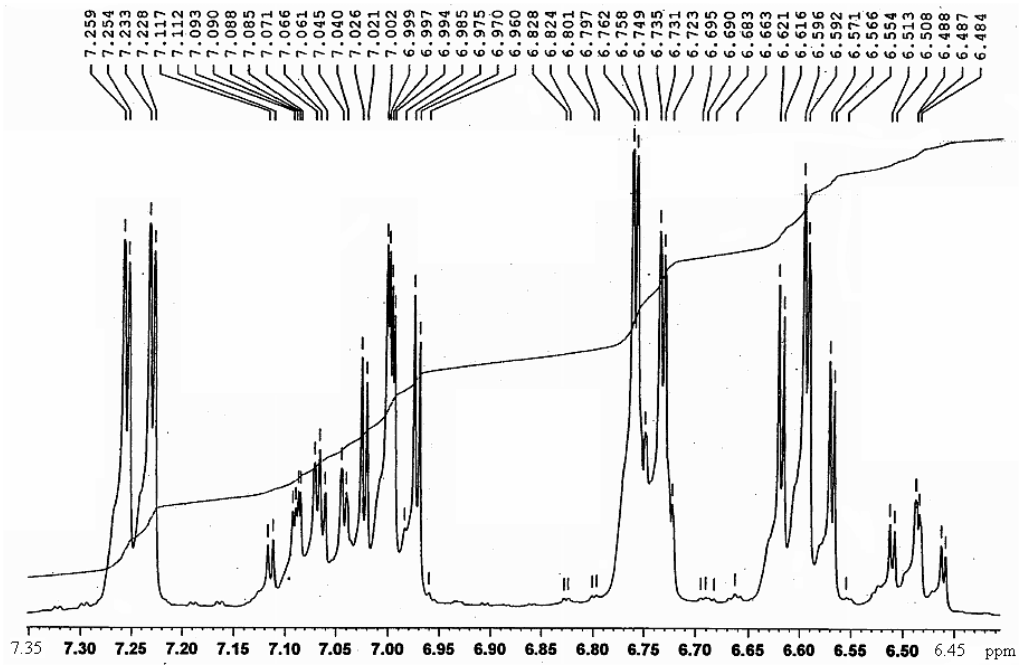

Fig.(III-24): ^{1}H NMR data of 2-aminothiophenol in CD_3OD vs. TMS, over the region δ7.35- 6.40.

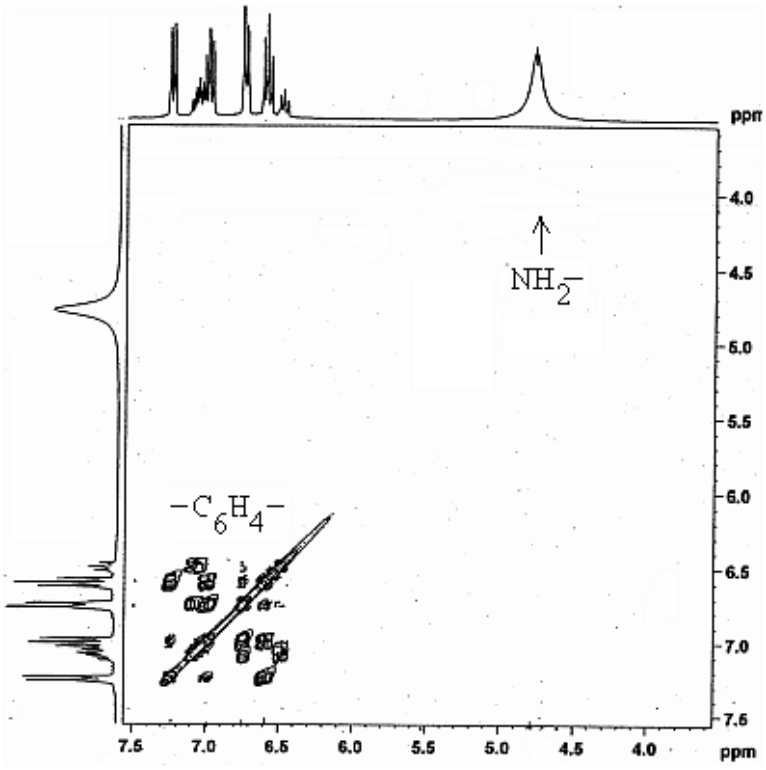

Fig.(III-25): ^{1}H-^{1}H COSY data (symmetrized) of 2-aminothiophenol in CD_3OD vs. TMS, over the region δ 7.5-3.5.

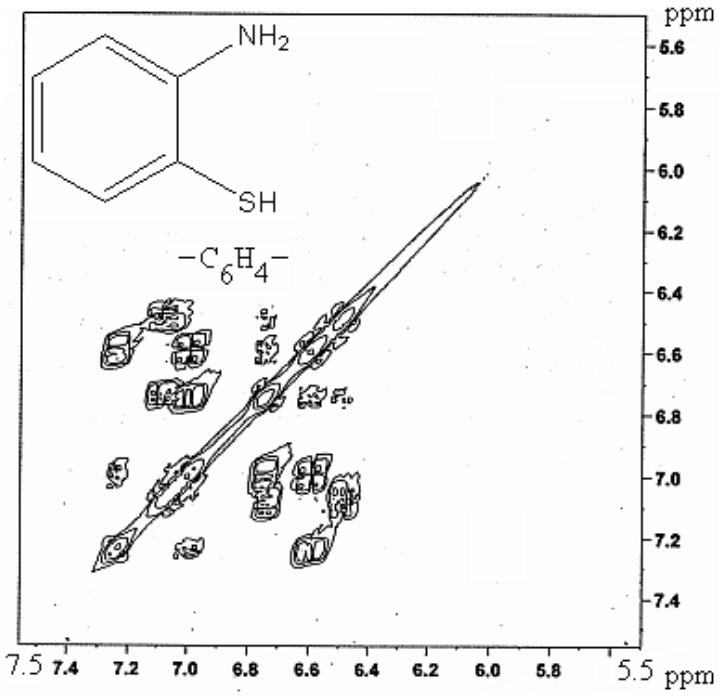

Fig.(III-26): ^{1}H-^{1}H COSY data (symmetrized) of 2-aminothiophenol in CD_3OD vs. TMS, over the region δ7.5-5.5.

Fig. (III-30) to Fig. (III-32) represent the 1-D and 2-D NMR data of compound **(3)**. Here the CH(1′) signal is assigned at δ6.25; the NH(8) and OH(CH_3OH) signals are assigned at δ12.30 and δ13.62 respectively. The 1H-NMR of oxine (8-quinolinol) has been assigned by Baker and Sawer [51]. Such assignments have been helpful here in assigning the ^{1}H-NMR signals of the $(thiox)^{1-}$ residue over the region δ7.5- δ9.8 in terms of both 1-D and 2-D NMR data. 2-D NMR data also help to assign the CH_3(2″) signal and NH(2) signal in terms of cross-peaks at δ1.15 and δ3.45 respectively. Now a closer look at relevant 1-D NMR data help to assign CH_3(2′) signal at δ1.31. As evident from Table (III-2), bidented pterin coordination can be inferred. Now considering the ancillary ligand residue as bidented N,S donor, the [Mo(IV)] centre attains a coordination number of six in this complex as shown in the Scheme (III-5). A noteworthy feature is the shielding of the NH(2) signal from its free ligand position of δ4.30;increase of electron density around this functional group occurs during complex formation. This aspect together with electron depletion around NH(8), highlights the redox non-innocent behaviour of the pterin ligand, possible enhanced by the N,S donor ligand. Minor contributions from an isomer could be located at δ11.11, δ6.06 and over the region δ1.1- δ1.6 respectively. This is consistent with the x-ray structural data of the

Zn(II)-pterin complex reported in Chapter II; here on complex formation, the NH_2 – C(2) bond acquires double bond character due to electronic redistribution of the redox non-innoent pterin ligand.

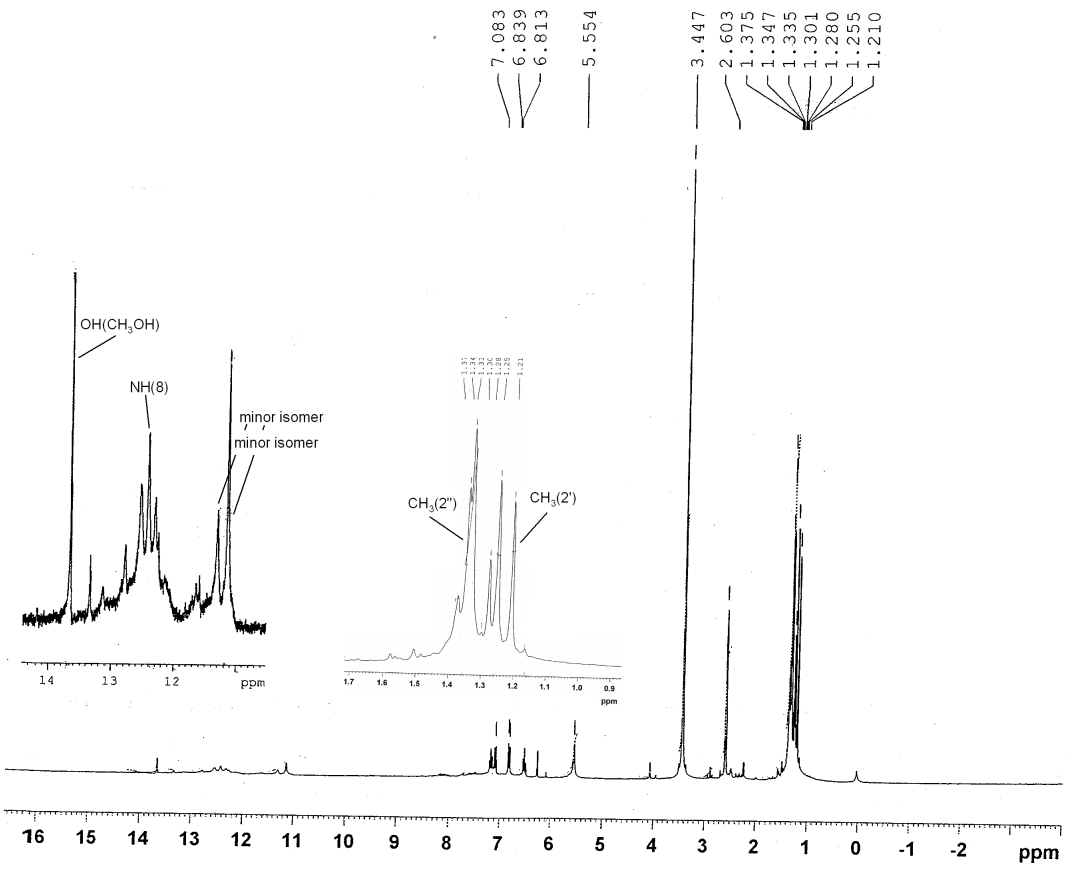

Fig.(III-27): ^{1}H NMR data of compound (**2**) in DMSO-d_6 over the region δ16.0-0.0(vide text for details).

Fig. (III-33) represent the 2-D NMR data of the ancillary ligand 2-aminoetahnethiol hydrochloride along with assignments.

The 1-D and 2-D NMR data of **(4)** are shown in Fig. (III-34) to Fig. (III-36). The NH(8), OH(CH_3OH) and CH(1′) signal could be assigned at δ12.40, δ13.30 and δ6.25 respectively. 2-D NMR data help to assign the NH(2) and CH_3(2″) signals at δ4.45 and δ1.30 respectively. An examination of Fig. (III-35) helps to assign the CH(1′) signal at δ1.21. As par Table. (III-2) the relevant Δ value points out non-participation of the 2′-carbonyl group in the metal coordination process and bidented pterin coordination (O,N donor) takes place as

usual. 2-D NMR is helpful in assigning the ancillary ligand proton signals as usual; the NH_2, $CH_2(2)$ and $CH_2(1)$ are assigned at δ7.70, δ3.35 and δ2.80 respectively.

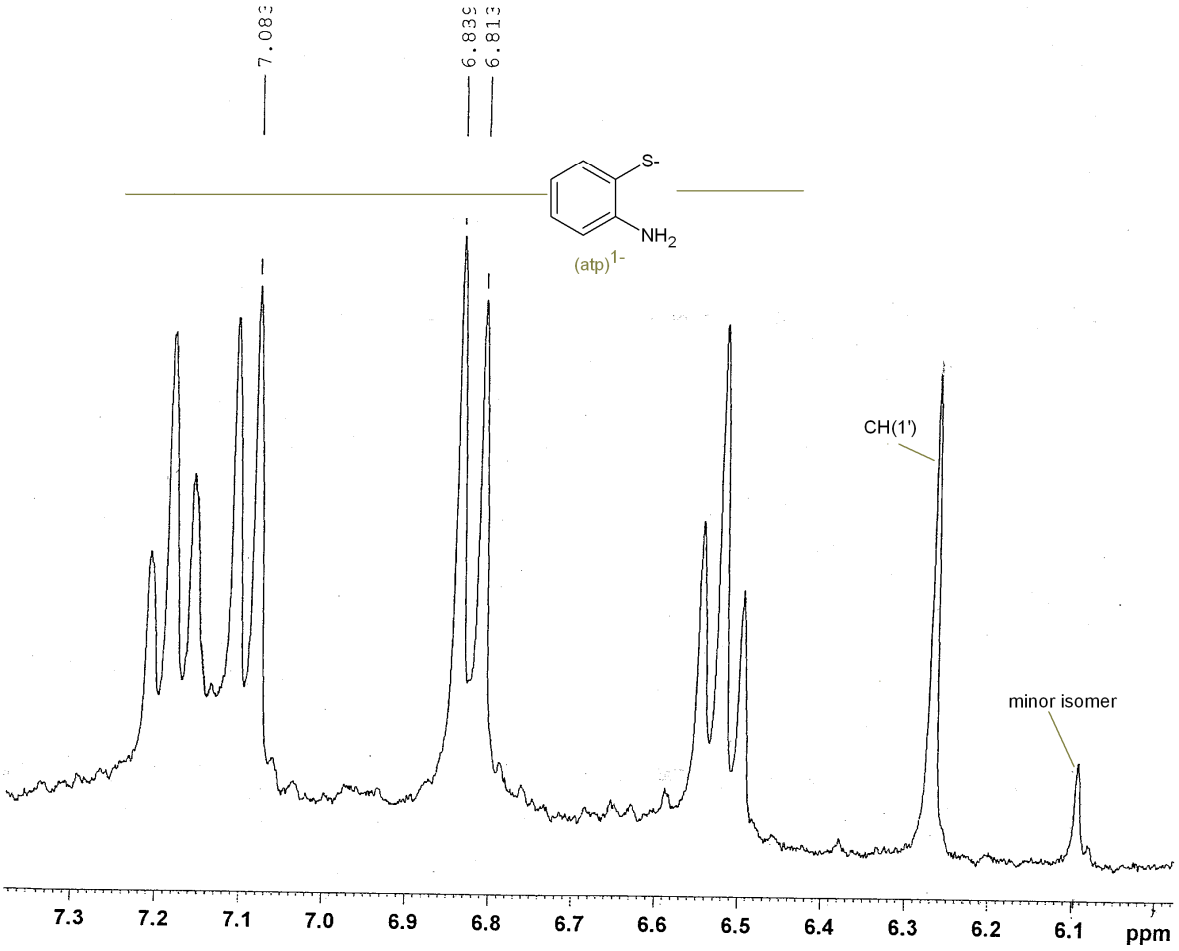

Fig.(III-28): ^{1}H NMR data of compound **(2)** in DMSO-d_6 over the region δ6.0-7.3(vide text for details).

For the free ancillary ligand [Fig. (III-33)] such signals appear at δ8.14, δ3.19 and δ2.91 respectively. Deprotonation of the NH_2 group during metal coordination is responsible for the observed shielding of the NH_2 signal in compound **(4)**. The $CH_2(2)$ signal also undergoes distinct shielding. Contributions from a minor isomer could be located at δ11.15 and δ6.07 respectively [Fig.(III-36)].

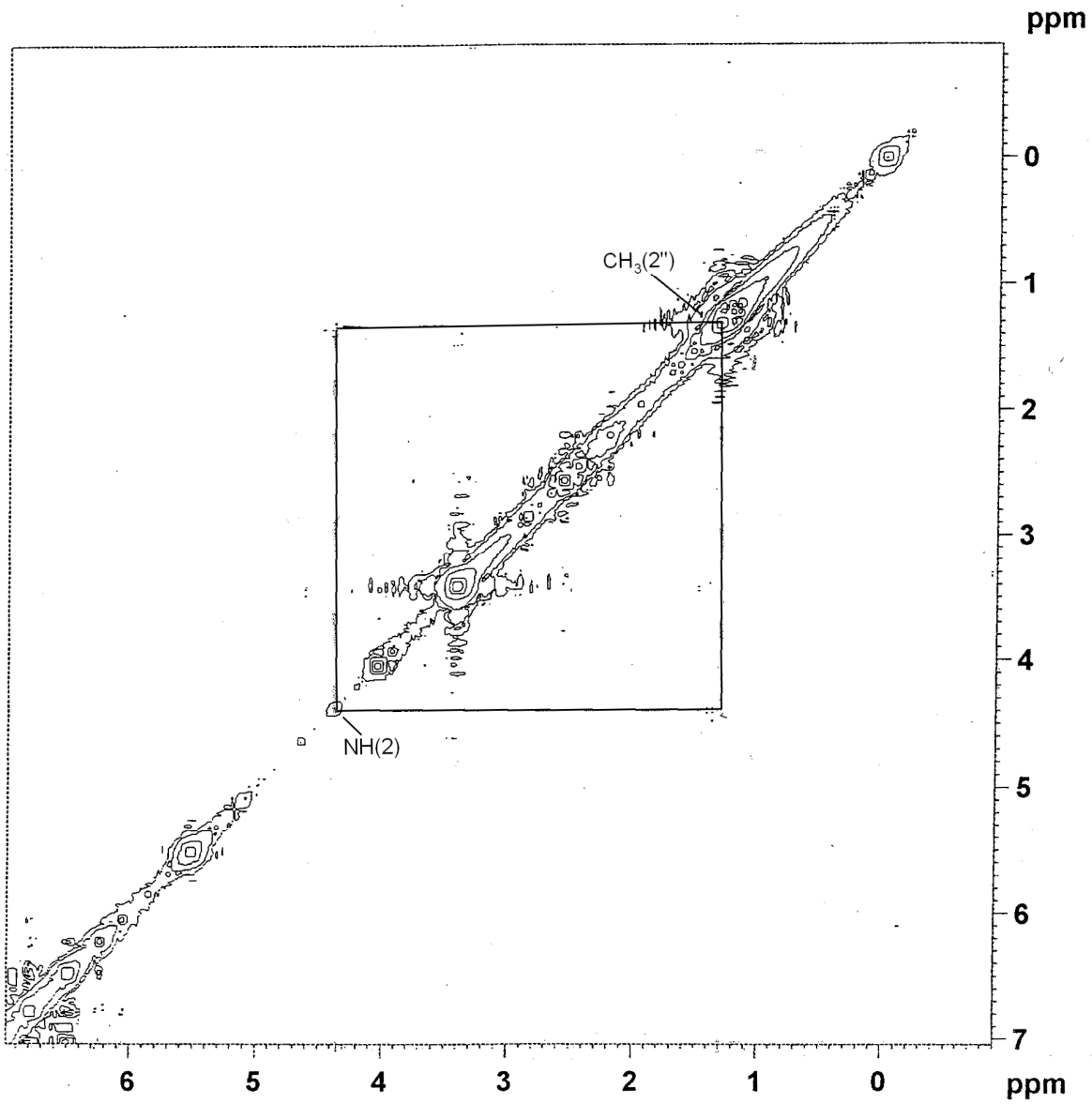

Fig.(III-29): ^{1}H-^{1}H COSY data (symmetrized) of compound **(2)** in DMSO-d_6 vs. TMS, over the region δ7.0-0.0.

The 2-D spectra of Ph_4PBr and the ancillary ligand H_2(cys) are shown in Fig. (III-37) and Fig. (III-38) respectively. Fig. (III-39) to Fig. (III-41) represent the 1-D and 2-D NMR spectra of compound **(5)**. The OH(CH_3OH), NH(8) and CH(1′) signals appear at δ13.60, δ12.40 and δ6.22 respectively. The phenyl ring protons [$(Ph_4P)^+$] are spread over δ8.2 to δ7.5 (both 1-D and 2-D NMR data). 2-D NMR data help to locate the NH(2) and CH_3(2″) signals at δ3.45 and δ1.21 respectively. A closer look at the relevant 1-D NMR data help to locate the CH_3(2′) signal at δ1.31. Both these CH_3 signals are highly distorted doublet due to the

intervening carbonyl group from the nearest coupling proton [NH(2) or CH(1′)]. 2-D NMR data also help to assign the signals of the ancillary ligand residue $(cys)^{2-}$ [Fig. (III-41)]. Signals from additional isomer could also be located in this spectrum (δ11.60, δ11.0, δ6.02, δ5.80, δ1.13). Now the chemical shift value of the NH(2) signal needs a closer attention as it is shielded considerably from its free ligand position (Δ = 0.85). It is comparable to that of compound **(3)** containing thiooxine as ancillary ligand. Comparable L→M π-bonding, as discussed in case of thiooxine may be valid here as well. This electron transmission ability of the $(cys)^{2-}$ residue, as highlighted by the role in the cytochrome P-450 enzyme may be valid here also.

Fig. (III-42) to Fig. (III-44) represent the 1-D and 2-D NMR data of **(6)**. The high resolution ^{1}H-NMR signals are consistent with its formulation as par Scheme (III-8), indicating a di-μ-oxo bridged –Mo(V) dimer (diamagnetic species). The two sharp signals at δ6.22 and δ5.79 assignable to the CH(1′) signal indicate that two pterin ligand residues are slightly different on NMR time scale. The $C_6H_5[(Ph_4P)^{+}]$ functional group is represented by the signal spread over δ7.6- δ8.2. The NH(8) proton of the two pterin ligand residue give rise to two signals at δ12.33 and δ12.20, in accordance with the above inference. The OH(CH_3OH) signal is identified at δ13.60. 2-D NMR data [Fig. (III-44)] help to assign the ancillary ligand, $(cys)^{2-}$ residue at δ1.94, δ2.45 and δ3.6 corresponding to CH_2(2), CH(1) and NH_2(1) protons. Besides these, the 2-D NMR [Fig. (III-44)] data also help to assign the NH(2) and CH_3(2″) signals at δ4.18 and δ1.35 respectively. A closer examination of the 1-D NMR data help to locate two signals at δ1.13 and δ1.20 assignable to the CH_3(1′) protons of the two pterin ligand residues. Contributions from minor isomers can also be observed as usual.

The above signals indicate that compound **(6)** has been recovered in the pure form out of the reaction mixture consisting of compound **(5)** and Me_3NO. Oxygen atom transfer associated with di-μ-oxo dimer bridge formation is proposed as indicated in Scheme (III-8) and Scheme (III-10).

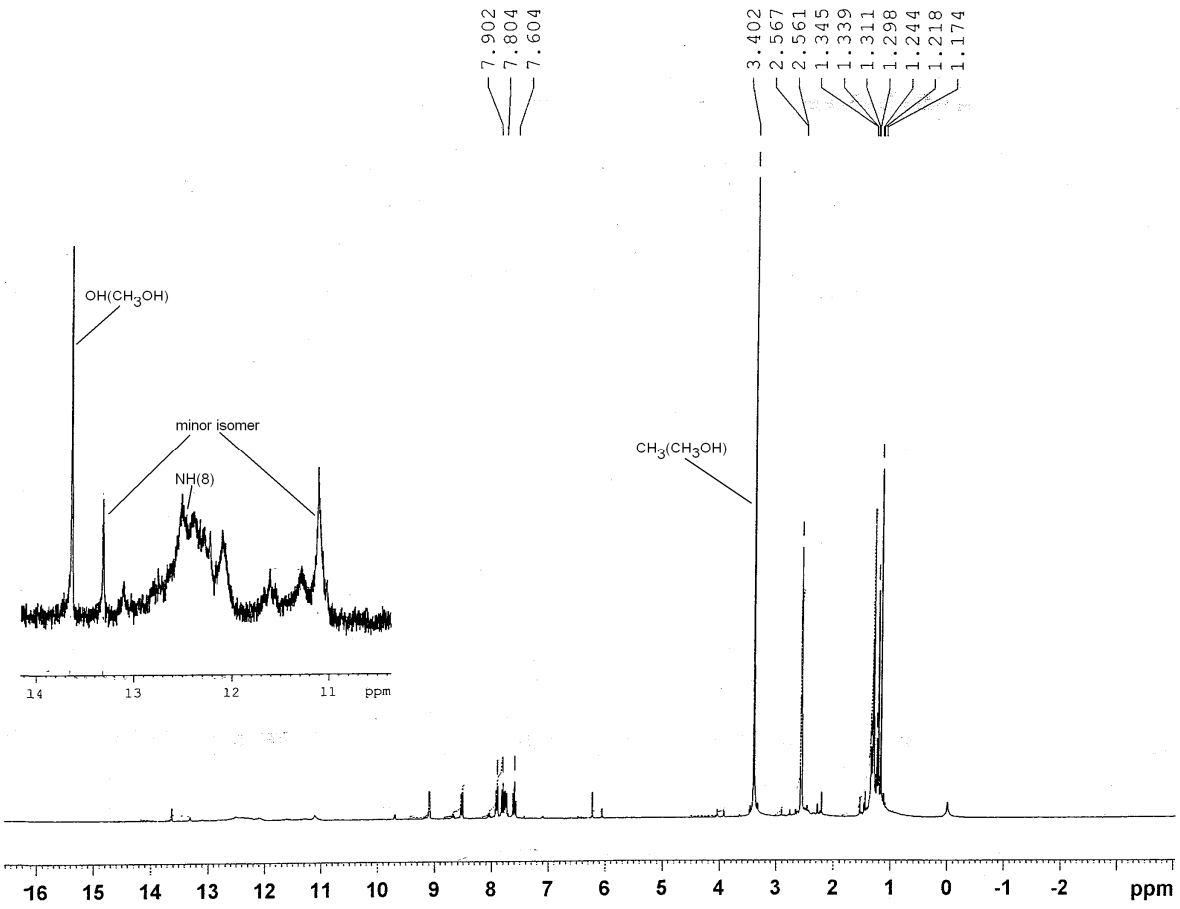

Fig. (III-30): ^{1}H NMR data of compound **(3)** in DMSO-d_6 over the region δ16.0-0.0(vide text for details).

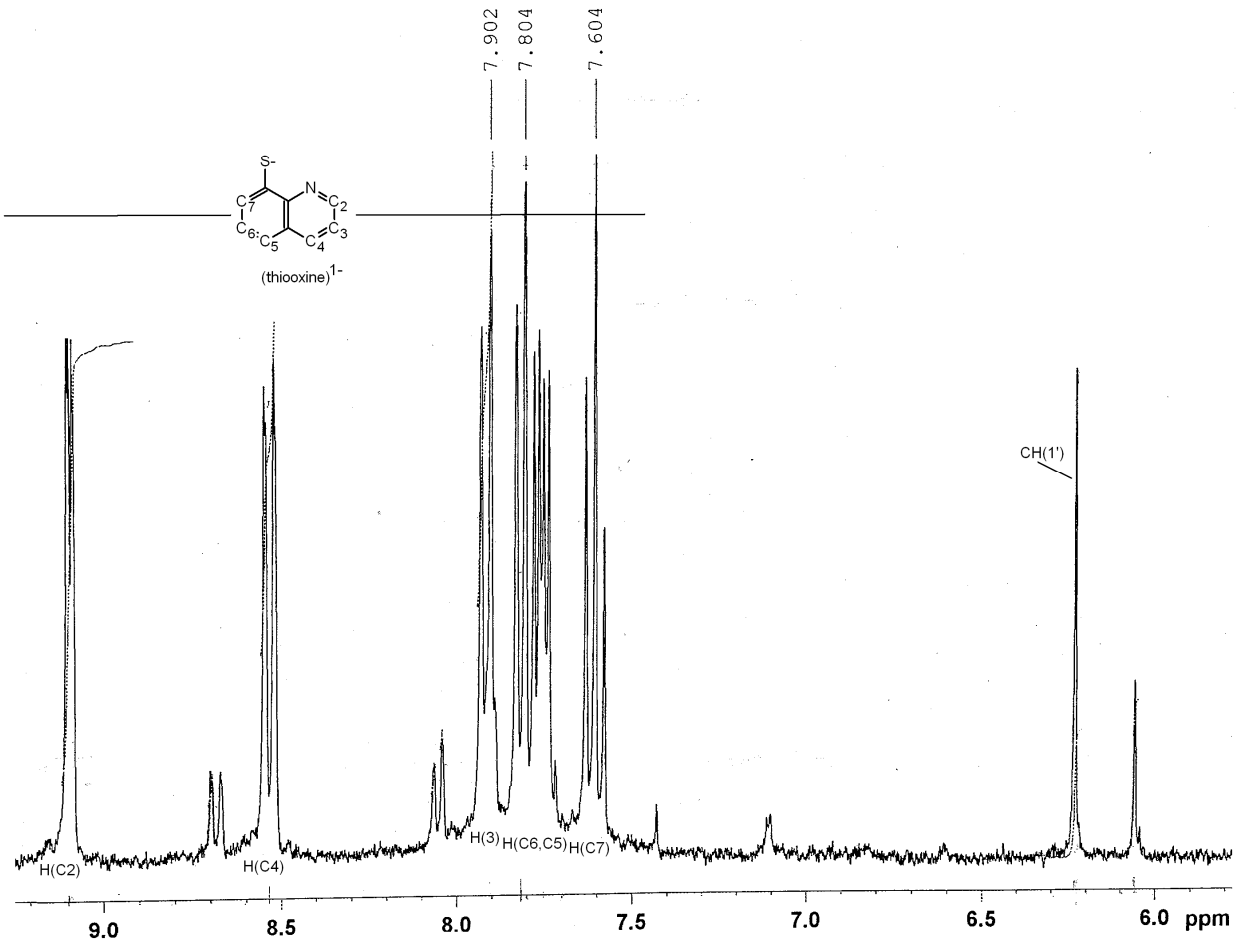

Fig. (III-31): ^{1}H NMR data of compound **(3)** in DMSO-d_6 over the region δ6.0-9.2(vide text for details).

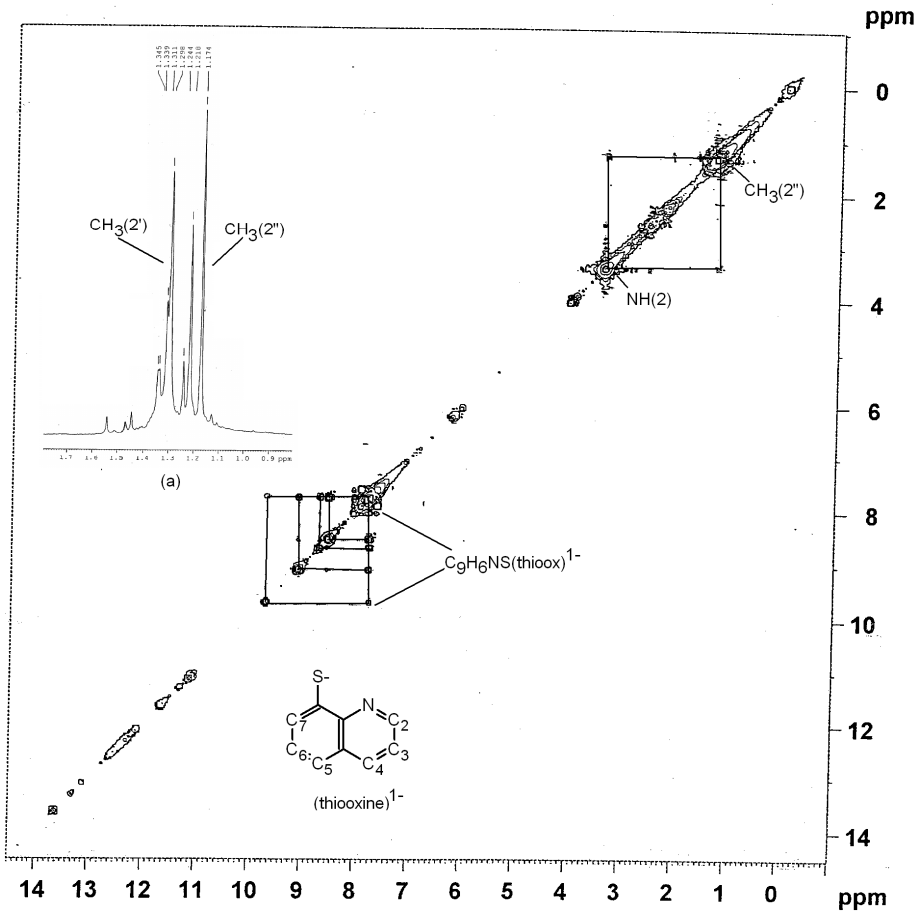

Fig. (III-32): ^{1}H-^{1}H COSY data (symmetrized) of compound **(3)** in DMSO-d_6 vs. TMS, over the region δ14.0-0.0; (a) (in set)different $CH_3(2')$ and $CH_3(2'')$signals of **(3)** are located here (vide text for details).

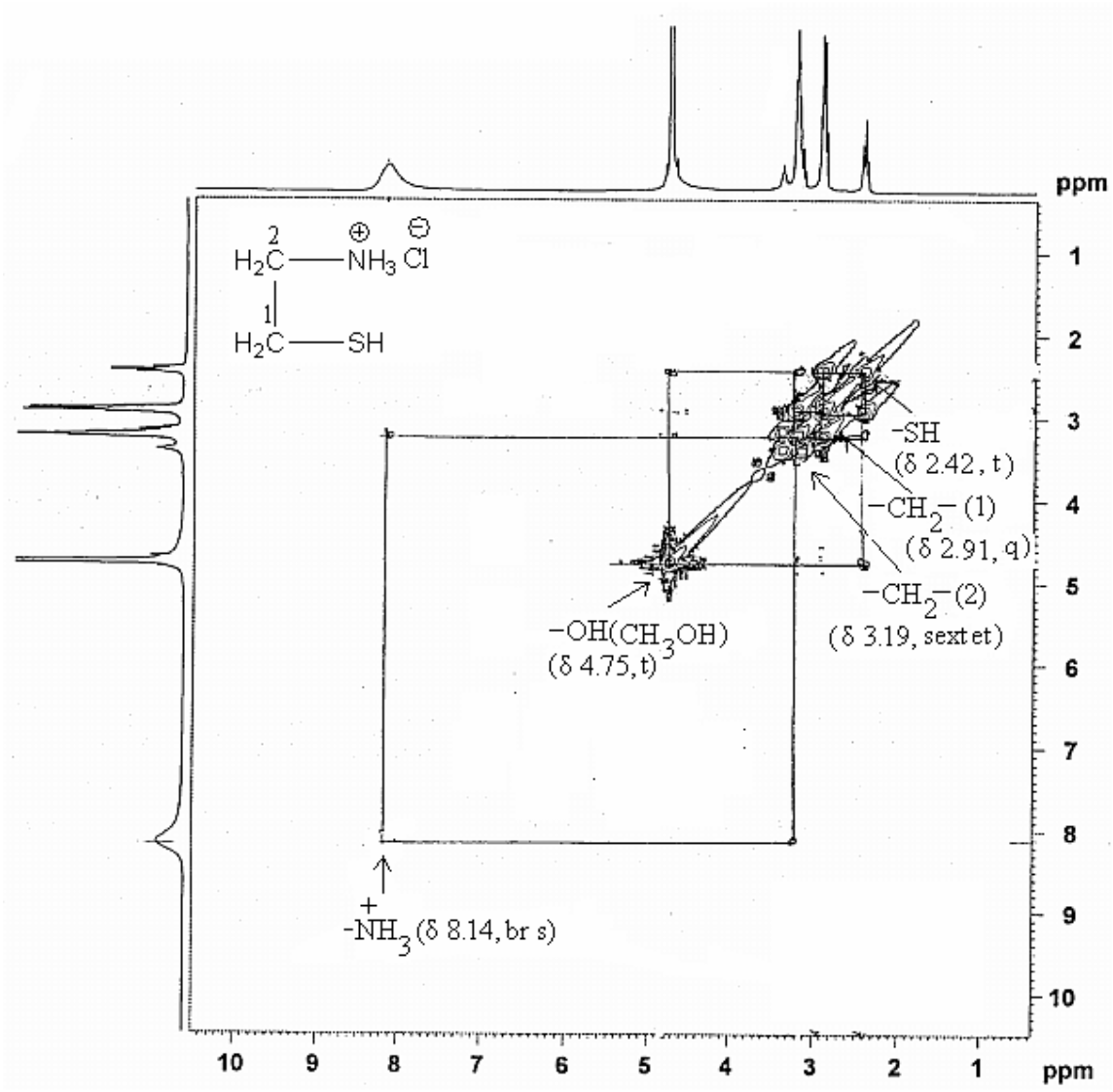

Fig. (III-33): ^{1}H-^{1}H COSY data (symmetrized) of H_2(aet) in CH_3OH-d_4, showing the assignments of different proton signals, including the long range hydrogen bonding interaction between the –SH group and the residual –OH signal of the solvent.

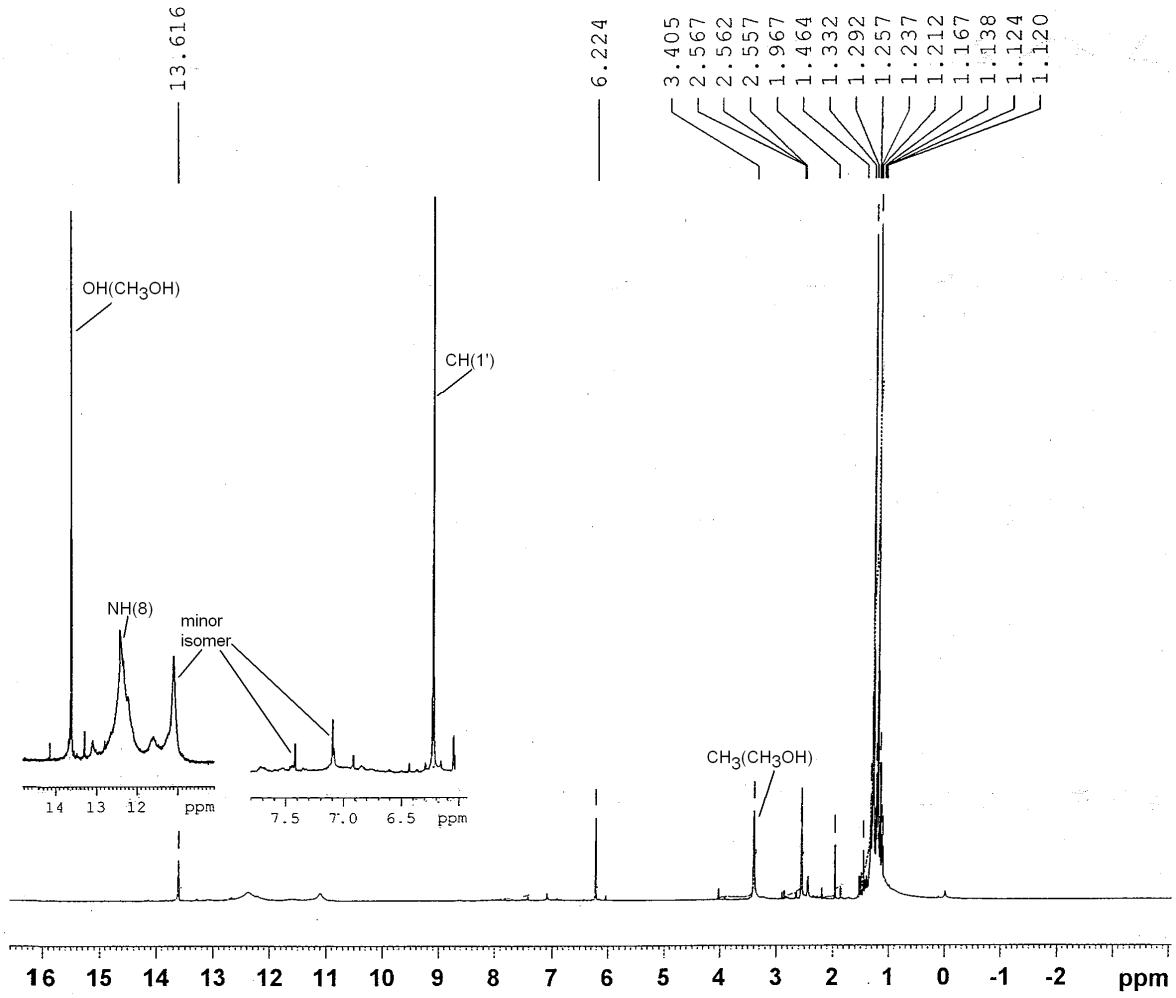

Fig. (III-34): ^{1}H NMR data of compound **(4)** in DMSO-d_6 over the region δ16.0-0.0(vide text for details).

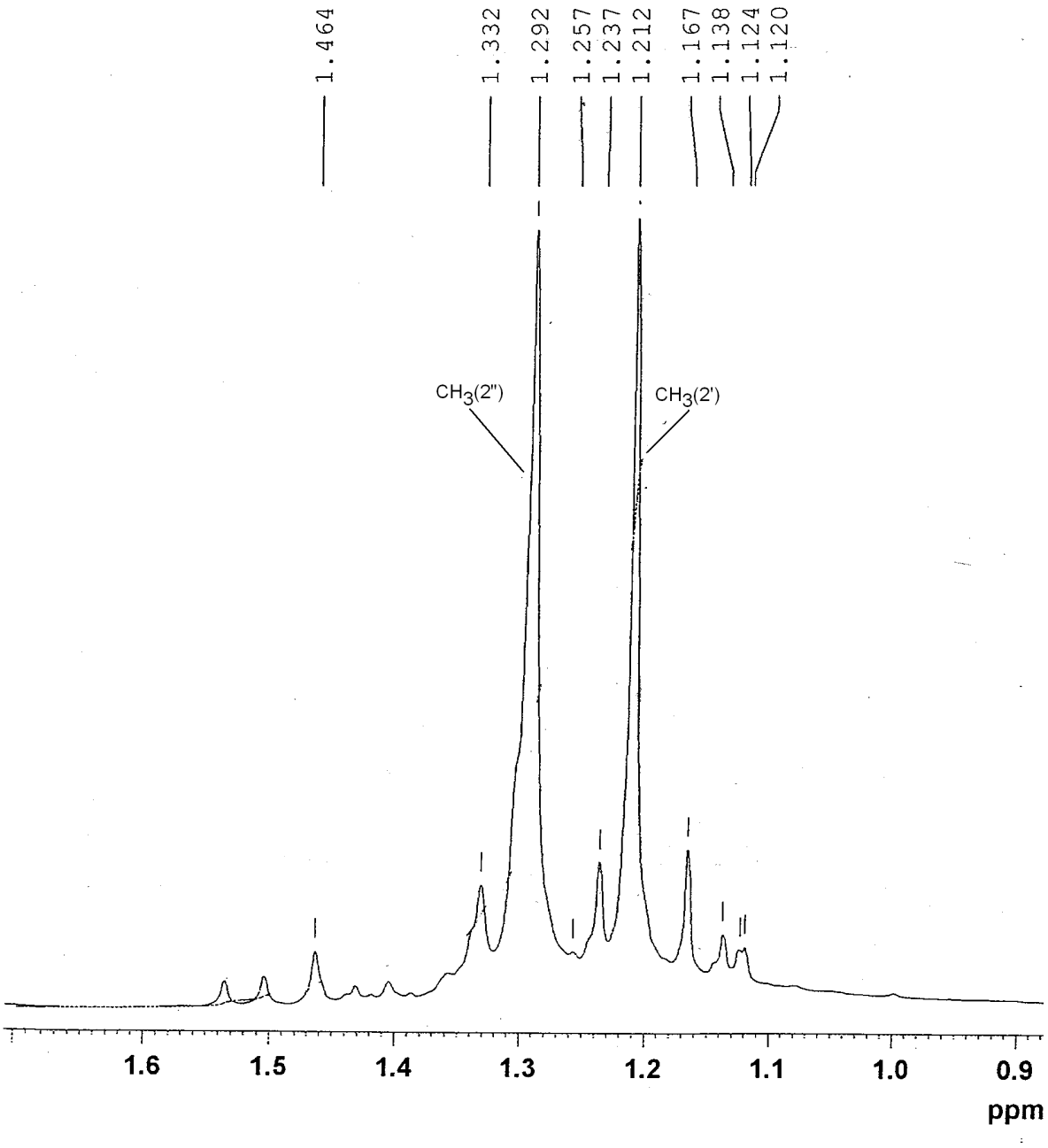

Fig. (III-35): ^{1}H NMR data of compound **(4)** in DMSO-d_6 over the region δ0.9-1.6(vide text for details).

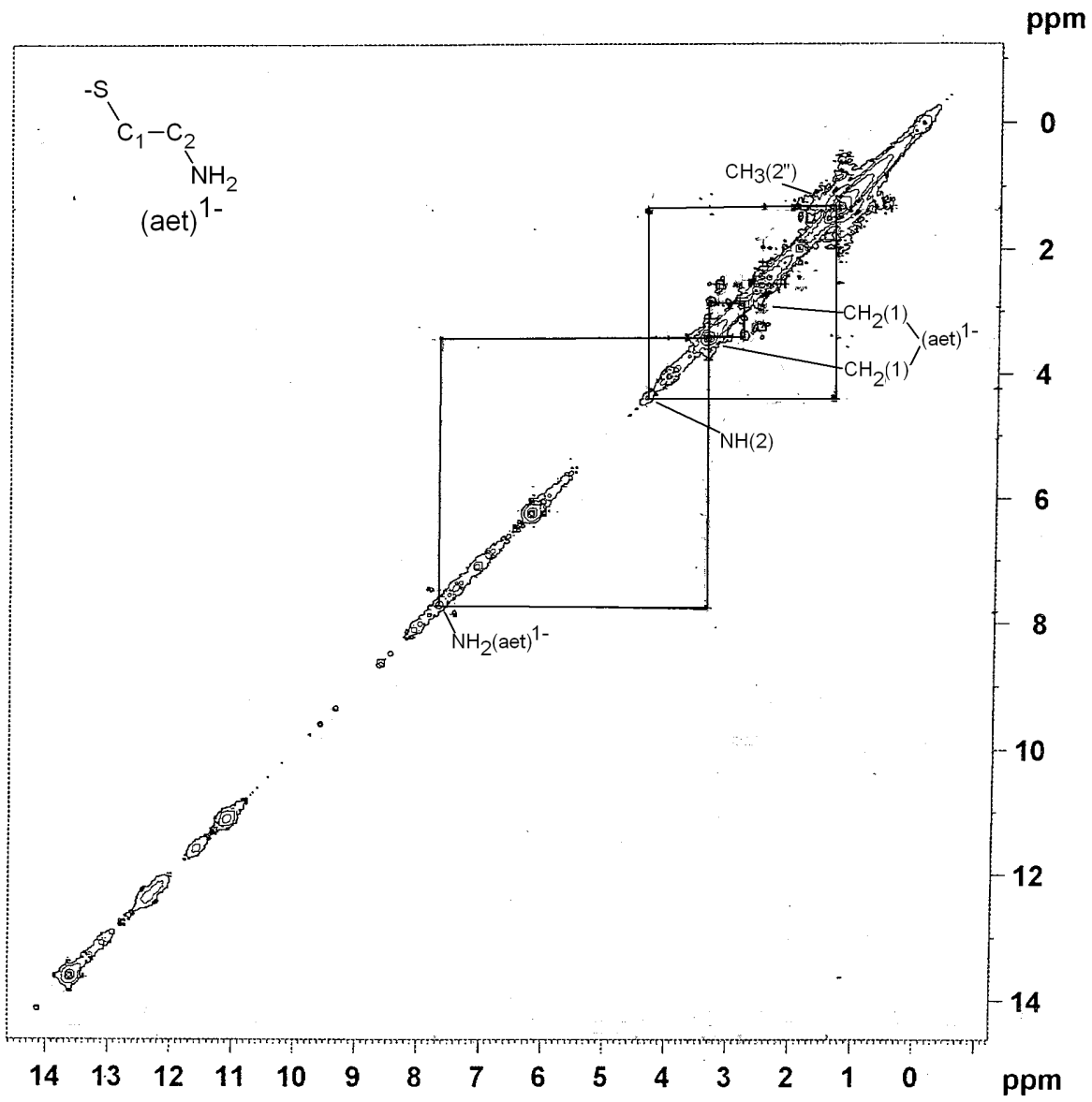

Fig. (III-36): ^{1}H-^{1}H COSY data (symmetrized) of compound **(4)** in DMSO-d_6 vs. TMS, over the region δ14.0-0.0(vide text for detail)

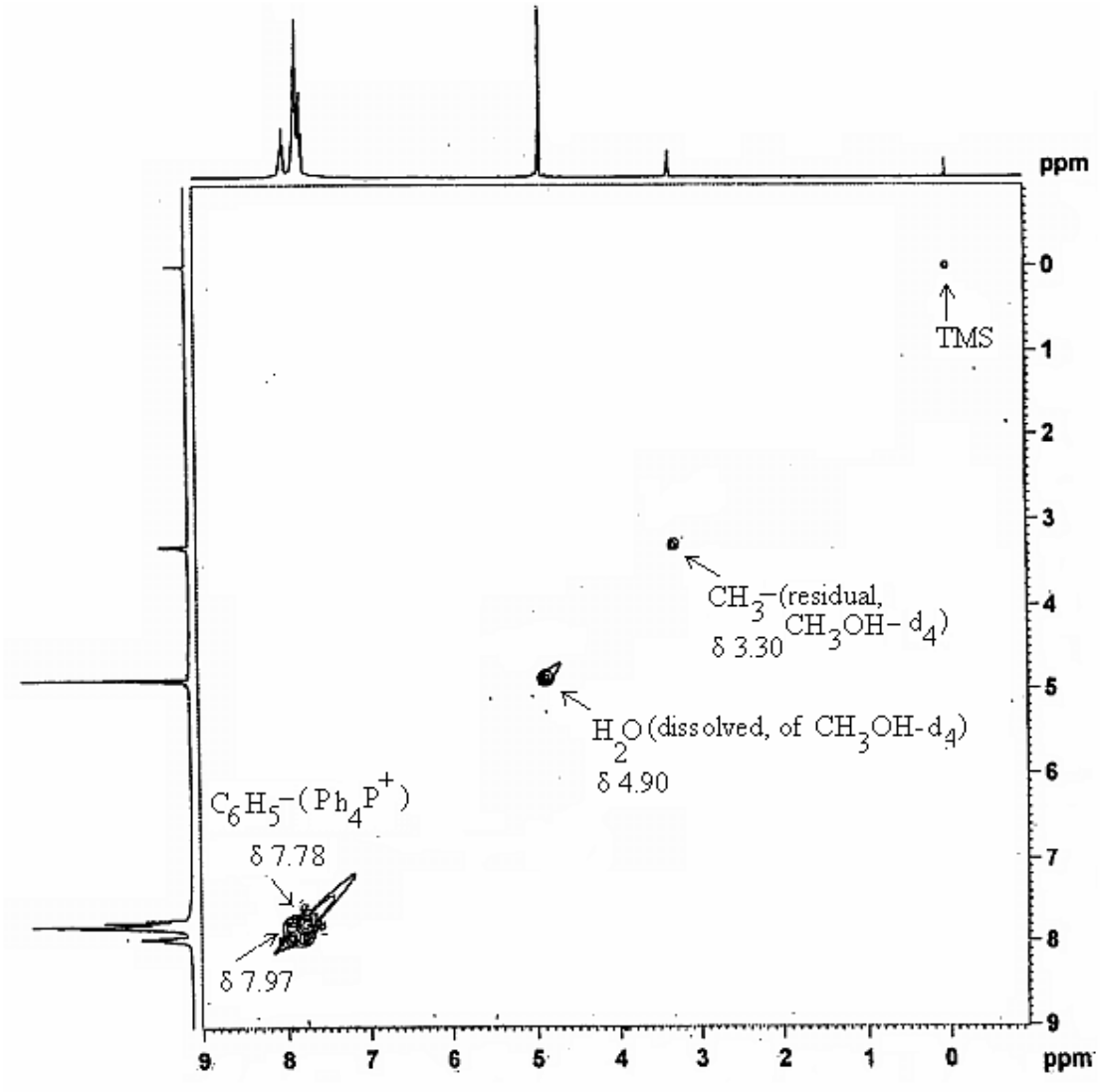

Fig. (III-37): ^{1}H-^{1}H COSY data of Ph_4PBr in CH_3OH-d_4, showing the assignments of the phenyl ring protons (2H, δ 7.97; 3H, δ 7.78; both multiplets)

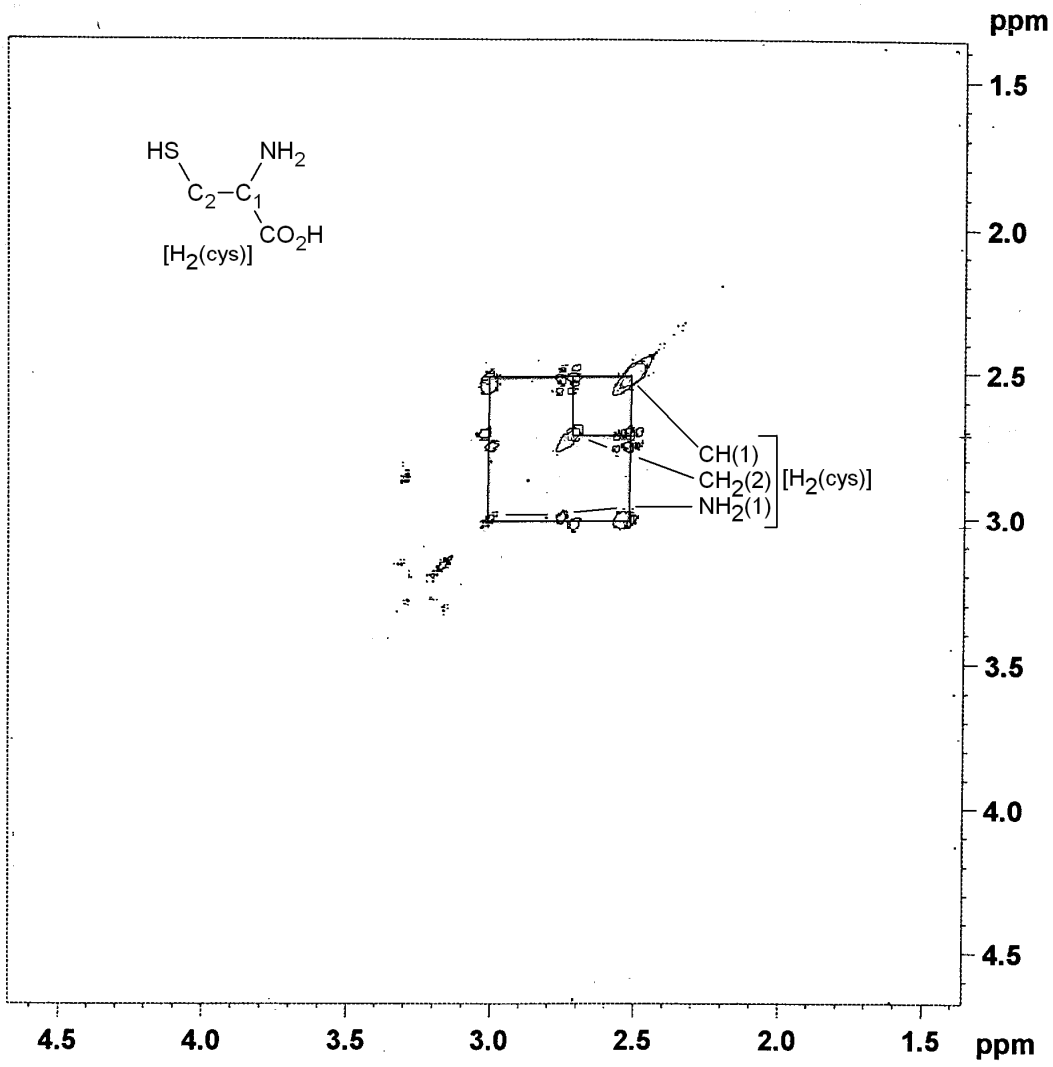

Fig. (III-38): ^{1}H-^{1}H COSY data (symmetrized) of H_2(cys) in DMSO-d_6 vs. TMS, over the region δ4.7-1.4.

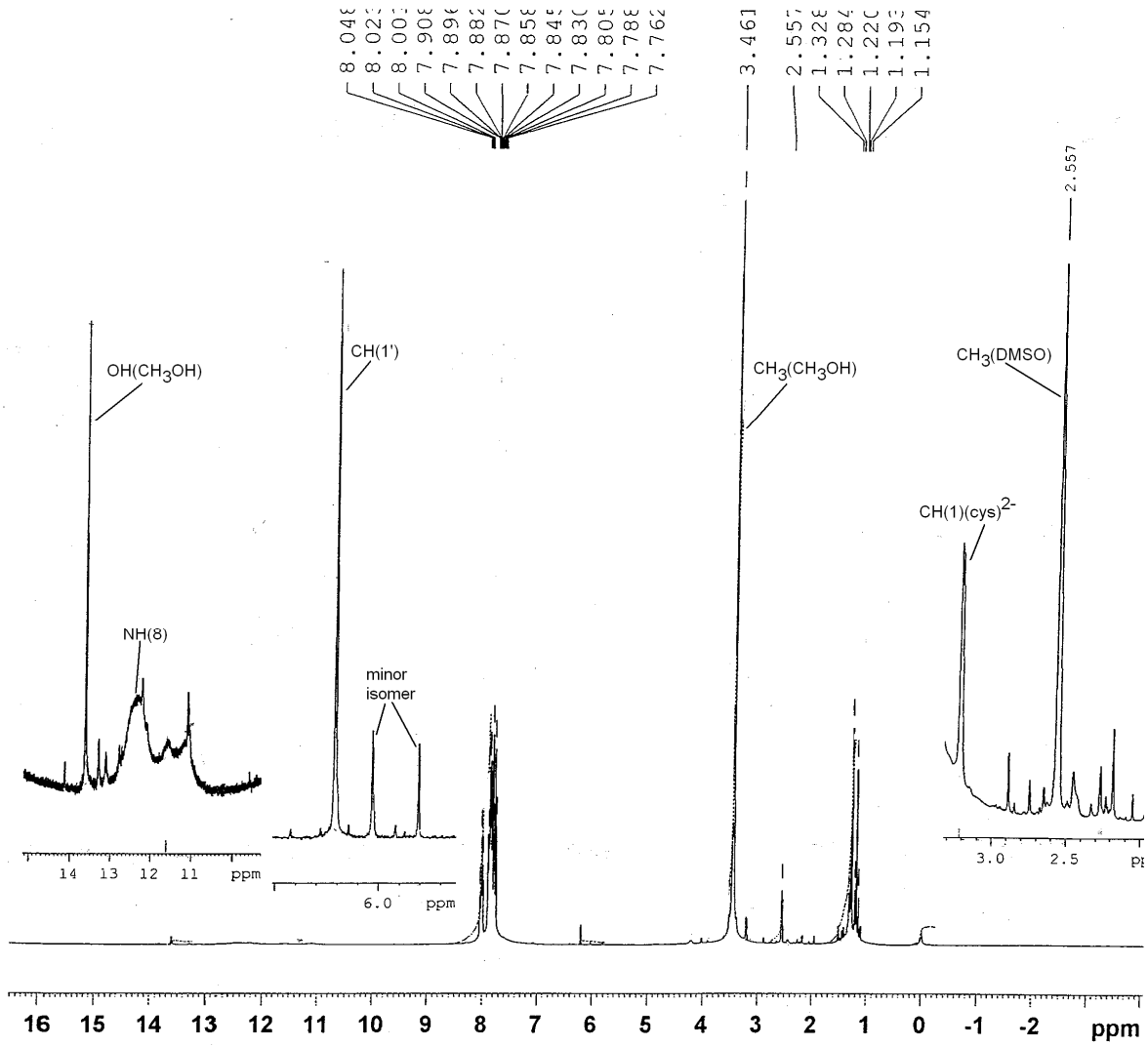

Fig. (III-39): ^{1}H NMR data of compound **(5)** in DMSO-d_6 over the region δ16.0-0.0(vide text for details).

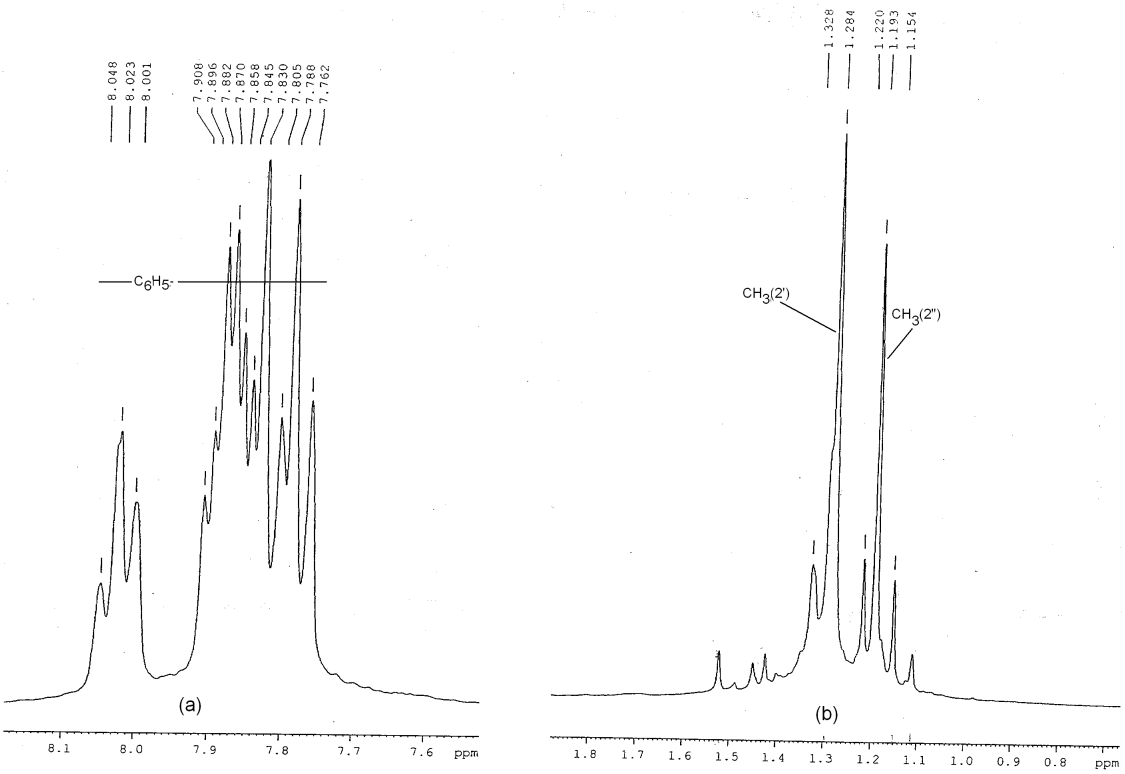

Fig. (III-40): (a) ^{1}H NMR data of compound **(5)** in DMSO-d_6 over the region δ8.1-7.6; **(b)** ^{1}H NMR data of compound **(5)** in DMSO-d_6 over the region δ1.8-08(vide text for details).

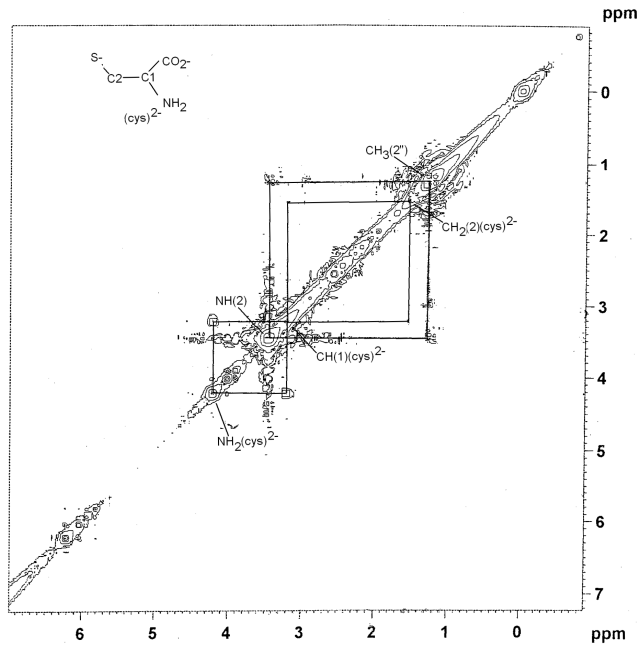

Fig. (III-41): ^{1}H-^{1}H COSY data (symmetrized) of compound **(5)** in DMSO-d_6 vs. TMS, over the region δ7.0-0.0(vide text for detail)

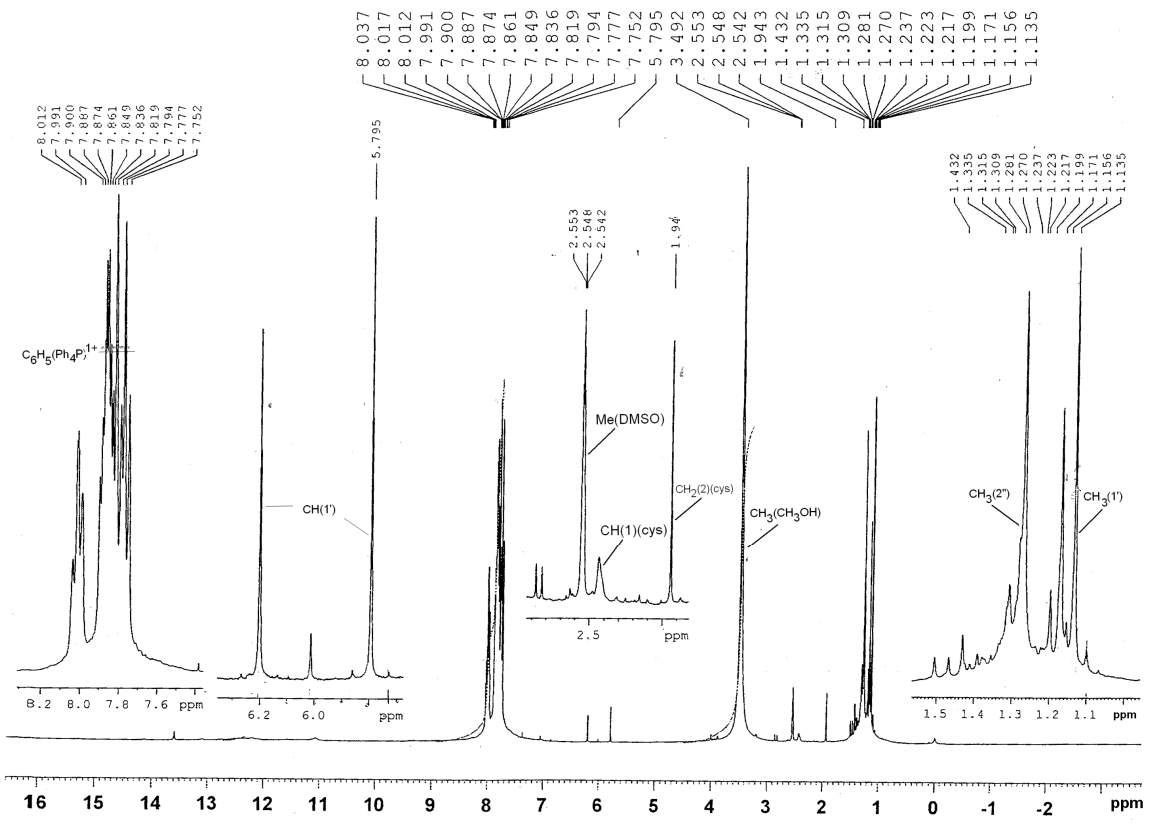

Fig. (III-42): ^{1}H NMR data of compound **(6)** in DMSO-d_6 over the region δ16.0-0.0(vide text for details).

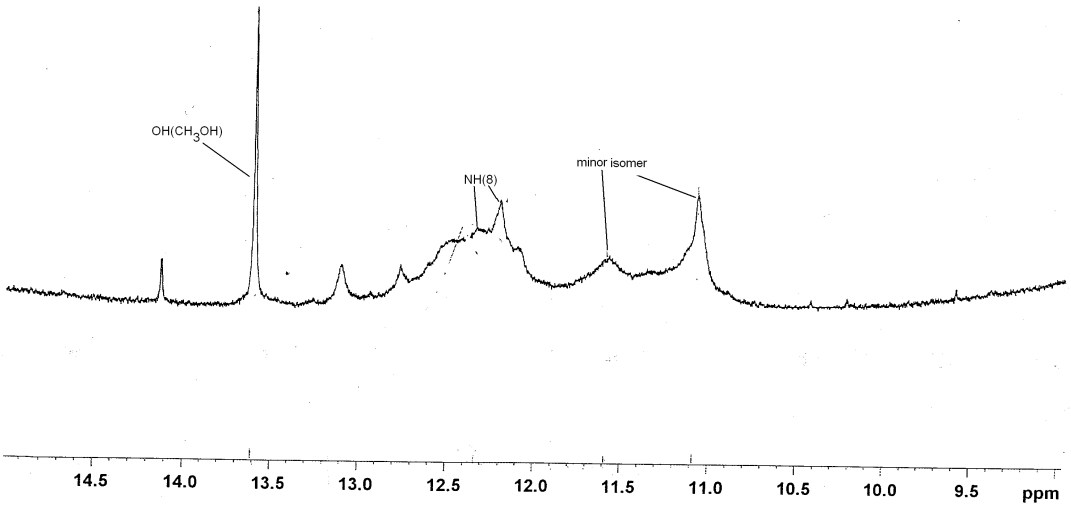

Fig. (III-43): ^{1}H NMR data of compound **(6)** in DMSO-d_6 over the region δ16.0-0.0(vide text for details).

Table (III-2): Relevant ^{1}H NMR signals in DMSO-d_6 (300 MHz, δ ppm, internal TMS) of the free ligand H_2L^2 and the corresponding complexes **(1)** – **(6)** and Δ ($=\delta_{complex} - \delta_{ligand}$) values ; vide Scheme (III-1) and (III-9).

Compound [a]	$CH_3(2')(\delta)$ Δ*	$CH(1')(\delta)$ Δ*	NH(8) (δ) Δ*	NH(2) (δ) Δ*
(H_2L^2)	1.097	6.15(ss)	10.90(wb)	4.30
(1) [b]	1.17 0.073	6.23(ss) 0.08	12.4(wb) 1.50	4.04 -0.26
(2) [b]	1.26 0.126	6.27(ss) 0.12	12.40(wb) 1.50	4.35 0.05
(3) [b,c]	1.31 0.213	6.25(ss) 0.01	12.30(wb) 1.40	3.45 -0.85
(4) [b]	1.21 0.113	6.25(ss) 0.1	12.40(wb) 1.50	4.45 0.15
(5) [b,c,d]	1.31 0.213	6.22(ss) 0.7	12.40(wb) 1.5	3.48 0.82
(6) [b,d]	1.35 0.253	6.22; 5.79(ss) 0.7;0.36	12.33; 12.20(wb) 1.43;1.3	4.18 -0.12

Abbreviations : ss = sharp singlet ; wb = weak broad

[a]vide Scheme (III-1) for the proton numbering system

[b]CH_3OH signals of these complexes appear at δ 13.60 – 13.65 (-OH) and δ 3.41 – 3.40 (CH_3-) respectively

[c]**the shielding of the NH(2) signal is associated with the electronic redistribution during complex formation process involving the redox non-innocent pterin ligand; concluding remarks of this thesis give a better picture**

[d]The phenyl ring proton signals of the Ph_4P^+ counter cation of **(5)**, appear at δ 8.02 (2 H, quartet) and δ 7.87 (3 H, complex multiplet); the corresponding signals of PPh_4Br appear at δ 7.97 and δ 7.78 respectively. In case of **(6)**, the corresponding phenyl ring proton signals appear at δ 7.99 (2H, quartet) and δ 7.87 (3H, complex multiplet). The 2D NMR data of PPh_4Br (in CH_3OH –d_4) is shown in Fig. (III-37).

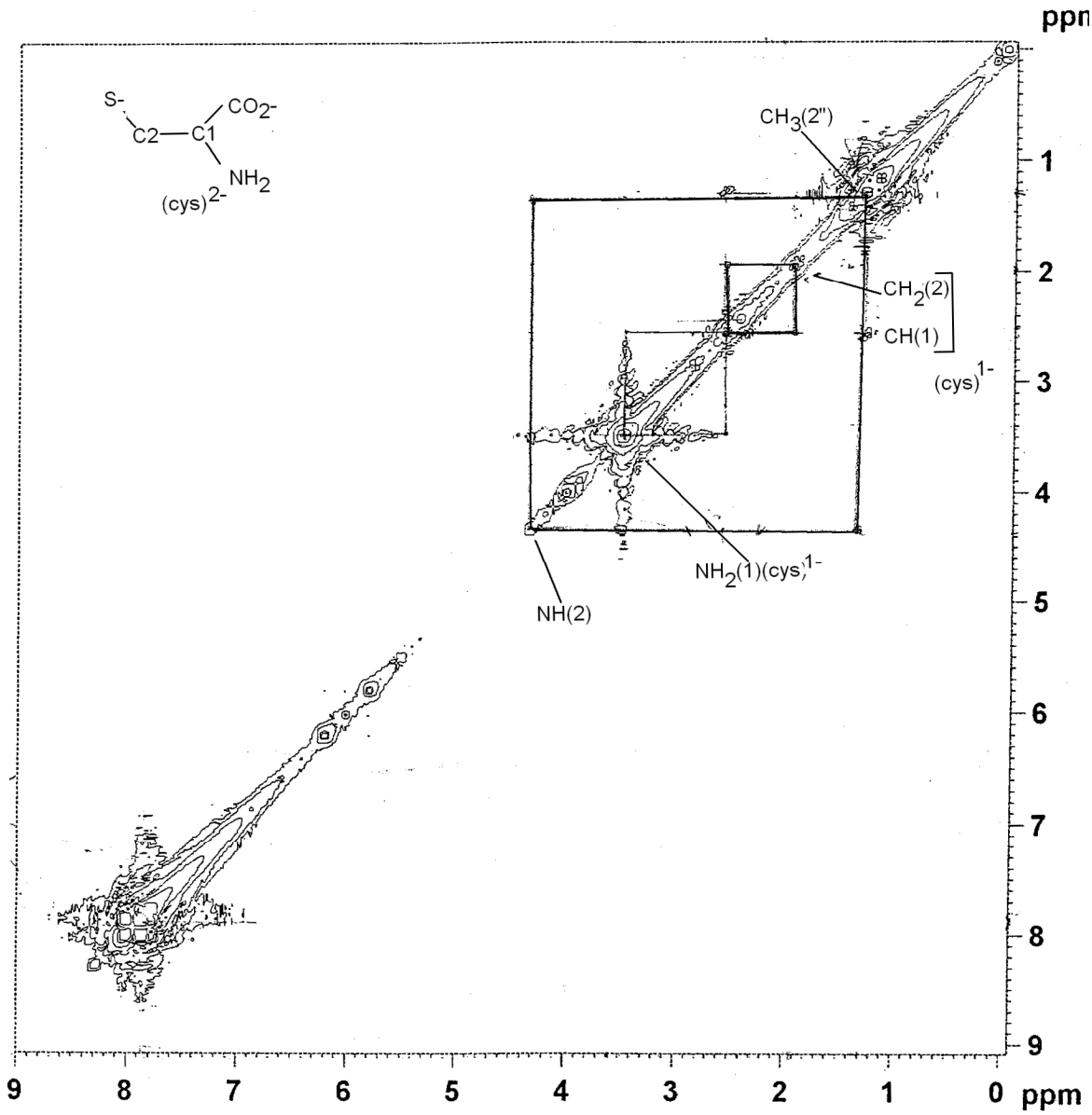

Fig. (III-44): ^{1}H-^{1}H COSY data (symmetrized) of compound **(6)** in DMSO-d_6 vs. TMS, over the region δ9.0-0.0(vide text for detail)

Fluorescence spectroscopy in CH_3OH

The aforesaid changes of ligand electronic structure during formation of these complexes can be inferred from their detected by the increase of fluorescence spectra [Fig. (III-45) to Fig. (III-50)], whereas the original ligand is non-fluorescent. This observation is due to the non-aromatic nature of the free pterin ligand (H_2L^2) (Scheme (III-1) [23]. But in the complex, the rigidity of the chelated ligand ring is sufficiently increased and dissipation

of excitation energy is not possible other than by fluorescence [23(a), (b)]. Thus the compound **(1)** shows the λ_{max} at 402 mm [Fig. (III-45)] in the fluorescence spectra. The moderate intensity of this fluorescence spectra, is possibly due to the non-aromatic nature of the 1, 4 diazine ring of $(L^2)^{2-}$ in the complex.

For the compound **(2)** the fluorescence spectrum is shown in Fig. (III-46). In this case also the increase in fluorescence intensity is observed on complex formation. This may be due to the achievement of aromaticity in the pyrimidine ring and also achieving the rigidity of the complex molecule, λ_{max} is observed at 410 nm.

Fig. (III-47) represents the fluorescence spectra (λ_{max} at 400.5 nm) of the compound **(3)**. It can be noted that the uncoordinated ligand (H_2L^2) is non-fluorescent and considerable increase in fluorescence occurs in this complex. This may be explained as pterin ligand gets rigidity by coordination with Mo atom as well as the presence of two thiox ligand coordinated to Mo atom. The electronic redistribution of the pterin ligand during the coordination with Mo atom can be proved by this spectrum.

The fluorescence spectrum of the compound **(4)** is presented in the Fig. (III-48), which shows the λ_{max} at 473 nm with moderate intensity. Its additional peaks over the region 350 – 400 nm may be ascribed to the ancillary ligand $(aet)^{1-}$ residue, with its aliphatic chain backbone [unlike the aromatic ones in compound **(1)** – **(3)**].

The fluorescence property [Fig. (III-49)] of compound **(5)** can also be correlated with a couple of factors, e.g., the aromatic nature of the pyrimidine ring [as par Scheme (III-9)] in the ligand residue,$(L^2)^{2-}$,as well as the overall rigidity of this complex molecule. The complex shows λ_{max} values at 368 nm and at 480 nm. The features at lower wavelengths can be ascribed to the aliphatic backbone of the ancillary ligand residue $(cys)^{2-}$.

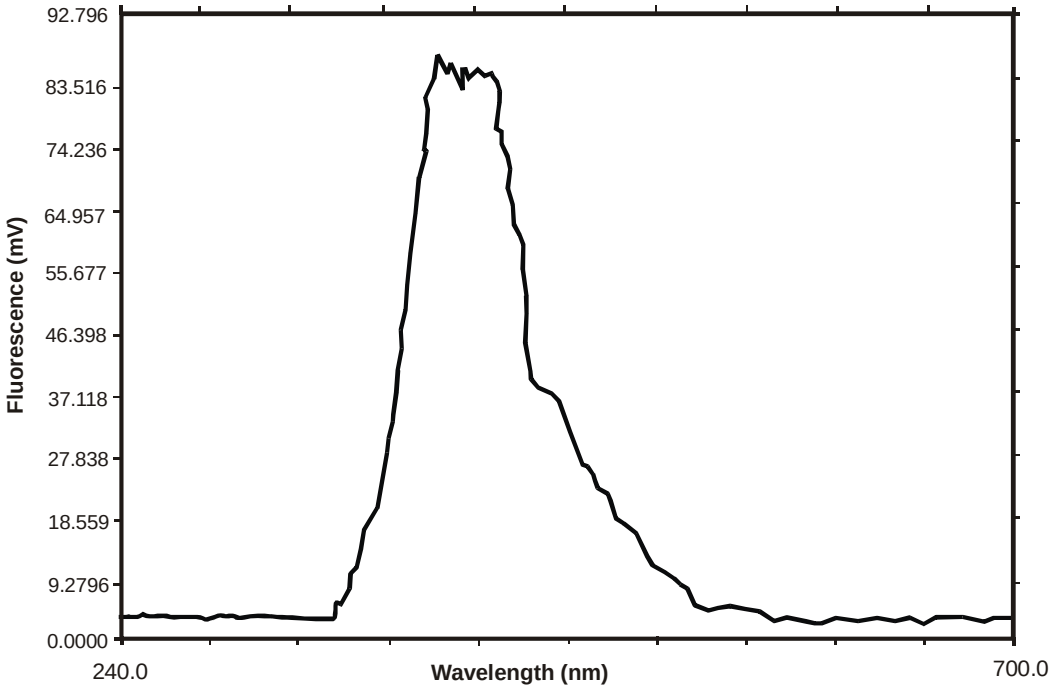

Fig. (III-45): Fluorescence spectra in methanol of compound **(1)** (1.42 x 10^{-6} mol dm^{-3})

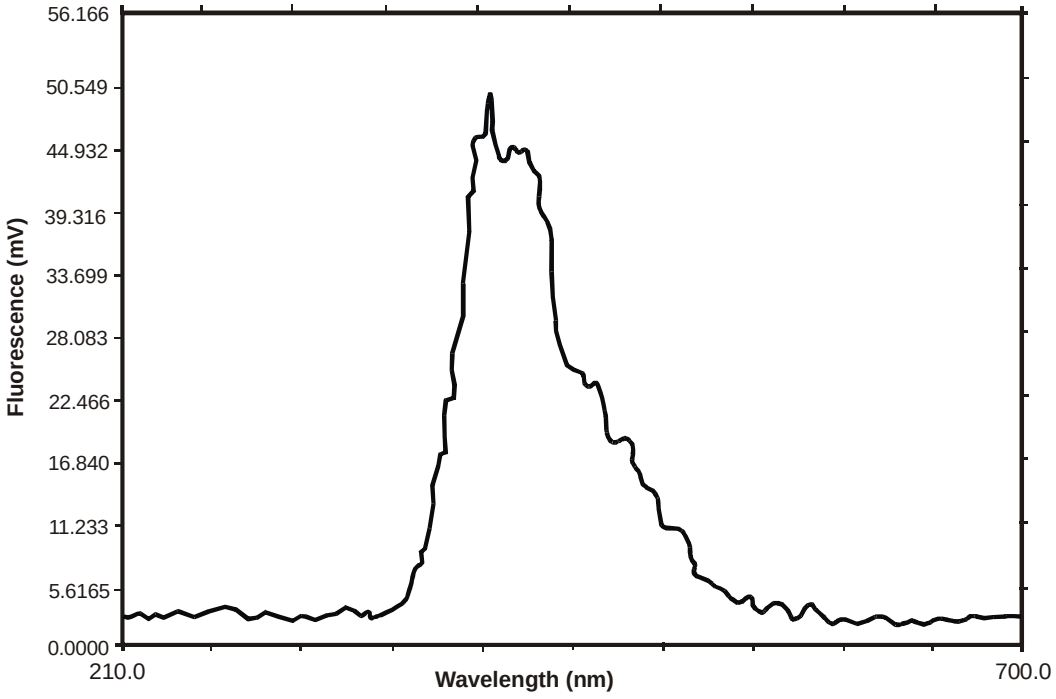

Fig. (III-46): Fluorescence spectra in methanol of compound **(2)** (1.05 x 10^{-6} mol dm^{-3}).

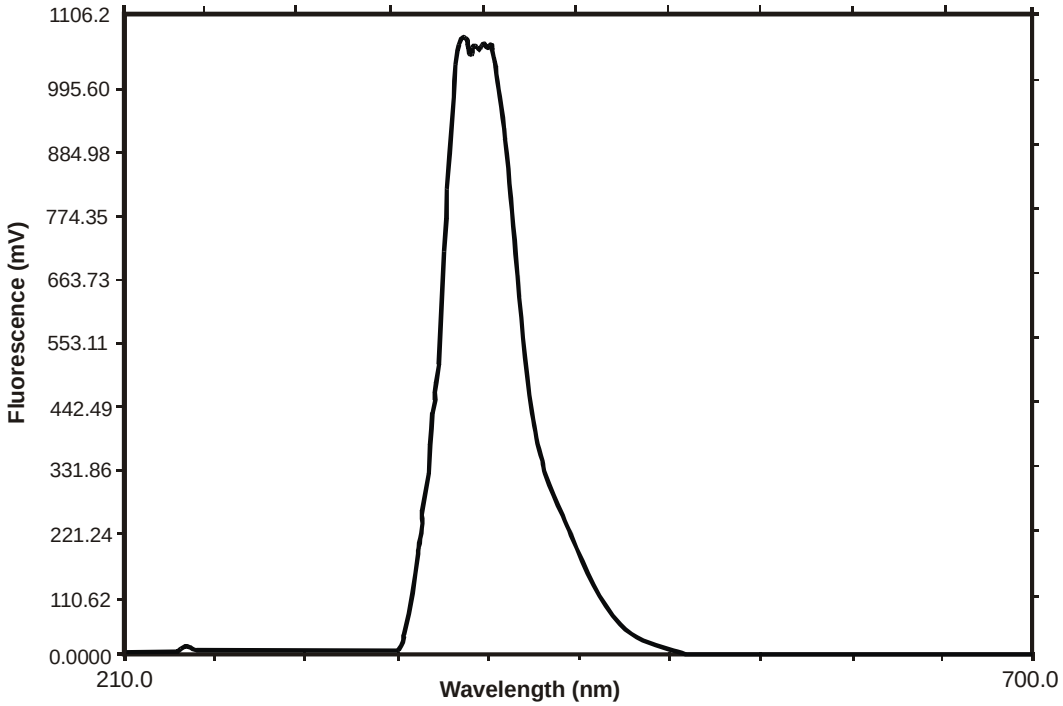

Fig. (III-47): Fluorescence spectra in methanol of compound **(3)** (1.36×10^{-6} mol dm^{-3}).

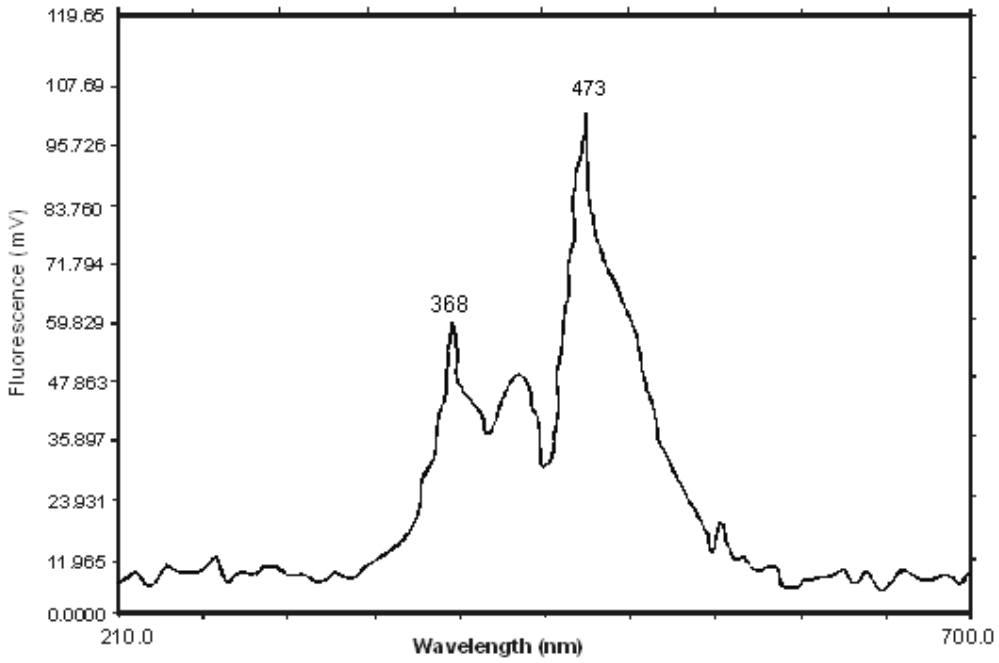

Fig. (III-48): Fluorescence spectra in methanol of compound **(4)** (2.12×10^{-6} mol dm^{-3}).

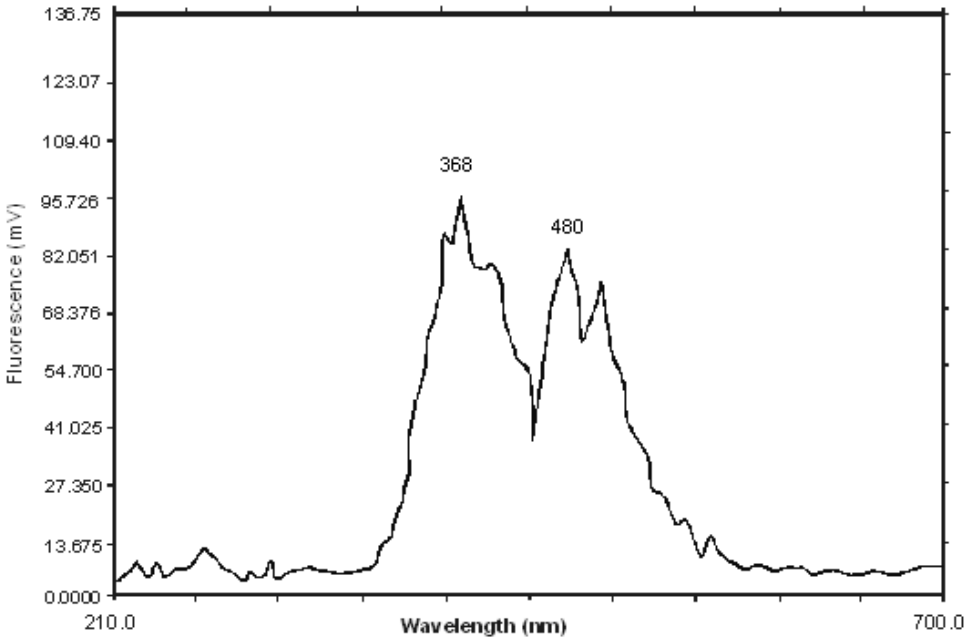

Fig. (III-49): Fluorescence spectra in methanol of compound **(5)** (1.01×10^{-6} mol dm^{-3}).

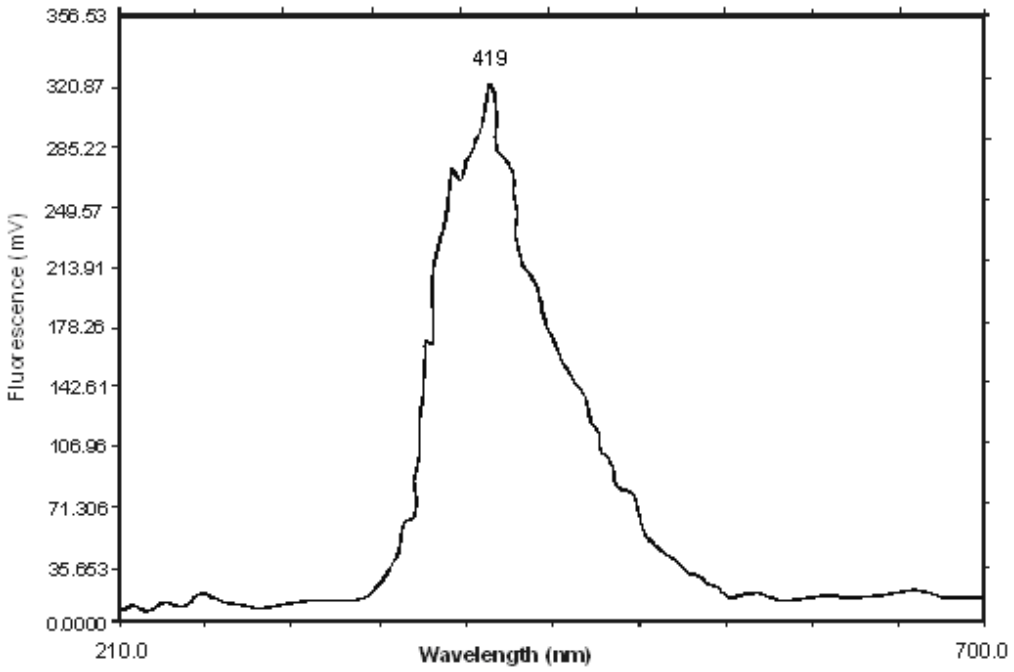

Fig. (III-50): Fluorescence spectra in methanol of compound **(6)** (1.77×10^{-6} mol dm^{-3})

CHEM3D models and frontier orbital energies

The schematic structure of the compound **(1)** was optimized by molecular mechanics calculation (MM2) [19(a)] giving the lowest steric energy (69.82 kcal/mol) CHEM3D model [Fig. (III-52)], whereas for the free ligand (H_2L^2) the steric energy is -0.051 kcal/mol [Fig. (III-51)] unveiling both its stability and geometry [19(b), (c)]. The four oxygen atoms [e.g., O(16), O(80), O(87) and O(90)] and the two nitrogen atoms [e.g., N(10) and N(50)] achieve a slightly distorted octahedral coordination geometry around the Mo(IV) atom in case of compound **(1)**, which is quite compact and stable, in conformity with its aforesaid ESIMS data [Fig. (III-7)]. The molecular modeling force field in use for molecular systems can be interpreted in terms of the four key contributions, e.g., bond stretching, angle bending, torsional terms and non-boding interactions [16a, 17b]. Apart from the CHEM3D model, the MM2 method provided with two basic parameters e.g., optimized bond lengths and angles, the most important of which are compared with the literature x-ray structural data of relevant molybdenum compounds in Table (III-3) [1]. It is evident that the optimized bond length data tally with the literature structural data especially well for the Mo-N(5) bonds, [Scheme (III-9) showing this atom numbering system, represents the dianion obtained through deprotonation of the ligand as par Scheme (III-1b)]; there is good agreement in most cases of optimized bond angles as well.

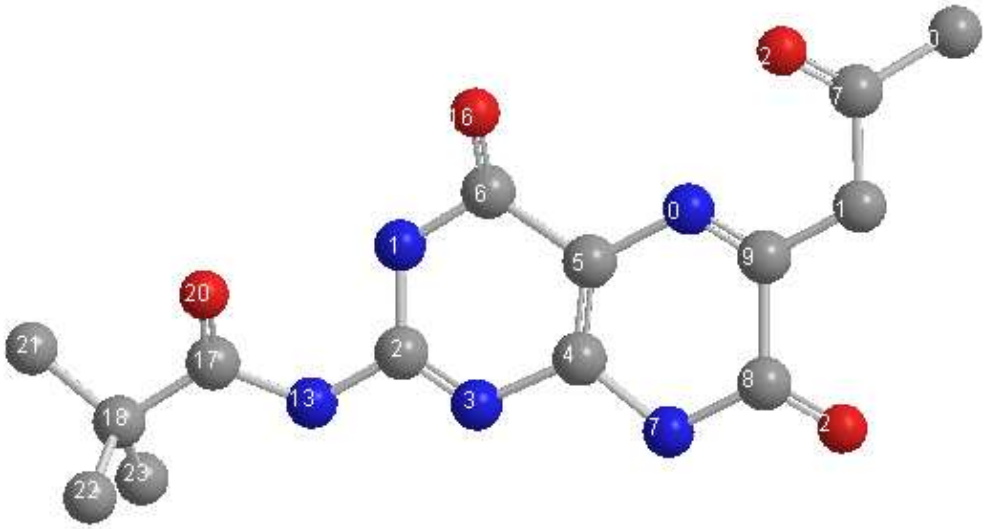

Fig.(III-51): The optimized geometry (CHEM3D model obtained through MM2 calculations) of (H_2L^2) with a steric energy of –0.05 Kcal /mol. Its numbering system is set by the software used [17, 19a] and is different from that in Scheme (III-1).

Table (III-4) compares the optimized bond lengths (CHEM3D model) of the free pterin ligand (H_2L^2) with the available x-ray structural data. Table (III-5) compares several optimized bond length data (Å) of the pterin ligand (H_2L^2) and compound **(1)**, some of which undergo change during the complex formation process; a perusal of these data supports the above inference regarding formation of the ligand dianion through tautomerism and deprotonation [Scheme (III-1(b) and Scheme (III-9)]. The changes in IR spectral data (mainly in the range 1650 – 1500 cm^{-1}) of the l igand (H_2L^2) during the complex formation process reflect the above changes in optimized bond length data associated with electronic redistribution.

Table (III-3). Comparison of selected computed (CHEM3D model) bond lengths (Å) and bond angles (deg) in compound **(1)** from the optimized geometry [Fig. (III-52), MM2 calculations] with the available literature data (in parentheses) from x-ray structural studies*.

Bond distances (Å) [+, †]	bond angles (deg) [+, ≠]
Mo(33)- O(16) 1.964	O(54) - Mo(33) - O(80)
Mo(33)- O(80) 1.969	96.52 (80.16 - 88.0)
(2.081-2.302)	
Mo(33)- N(10) 1.985	O(87) - Mo(33) - O(90)
Mo(33)- N(50) 1.984	167.06 (158.0 - 169.2)
(1.997-2.080)	
Mo(33)- O(87) 1.966	N(10) - Mo(33) - O(87)
Mo (33)- O(90) 1.965	89.24 (92.1 - 98.8)
(2.246-2.252)	
	N(10) - Mo(33) - O(16)
	85.279 (72 - 74)

*X-ray structural data have been collected from reference 1.

[+] Here O(16), O(80) and N(10), N(50) correspond to O(4) and N(5) donor atoms respectively, of the pterin ring as par Scheme (III-1), while O(87), O(90) correspond to CH_3OH substitutent.

[†] Bond length data for the two ligand residues in compound **(1)**.

[≠] One set of selected bond angle data involving Mo(33) is presented here.

Table (III-4). Comparison of selected computed bond length (Å) in (H_2L^2) from the optimized geometry (MM2 calculations) with the available x-ray structural data (in parentheses) from literature*, in the light of Scheme (III-1)

N(3)-C(4)		1.444	(1.390-1.400)
	C(4)-O(4)	1.212	(1.212-1.231)
	N(5)-C(6)	1.247	(1.359-1.468)
	C(7)-O(7)	1.213	(1.240)
C(7)-N(8)		1.551[+]	(1.303-1.443)
N(1)-C(2)		1.247	(1.306-1.334)
	C(2)-N(3)	1.452	(1.348-1.356)

*X-ray structural data have been collected from references 20.

[+]The only exception to a reasonable agreement between the computed bond length data (Å) and related x-ray data, in the C(7)-N(8) distance.

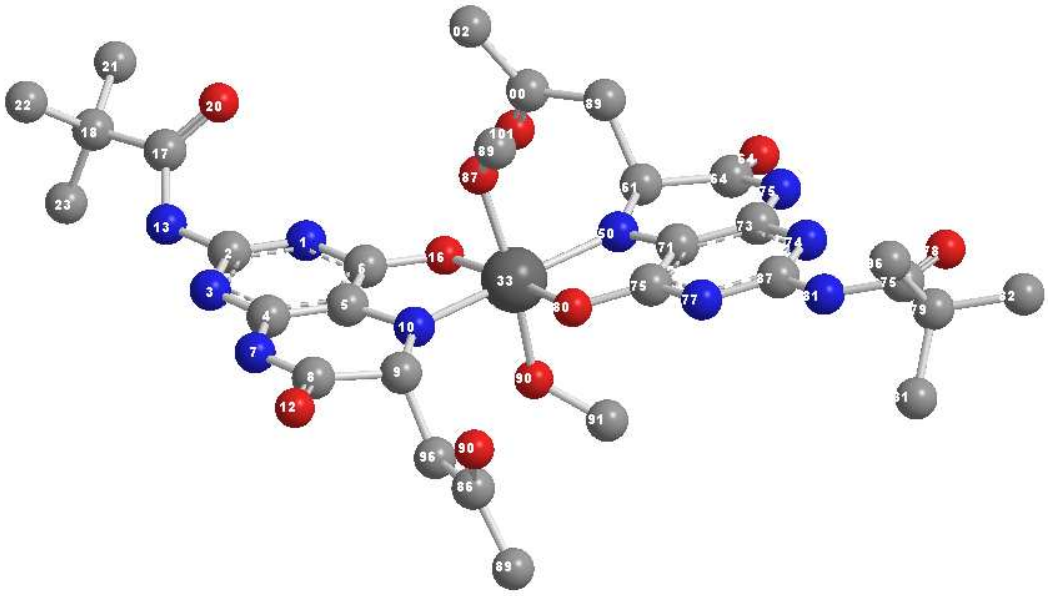

Fig. (III-52): The optimized geometry (CHEM3D model obtained through MM2 calculations) of compound **(1)** with a steric energy of 69.82 kcal/mol.

On the basis of the above discussions, a three dimensional model of the compound **(2)** [Fig. (III-53)] can be obtained by the (MM2) calculations by CHEM3D model software [19(a)] and calculating the lowest steric energy (15.35 kcal/mol). It also indicates both the geometry and stability of the complex. Its mass spectral data [appearance of the almost intact desolvated molecular ion peak in Fig. (III-8)] also

support its stability i.e., low steric energy value of its CHEM3D model. The bond lengths and bond angels of the compound are obtained from the calculation. Comparison of selected bond lengths and bond angels with the literature value are given in the Table (III-6). Concentrating on the bond length data (obtained from MM2 calculations [19(a)]) of free pterin ligand (H_2L^2) and that of this complex, the chelating nature of the ligand in this compound can also be understood. Table (III-7) contains some of the comparison of bond length data of both free ligand as well as those in complex.

Table (III-5) Comparison of selected optimized bond lengths (Å) of the pterin ligand (H_2L^2) and the compound **(1)** from the respective optimized geometries (MM2 calculations).

Bond[+]	**H_2L^2**	**compound (1)**[±]
N(3)-C(4)	1.379	1.336,1.335
C(4)-O(4)	1.234	1.565,1.562
N(5)-C(6)	1.282	1.580,1.584
C(6)-C(1′)	1.512	1.325,1.325
C(7)-O(7)	1.219	1.212,1.212
C(7)-N(8)	1.551	1.580,1.578

[+] Scheme (III-1) indicates the atom numbering system.

[±] Data for the two ligand residues in compound **(1)**.

The CHEM3D model of compound **(3)** was also obtained through MM2 calculation [19(a)] with a lowest steric energy 20.14 kcal/mol presented in Fig. (III-54). It indicates the stability of the coordination core. Some of the bond length and bond angle data is compared with standard literature data [1] and listed in the Table (III-8). Changes of bond length data of the free pterin ligand in this complex due to the coordination with Mo atom may be a valuable guide to interpret the coordination mode of the ligand, [$H_2L^2 \rightarrow (L^2)^{2-}$]; a few such bond length data are compared and listed in the Table (III-9).

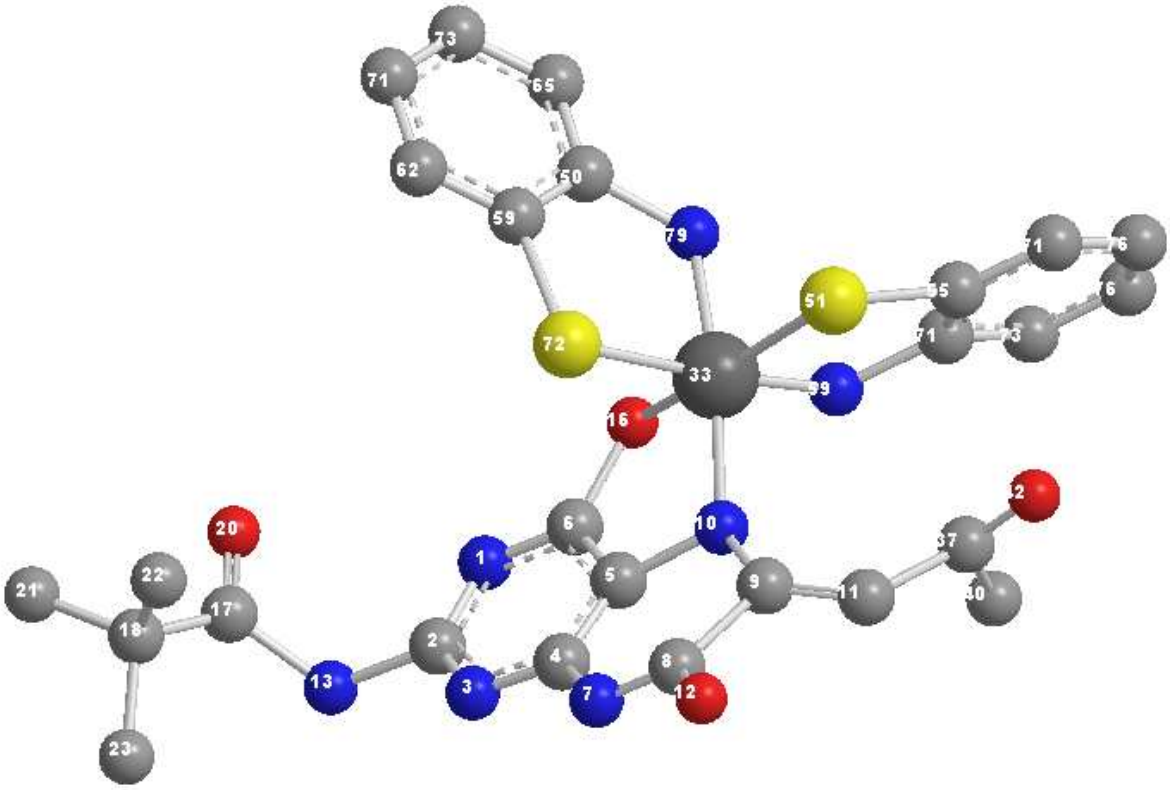

Fig. (III-53): The optimized geometry (CHEM3D model obtained through MM2 calculations) of compound **(2)** with a steric energy of 15.85 kcal/mol.

Table (III-6). Comparison of selected computed bond lengths (Å) and bond angles (deg) in compound **(2)** from the optimized geometry [Fig. (III-53), MM2 calculations] with the available literature data (in parentheses) from x-ray structural studies*.

Bond distances (Å) [+]	bond angles (deg) [+,#]
Mo(33) - N(10) 1.994 (1.997 - 2.080)	N(10) - Mo(33) - O(16) 85.05 (72 - 74)
Mo(33) - O(16) 1.972 (2.081 - 2.302)	
[±]Mo(33) - S(51) 2.341	N(10) - Mo(33) - N(59)
Mo (33) - S(72) 2.344 (2.393-2.460)	92.16 (92.1 – 98.8)
[±]Mo(33) - N(59) 1.993	N(10) – Mo(33) – N(79)

Mo (33) - N(79) 1.996 (1.997 - 2.080)		168.25 (158.0 - 169.2)
	S(51) – Mo(33) – S(72) 94.45 (83.69 - 96.6)	

*X-ray structural data have been collected from the reference 1.

[+] Here O(16) and N(10) correspond to O(4) and N(5) donor atoms respectively, of the pterin ring as par Scheme (III-1).

[±] Bond length data for the two $(atp)^{1-}$ ligand residues in compound **(2)**.

[#]One set of selected bond angle data involving Mo(33) for compound **(2)**, is presented here.

Table (III-7). Comparison of selected optimized bond lengths (Å) in the pterin ligand (H_2L^2) and the compound **(2)** from the respective optimized geometries (MM2 calculations).

Bond[+]	**H_2L^2**	**Compound (2)**
N(3)-C(4)	1.446	1.336
C(4)-O(4)	1.234	1.557
N(5)-C(6)	1.282	1.590
C(6)-C(1')	1.512	1.328
C(6)-C(7)	1.707	1.717
C(7)-O(7)	1.219	1.213
C(7)-N(8)	1.551	1.580
C(2')-O(2')	1.214	1.215

[+] Scheme (III-1) indicates the atom numbering system.

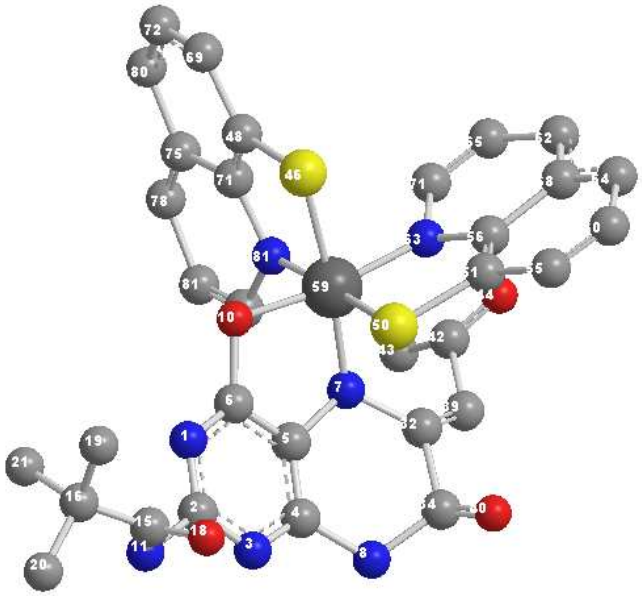

Fig. (III-54): The optimized geometry (CHEM3D model obtained through MM2 calculations) of compound **(3)** with a steric energy of 20.14 kcal/mol.

Table (III-8). Comparison of selected computed bond lengths (Å) and bond angles (deg) in compound **(3)** from the optimized geometry [Fig. (III-54), MM2 calculations] with the available literature data (in parentheses) from x-ray structural studies*.

Bond distances (Å) [+]	bond angles (deg) [+,#]
Mo(59) - N(7) 2.002 (1.997 - 2.080)	N(7) - Mo(59) - O(10) 87.34 (72 - 74)
Mo(59) - O(10) 1.964 (2.081 - 2.302)	
[±]Mo(59) - S(46) 2.350	N(7) - Mo(59) - N(81)
Mo (59) - S(50) 2.346 (2.393-2.460)	93.92 (92.1 – 98.8)
[±]Mo(59) - N(63) 2.002	O(10) – Mo(59) – S(50)
Mo (59) - N(81) 2.002 (1.997 - 2.080)	95.05 (92.2 – 94.8)
	S (46) - Mo(59) - S(50) 92.32 (83.69 - 96.6)

*X-ray structural data have been collected from the reference 1.

[+] Here O(10) and N(7) correspond to O(4) and N(5) donor atoms respectively, of the pterin ring as par Scheme (III-1).

[±] Bond length data for the two $(thioox)^{-1}$ ligand residues in compound **(3)**.

[#]One set of selected bond angle data involving Mo(59) for compound **(3)**, is presented here.

A CHEM3D model with low steric energy (17.17 kcal/mol) of the compound **(4)** was obtained through MM2 calculations [19(a)], is presented in the Fig. (III-55). The compactness of the compound can be reflected from the steric energy value. Appearance of the almost intact desolvated molecular ion peak in its mass spectra [Fig. (III-10)] corroborate this view. The comparison of some of the bond length and bond angle data (the available literature x-ray data) given in the Table (III-10). Some of the bond lengths of pterin ligand are compared with that in compound **(4)** as shown in Table (III-11).

Table (III-9). Comparison of selected optimized bond lengths (Å) in the pterin ligand (H_2L^2) and the compound **(3)** from the respective optimized geometries (MM2 calculations).

Bond[+]	**H_2L^2**	**Compound (3)**
N(3)-C(4)	1.446	1.336
C(4)-O(4)	1.234	1.557
N(5)-C(6)	1.282	1.590
C(6)-C(1')	1.512	1.328
C(6)-C(7)	1.707	1.717
C(7)-O(7)	1.219	1.213
C(7)-N(8)	1.551	1.580
C(2')-O(2')	1.214	1.215

[+] Scheme (III-1) indicates the atom numbering system.

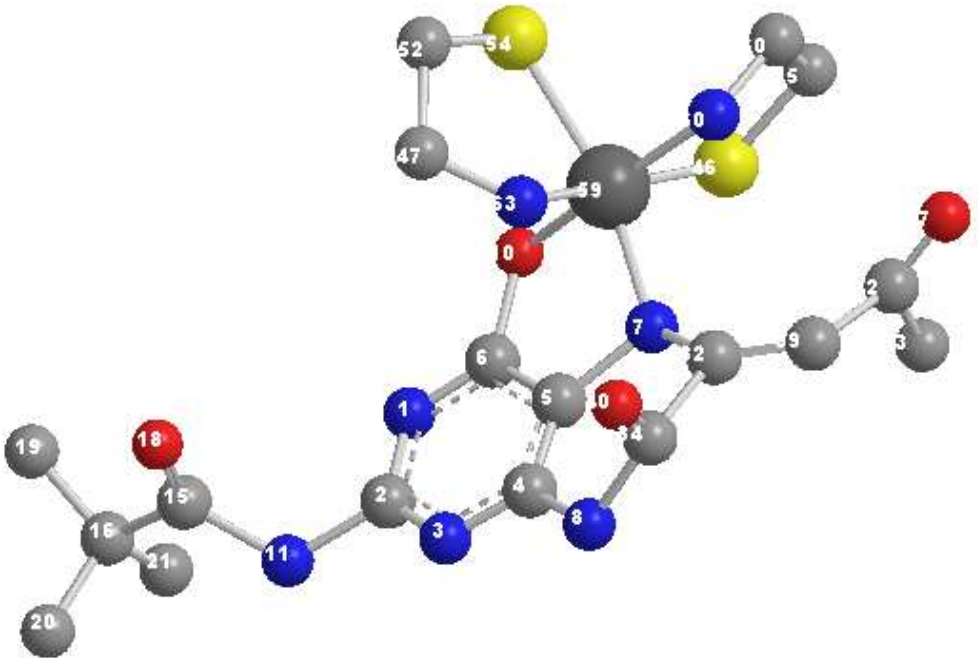

Fig. (III-55): The optimized geometry (CHEM3D model obtained through MM2 calculations) of compound **(4)** with a steric energy of 17.17 kcal/mol.

Table (III-10). Comparison of selected computed bond lengths (Å) and bond angles (deg) in compound **(4)** from the optimized geometry [Fig. (III-55), MM2 calculations] with the available literature data (in parentheses) from x-ray structural studies*.

Bond distances (Å) [+]	bond angles (deg) [+, #]
Mo(59) - N(7) 1.999	N(7) - Mo(59) - O(10)
(1.997 - 2.080)	86.26 (72 - 74)
Mo(59) - O(10) 1.964	
(2.081 - 2.302)	
[±] Mo(59) - S(46) 2.332	N(7) - Mo(59) - N(60)
Mo (59) - S(54) 2.338	95.96 (92.1 – 98.8)
(2.393-2.460)	
[±]Mo(59) - N(60) 1.996	O(10) – Mo(59) – S(46)
Mo (59) - N(63) 2.000	87.49 (92.2 – 94.8)
(1.997 - 2.080)	
	S (46) - Mo(59) - S(54)
	98.18 (83.69 - 96.6)

*X-ray structural data have been collected from the reference 1.

[+] Here O(10) and N(7) correspond to O(4) and N(5) donor atoms respectively, of the pterin ring as par Scheme (III-1).

[±] Bond length data for the two $(aet)^{1-}$ ligand residues in compound **(4)**.

[#]One set of selected bond angle data involving Mo(59) for compound **(4)**, is presented here.

Possible schematic structure of compound **(5)** was optimized by molecular mechanics calculations (MM2) [19(a)] giving the lowest steric-energy (16.28 kcal /mol) CHEM3D model [Fig. (III-56)], indicating both its stability and geometry. Some of the bond length and bond angle data are compared in Table (III-12). Comparison of bond length data of free pterin ligand (H_2L^2) and to that of in complex is listed in the Table (III-13).

Table (III-11). Comparison of selected optimized bond lengths (Å) in the pterin ligand (H_2L^2) and the compound **(4)** from the respective optimized geometries (MM2 calculations).

Bond[+]	**H_2L^2**	**Compound (4)**
N(3)-C(4)	1.446	1.336
C(4)-O(4)	1.234	1.551
N(5)-C(6)	1.282	1.601
C(6)-C(1')	1.512	1.327
C(6)-C(7)	1.707	1.726
C(7)-O(7)	1.219	1.213
C(7)-N(8)	1.551	1.584
C(2')-O(2')	1.214	1.214

[+] Scheme (III-1) indicates the atom numbering system.

Table (III-12). Comparison of selected computed bond lengths (Å) and bond angles (deg) in compound **(5)** from the optimized geometry [Fig. (III-56), MM2 calculations] with the available literature data (in parentheses) from X-ray structural studies*.

Bond distances (Å) [+]	bond angles (deg) [+, #]
Mo(59) - N(7) 2.001	N(7) - Mo(59) - O(10)

(1.997 - 2.080)	85.39 (72 - 74)
Mo(59) - O(10) 1.965	
(2.081 - 2.302)	
[±] Mo(59) - S(69) 2.337	O(10) – Mo(59) – S(69)
Mo (59) - S(98) 2.338	87.31 (92.2 – 94.8)
(2.393-2.460)	
[±]Mo(59) - O(57) 1.958	S (69) - Mo(59) - S(98)
Mo (59) - O(97) 1.958	92.87 (83.69 - 96.6)
(2.081 - 2.302)	

*X-ray structural data have been collected from the reference 1.

[+] Here O(10) and N(7) correspond to O(4) and N(5) donor atoms respectively, of the pterin ring as par Scheme (III-1).

[±] Bond length data for the two $(cys)^{2-}$ ligand residues in compound **(5)**.

[≠]One set of selected bond angle data involving Mo(59) for compound **(5)**, is presented here.

Table (III-13). Comparison of selected optimized bond lengths (Å) in the pterin ligand (H_2L^2) and the compound **(5)** from the respective optimized geometries (MM2 calculations).

Bond[+]	**H_2L^2**	**Compound (5)**
N(3)-C(4)	1.446	1.340
C(4)-O(4)	1.234	1.551
N(5)-C(6)	1.282	1.559
C(6)-C(1')	1.512	1.327
C(6)-C(7)	1.707	1.724
C(7)-O(7)	1.219	1.213
C(7)-N(8)	1.551	1.581
C(2')-O(2')	1.214	1.214

[+] Scheme (III-1) indicates the atom numbering system.

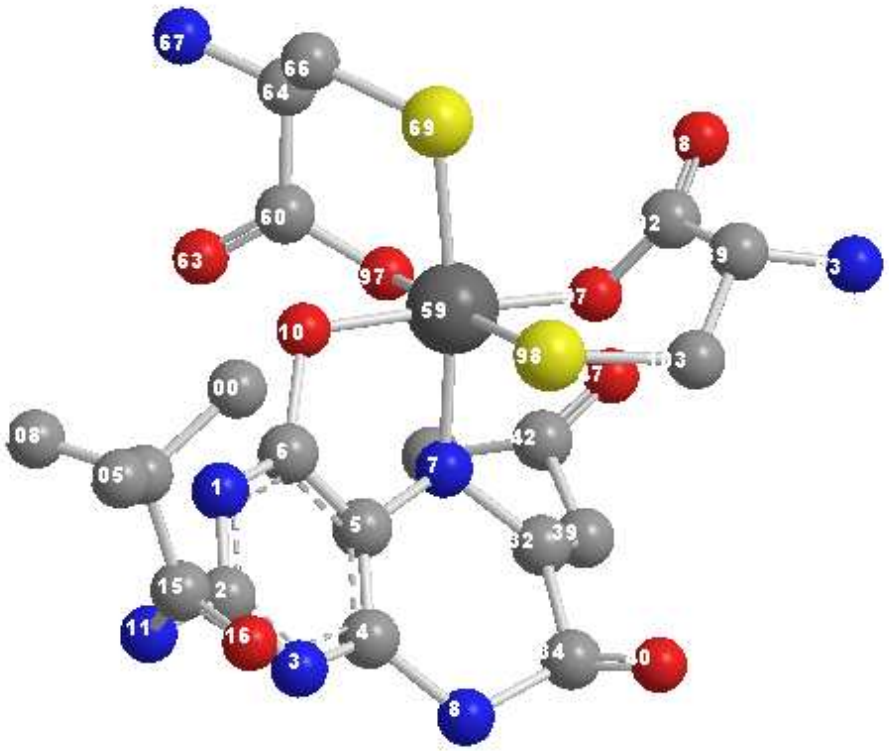

Fig. (III-56): The optimized geometry (CHEM3D model obtained through MM2 calculations) of compound **(5)** with a steric energy of 16.28 kcal/mol.

A 3D structure was constructed by MM2 calculations [19(a)] (CHEM3D model) giving the lowest steric energy (24.81 kcal/mol) for compound **(6)** and is presented in Fig. (III-57). From the Fig. (III-57) it may be noted that it is a binuclear di-μ-oxo complex. The comparison of some selected bond length and bond angle data with literature value is given in the Table (III-14). The bond length data of pterin ligand residue [$(L^2)^{2-}$] obtained from MM2 calculation compared with the free ligand (H_2L^2) value and listed in Table (III-15).

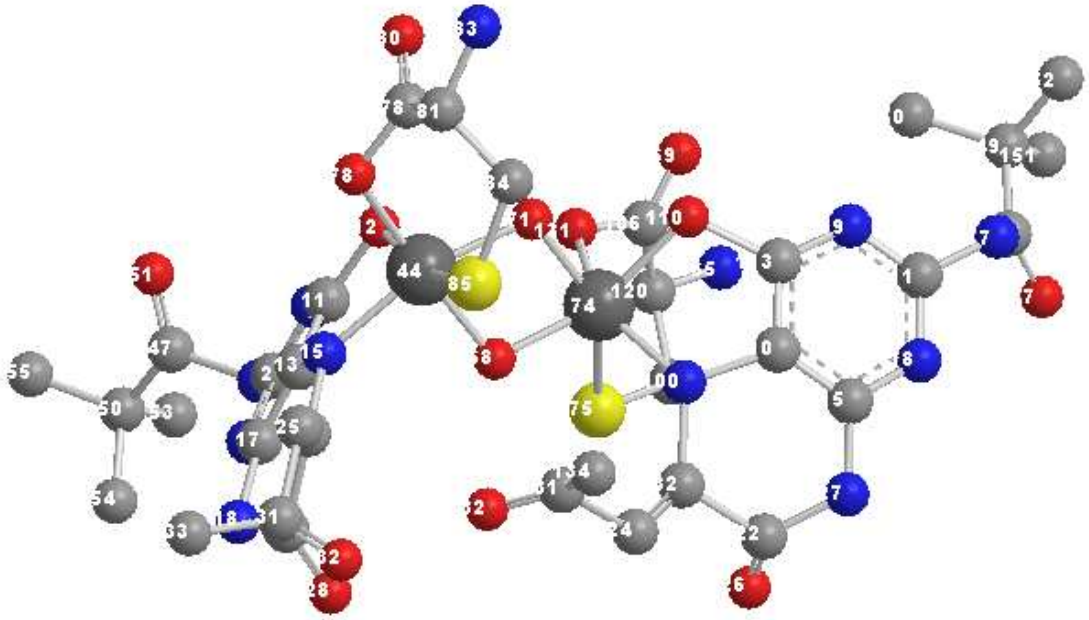

Fig. (III-57): The optimized geometry (CHEM3D model obtained through MM2 calculations) of compound **(6)** with a steric energy of 24.81 kcal/mol.

Concentrating on the chelating aspect the pterin ligand towards molybdenum, the Mo-N(5) bond plays a pivotal role here [Fig. (III-52) to Fig. (III-57) [1]; it has significant multiple bond character as verified through x-ray structural data [1]. Joule and coworkers concluded from both chemical and x-ray structural studies that sufficiently greater basicity/ nucleophilicity resides at N(5) than N(8), thereby supporting such coordination property [20]. The pterin ring is attached to the Mo(IV) atom in compound **1, 2, 3, 4, 5** and **6** through O(4) and N(5) atoms resulting from the dianion formation involving the amide function in position 3, 4 and the vinylogous amide in position 5 including the adjacent side chain [i.e., the proton from C(1') is located at N(5); Scheme (III-3) to (III-8)] [1]; the pterin ligand residue $(L^2)^{2-}$ acts as a binegative bidentate one here [Scheme (III-9)]. Tautomerism of the above type involving a heterocyclic nucleus and its side chain, is well characterized. ^{1}H NMR data supports the presence of the tautomer shown in the scheme (III-1b) and (III-9).

Table (III-14). Comparison of selected computed bond lengths (Å) and bond angles (deg) in compound **(6)** from the optimized geometry [Fig. (III-57)], MM2 calculations] with the available literature data (in parentheses) from x-ray structural studies*.

Bond distances (Å) [+]	bond angles (deg) [+,#]
Mo(44) - N(15) 1.997	N(15) - Mo(44) - O(12)
Mo(74) - N(100) 2.005	86.29 (72 - 74)
(1.997 - 2.080)	
Mo(44) - O(10) 1.966	
Mo(74) - O(110) 1.970	O(78) – Mo(44) – S(85)
[±]Mo(44) - O(78) 1.957	84.51 (92.2 – 94.8)
Mo(74) - O(131) 1.966	
(2.081 - 2.302)	
[±]Mo(44) - S(85) 2.337	O(68) – Mo(44) – O(71)
Mo (74) - S(54) 2.342	70.60 (93.2)
(2.393-2.460)	
Mo(44) - O(68) 1.954	O(71) - Mo(44) - O(78)
Mo (44) - O(71) 1.953	105.27 (107.6)
Mo (74) - O(68) 1.955	
Mo (74) - O(71) 1.960	
(1.91 – 1.95)	

*X-ray structural data have been collected from the reference 1.

[+] Here O(12) and O(110) correspond to O(4) and N(15) and N(100) correspond to N(5) donor atoms, of the pterin ring as par Scheme (III-1).

[±] Bond length data for the two $(cys)^{2-}$ ligand residues in compound **(6)**.

[#]One set of selected bond angle data involving Mo(44) for compound **(6)**, is presented here.

The visualized frontier orbitals with energies (eV) of the complexes

The visualized frontier orbitals with corresponding energies are presented in Fig. (III-58) and Fig. (III-59). They are calculated from the CHEM3D models as extended Huckel surfaces [17,19]. A closer look at this figures reveal that in case of compounds **2** – **5** , there is an increase in electron density on the Mo(IV) centers, as compared to that in compound **(1).**

This is due to the coordination of the Mo(IV) center with S-donor atoms of ancillary ligands along with the pterin ligand [H_2L^2] in complex **2** – **5**. This localized electron density facilitates the reactivity of these compounds with an enzyme substrate like $Me_3N{\rightarrow}O$, as described below. Again the relatively large energy gap between the HOMO and LUMO levels of these compounds [$\Delta(E_3 - E_2)$], indicates relatively lower tendency to react under control conditions. For example the freshly prepared compounds are susceptible to moisture under aerobic conditions, but once dried in vacuuo they are relatively stable for some time (absence of simultaneous attack by O_2 and H_2O). The small energy band gaps involving other frontier orbitals for these complexes predicts interesting reactivities, as described later.

Table (III-15). Comparison of selected optimized bond lengths (Å) in the pterin ligand (H_2L^2) and the molybdenum complex from the respective optimized geometries (MM2 calculations).

Bond[+]	**H_2L^2**	**Compound (6)**[±]
N(3)-C(4)	1.379	1.335,1.333
C(4)-O(4)	1.234	1.566,1.566
N(5)-C(6)	1.282	1.596,1.605
C(6)-C(1′)	1.512	1.328,1.327
C(6)-C(7)	1.707	1.719,1.721
C(7)-O(7)	1.219	1.213,1.211
C(7)-N(8)	1.551	1.577,1.448
C(2')-O(2')	1.214	1.214,1.214

[+] Scheme (III-1) indicates the atom numbering system.

[±] Data for the two pterin ligand [$(L^2)^{2-}$] residues in compound **(6)**.

Compound **(1)**	Compound **(2)**	Compound **(3)**
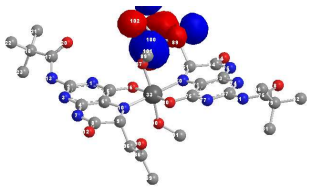	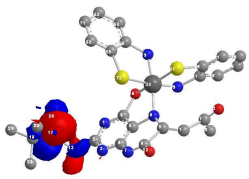	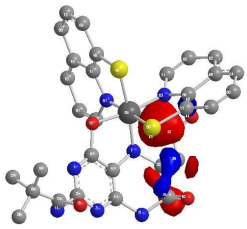
E_4(LUMO+1)= -1.544	E_4(LUMO+1)= -1.547	E_4(LUMO+1)= -3.081
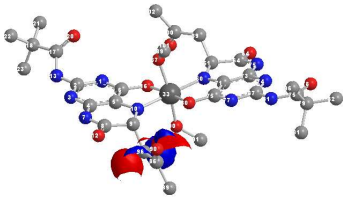	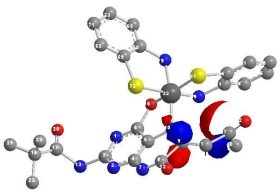	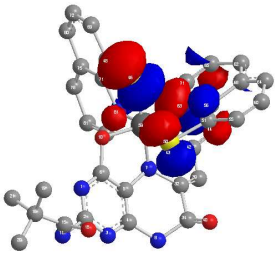
E_3(LUMO)= -1.671	E_3(LUMO)= -3.005	E_3(LUMO)= -6.603
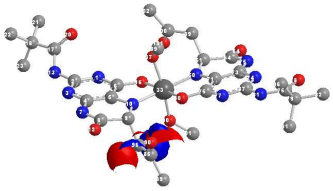	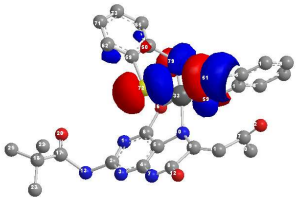	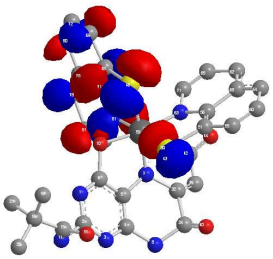
E_2(HOMO)= -7.340	E_2(HOMO)= -7.928	E_2(HOMO)= -7.587
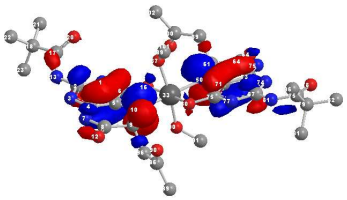	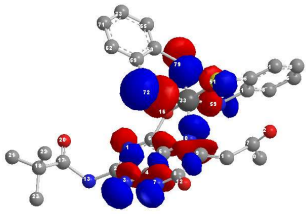	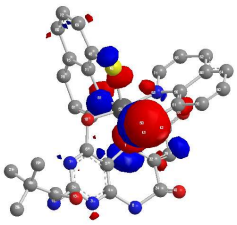
E_1(HOMO-1)= -7.365	E_1(HOMO-1)= -8.601	E_1(HOMO-1)= -7.964
$\Delta(E_2-E_1)$ = 0.025 eV	$\Delta(E_2-E_1)$ = 0.673eV	$\Delta(E_2-E_1)$ = 0.377eV
$\Delta(E_3-E_2)$ = 5.669 eV	$\Delta(E_3-E_2)$ = 4.923 eV	$\Delta(E_3-E_2)$ = 0.984 eV
$\Delta(E_4-E_3)$ = 0.127 eV	$\Delta(E_4-E_3)$ = 1.458 eV	$\Delta(E_4-E_3)$ = 3.522 eV

Fig.(III-58): The visualized frontier orbitals with energies (E, eV) of **(1)**, **(2)** and **(3)** (using Chem Office 2004, version 8.0).

Compound **(4)**	Compound **(5)**	Compound **(6)**
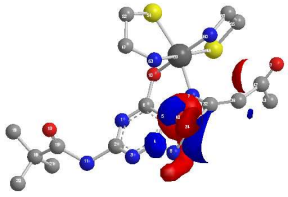	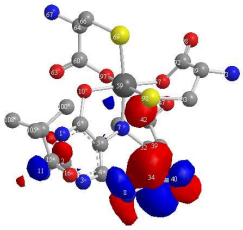	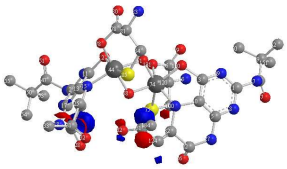
E_4(LUMO+1)= -2.292	E_4(LUMO+1)= -2.225	E_4(LUMO+1)= -2.683
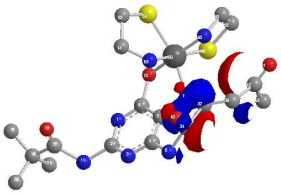	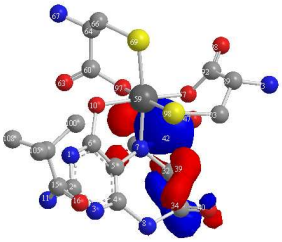	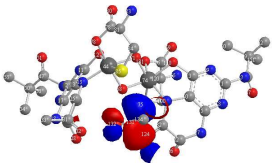
E_3(LUMO)= -2.945	E_3(LUMO)= -2.853	E_3(LUMO)= -2.782
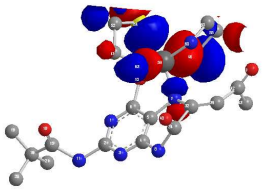	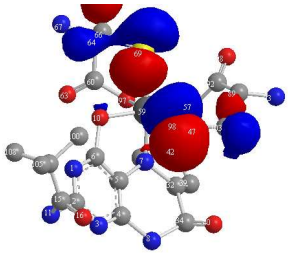	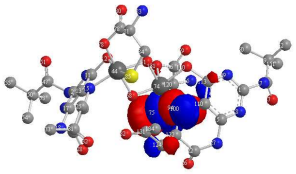
E_2(HOMO)= -7.574	E_2(HOMO)= -7.517	E_2(HOMO)= -7.646
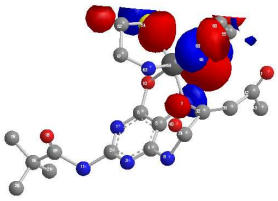	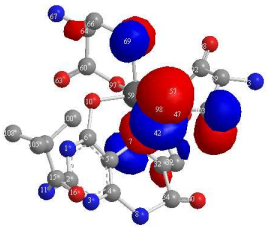	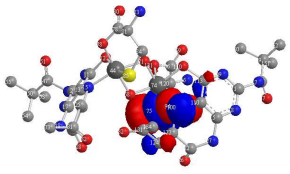
E_1(HOMO-1)= -8.302	E_1(HOMO-1)= -8.251	E_1(HOMO-1)= -8.667
$\Delta(E_2-E_1)$ = 0.728 eV	$\Delta(E_2-E_1)$ = 0.734eV	$\Delta(E_2-E_1)$ = 1.021eV
$\Delta(E_3-E_2)$ = 4.629 eV	$\Delta(E_3-E_2)$ = 4.664 eV	$\Delta(E_3-E_2)$ = 4.864 eV
$\Delta(E_4-E_3)$ = 0.653 eV	$\Delta(E_4-E_3)$ = 0.628 eV	$\Delta(E_4-E_3)$ = 0.099 eV

Fig.(III-59): The visualized frontier orbitals with energies (E, eV) of **(4)**, **(5)** and **(6)** (using Chem Office 2004, version 8.0).

UV – VIS spectroscopy and reactivity study (in CH_3OH)

The UV-VIS spectra of pterins depend on the oxidation state of the constituent pyrimidine and 1,4-diazine rings. The free ligand (H_2L^2) absorbs at 294 nm due to intraligand ($\pi\rightarrow\pi^*$) transition. For compound **(1)** the 280 nm band is due to an intraligand ($\pi\rightarrow\pi^*$) transition, the bands at 376 nm and 415 nm (broad shoulder) with large molar extinction coefficient values are assigned to charge transfer [L→Mo(IV)] transitions and intensity stealing respectively. The last two types of bands are responsible for deep brown colour of this compound. The Mo(IV) center is a spin paired d^2 system and the 'd – d' transitions are occluded by the aforesaid CT transitions.

In UV-VIS spectra of the compound **(2)** the bands at 373.5 nm and 414.5 nm (broad shoulder) with large molar extinction coefficient values are assigned to charge transfer [L→Mo(IV)] transitions. The last band account for the snuff red colour of this complex.

For the compound **(3)** the 239 nm band is due to an intraligand ($\pi\rightarrow\pi^*$) transition and the bands at 348 nm and 410 nm with large molar extinction coefficient values are assigned to charge transfer [L→Mo(IV)] transition. The last two bands account for the yellow-brown colour of this complex.

The bands at 377 nm and 414 nm (broad shoulder) in UV-VIS spectra of compound **(4)** with moderate molar extinction coefficient values are assigned to charge transfer [L→Mo(IV)] transition causes the dark brown colour of this compound, whereas the intraligand ($\pi\rightarrow\pi^*$) transition occurs at 218 nm.

In UV-VIS spectrum of compound **(5)** the bands at 347 nm and 416 nm with moderately large molar extinction coefficient values are assigned to charge transfer [L→Mo(IV)] transition in complex and the intraligand charge transfer ($\pi\rightarrow\pi^*$) occurs at 268 nm. The former bands are responsible for the reddish brown colour of the compound. In case of compound **(6)** the intraligand ($\pi\rightarrow\pi^*$) transition occurs at 270 nm with slight red shift occurred compared to compound **(5)**. The 350 and 410 nm bands in this complex are responsible for charge transfer [L→Mo(V)] band causes dark brown colour of this complex.

Reactivity

The oxomolybdoenzymes like dimethylsulfoxide reductase (DMSOR), trimethyl N-oxide reductase (TMAOR), sulphite oxidase, etc., undergo reactions with suitable substrates; PPh_3 is a standard substrate for oxomolybdenum compounds in the higher oxidation states, especially with dioxo Mo(VI) core [6]. Here the spectrophotometric monitoring of the reaction of compound **(1)** with $Me_3N{\rightarrow}O$ (that is, oxidation of the Mo centre) at 318K in CH_3OH is represented in Fig. (III-60). A continuous increase in optical density at 341 nm and 414 nm is observed. The lack of tight isosbestic points here indicates the presence of appreciable amounts of reaction intermediates [7]; as delineated here, an associated type intermediate is formed which is ultimately converted to di-μ-oxo binuclear Mo(V) complex through a couple of steps. A blank experiment using the free pterin ligand (H_2L^2) and $Me_3N{\rightarrow}O$ shows no such spectral change [Fig. (III-61)]. Again when the complex was treated with PPh_3 under the same condition as above, no spectral change is observed as in Fig. (III-62). The growth kinetics for the reaction of the compound **(1)** with $Me_3N{\rightarrow}O$ was followed at 342 nm under pseudo first order conditions (maintaining ca. 8-61 times excess of $Me_3N{\rightarrow}O$ in CH_3OH). Observed rate constants are determined by least square method from the plots of log $(A_\infty - A_t)$ versus time. Pseudo-first order rate constants (K_{obs}, s^{-1}) are determined at four different temperatures (313-328K) for determining the activation parameter ($\Delta S^{\neq}$ = - 197.52 J K^{-1} mol^{-1}). The negative $\Delta S^{\neq}$ value supports the associative nature of the reaction. From the above observation it can be inferred that oxidation state of the molybdenum atom is the (IV) in compound **(1)**. The same is true for compounds **(2) – (5)** of this series.

Now a closer look may be taken at the above reativities in terms of the frontier orbital energies of the compound **(1)** [Fig. (III-58)]. Here both $\Delta(E_4 - E_3)$ and $\Delta(E_2 - E_1)$ energy gaps have low values, with the later one being significantly low. This helps oxygen atom addition to the Mo(IV) center [Mo(IV) → Mo(VI) oxidation], mimicking the functional behaviour of trimethyl N-oxide reductase (TMAOR). As it reacts terminal oxo group attached to the Mo(IV) center, no reactivity towards PPh_3 is exhibited. Even the traces of moisture/O_2 present in the solvent fail to react with compound **(1)** [Fig. (III-62)], due to large HOMO – LUMO band gap (4.629 eV)

As far as reaction stoichiometry is concerned, this has been established for another compound **(5)** of this series, where a di-μ-oxomolybdenum(V) complex is isolated and

characterized as the end product of the reaction that is compound **(6)**. Initially the following reaction (equation (III-1) takes place, leading to a μ-oxo Mo(V) compound, as par the amount of Me_3N recovered from the reaction medium:

2 compound **(5)** + $Me_3N{\rightarrow}O$ $\rightleftharpoons$ [2 compound **(5)**.$Me_3N{\rightarrow}O$]

↓

μ-oxo Mo(V) compound + Me_3N …..Equation (III-1)

Traces of moisture present in the solvent (CH_3OH) ultimately leads to the formation [Equation (III-2)] of the di-μ-oxo Mo(V) compound [compound **(6)**] as the final product [Scheme (III-10)]:

μ-oxo Mo(V) compound + H_2O ⟶ di-μ-oxo Mo(V) compound **(6)**+ $2H^+$

……Equation (III-2)

$2(LnMo^{IV}) + Me_3NO \longrightarrow LnMo^{V} - O - Mo^{V}Ln \xrightarrow[H_2O]{} LnMo^{V}$ (O, O) $Mo^{V}Ln + 2H^+$

Scheme (III-10)

The nitrogen atoms of the pterin ligand are basic enough for abstracting the two protons released as par Equation (III-2); this may involve a couple of acid-base equilibrium type steps as discussed later. In an important review on different facets of molybdenum chemistry, Stifel [9] pointed out the existence of well-characterized di-μ-oxo Mo (V) complexes especially in presence of H_2O; beside this, the role of higher oxidation states of molybdenum [e.g., Mo(V)] in enhancing acidity of the coordinated ligand (e.g., of H_2O) is relevant in the present context for the reaction represented by Equation (III-2).

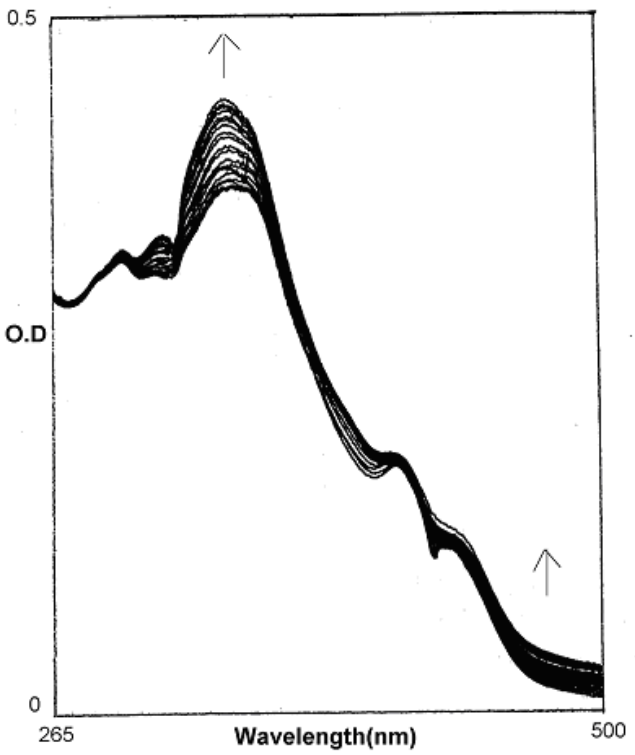

Fig. (III-60): Absorption spectral changes recorded at 10 min interval during the reaction of compound **(1)** (1.42 x 10^{-5} mol) with $Me_3N\rightarrow O$ (3.2 x 10^{-3} mol) in CH_3OH at 318K.

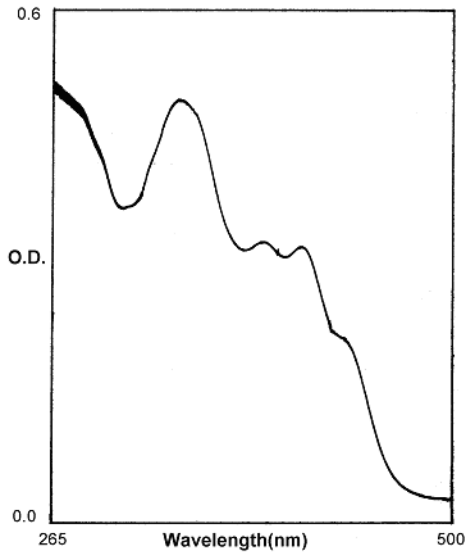

Fig. (III-61): Spectrophotometric monitoring of the reaction between ligand (H_2L^2) (3.5 x 10^{-5} mol) and $Me_3N\rightarrow O$ (3.2 x 10^{-3} mol) at 360K.

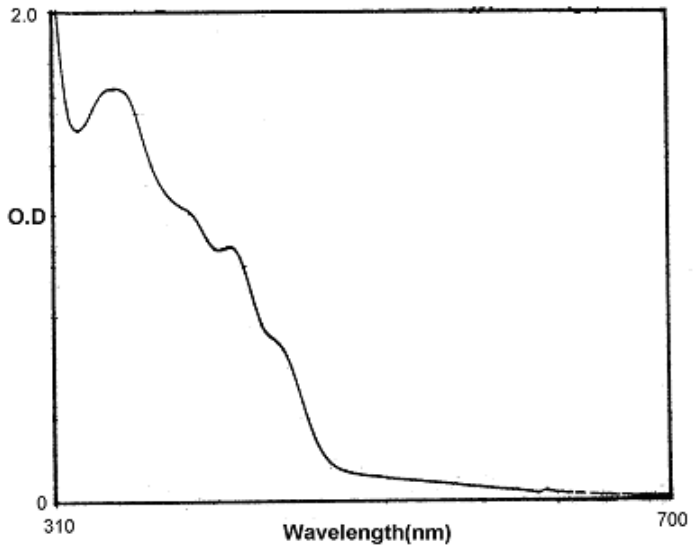

Fig. (III-62) Spectrophotometric monitoring of the reaction between compound **(1)** (1.42×10^{-5} mol) and PPh_3 (2.08×10^{-3} mol) under the same condition as in Fig. (III-60).

Fig. (III-64), (III-66), (III-67) and (III-69) represent reactivities of other compounds of this chapter towards Me_3NO. The corresponding plots of reaction profiles (that is, k_{obs}, s^{-1} versus $Me_3N\rightarrow O$ concentration) of the relevant compounds [Fig. (III-63, 65, 68 and 70)] are quite interesting, e.g., they range from sigmoidal type to bell-shaped curve or even a combination of both types. The above plots closely resemble the pH dependence curves of group transfer reactions of complex compounds.

As par Equation (III-1) and (III-2), the reaction of two molecules of the Mo(IV) complex (e.g., compound **(2)** with a molecule of substrate ($Me_3N\rightarrow O$), in combination with the acid-base equilibrium involving the protons released in the second stage and accepted by pterin nitrogen atoms, can give rise to the interesting type of reaction profiles observed here. Each of the pertinent profiles as stated above, reflects a mixed order reaction with respect to the substrate ($Me_3N\rightarrow O$) concentration.

In enzymes kinetic studies the role of pH on reaction rates (sometimes giving bell-shaped curves) is quite important [6(d), (e)]; of course, assigning $[H^+]$ terms in the rate law is an involved task.

The compound **(2)** was found to react with $Me_3N \rightarrow O$ (one of the substrates of molybdoenzymes) at 310.5K. A spectroscopic monitoring of this reaction was done by UV-VIS spectra and represented in the Fig. (III-64) and no isosbestic point is observed. This is due to the formation of intermediate during the course of the reaction. The decrease in absorbance here is extended up to 500 nm due to the presence of sulfur as donor atom.

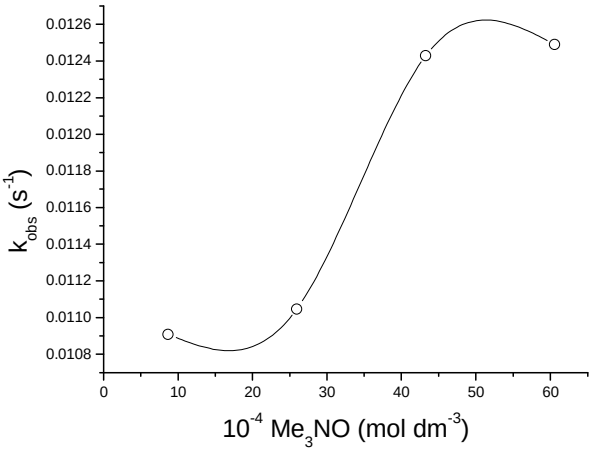

Fig. (III-63): Plot of k_{obs} (s^{-1}) at different concentrations of $Me_3N \rightarrow O$ at 318K, for the reactivity stated in Fig. (III-60).

The decay kinetics for the reaction of $Me_3N \rightarrow O$ with this complex is studied at 340 nm under pseudo first order condition (maintaining c.a., 13-101 times excess of $Me_3N \rightarrow O$ in CH_3OH). The least square method (plotting of $\log(A_\infty - A_t)$ versus time at 310.5K) was employed to determine the pseudo first order rate constant (k_{obs}, s^{-1}). The rate constants are plotted against the different $Me_3N \rightarrow O$ concentration and a bell shaped curve is obtained giving a maximum at 6.02×10^{-4} mole dm^{-3} of $Me_3N \rightarrow O$ concentration [Fig. (III-65)].

The pseudo first order rate constants are also determined at different temperature (313.15 – 328.15K) keeping the $Me_3N \rightarrow O$ concentration unchanged (keeping thirteen fold excess) to obtain the activation parameter ($\Delta S^{\neq}$ = - 197.51 J K^{-1} mol^{-1}) (obtained from the Eyring Plot [ln(k/T) versus 1/T]). The negative $\Delta S^{\neq}$ value indicates the associative nature of the complex during the reaction.

The reaction between $Me_3N \rightarrow O$ and compound **(3)** occurred at 311K. The spectroscopic monitoring of this reaction was done and represented in the Fig. (III-66). A

regular decrease in the optical density from 265 nm to 500 nm wavelength is observed in the reaction. Absence of any definite is isosbestic point indicates presence of an intermediate complex during the reaction.

The compound **(4)** is reactive towards $Me_3N\rightarrow O$. The reaction between this complex and $Me_3N\rightarrow O$ took place at 318K. The reaction was followed spectrophotometrically and the reaction time course is shown in the Fig. (III-67). From the Fig. (III-67) it may be noted that at 361.6 nm there is a isosbestic like point. The decrease in optical density occurs at longer wavelength to the isosbestic like point and reverse is observed at lower wave length.

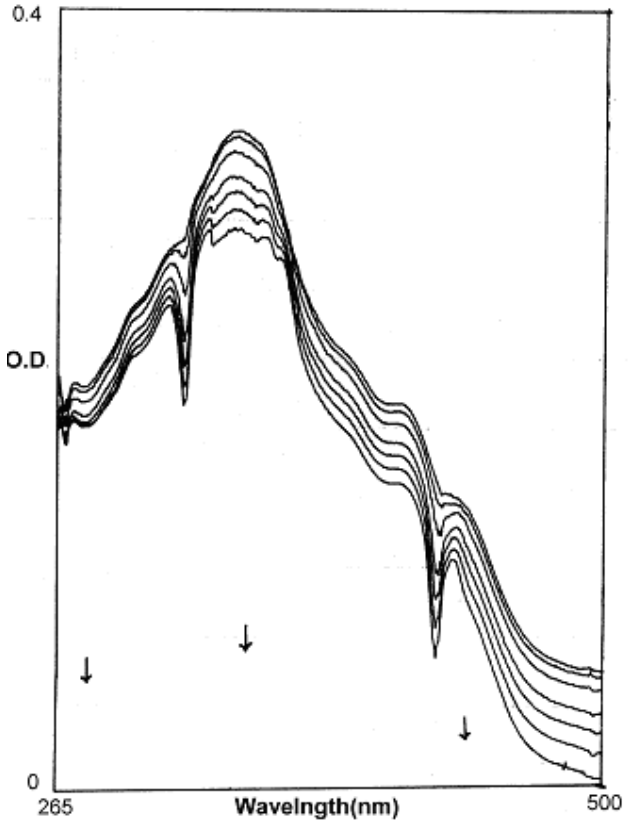

Fig. (III-64): Absorption spectral changes recorded at 10 min interval during the reaction of compound **(2)** (2.01×10^{-5} mol) with $Me_3N\rightarrow O$ (4.33×10^{-3} mol) in CH_3OH at 310.5K.

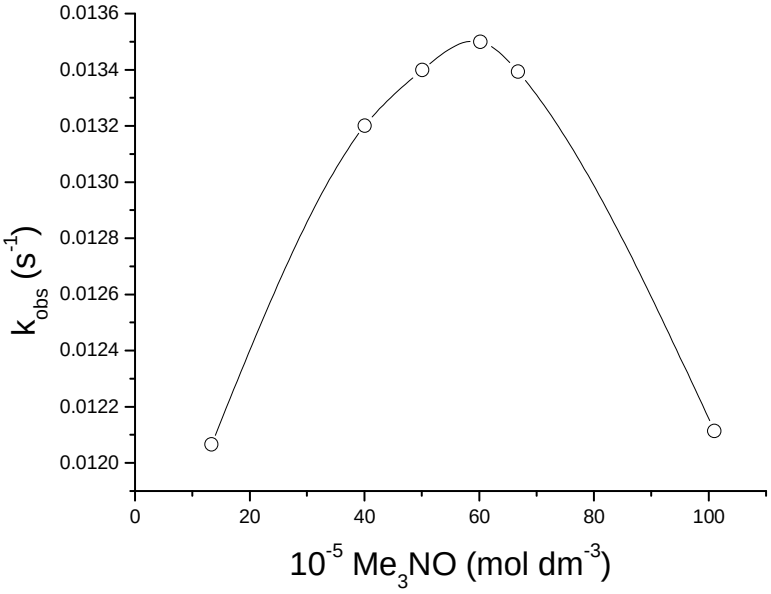

Fig. (III-65): Plot of k_{obs} (s^{-1}) at different concentrations of $Me_3N\rightarrow O$ at 310K, for the reactivity stated in Fig. (III-64).

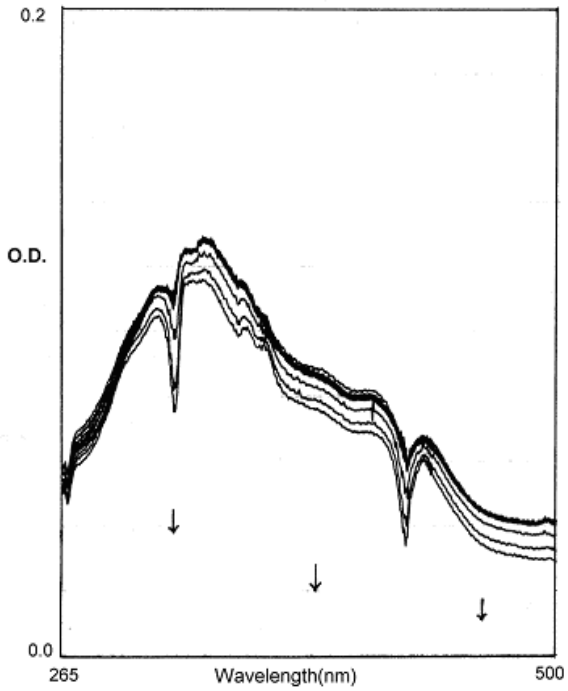

Fig. (III-66): Absorption spectral changes recorded at 10 min interval during the reaction of compound **(3)** (2.72 x 10^{-5} mol) with $Me_3N\rightarrow O$ (4.33 x 10^{-3} mol) in CH_3OH at 311K.

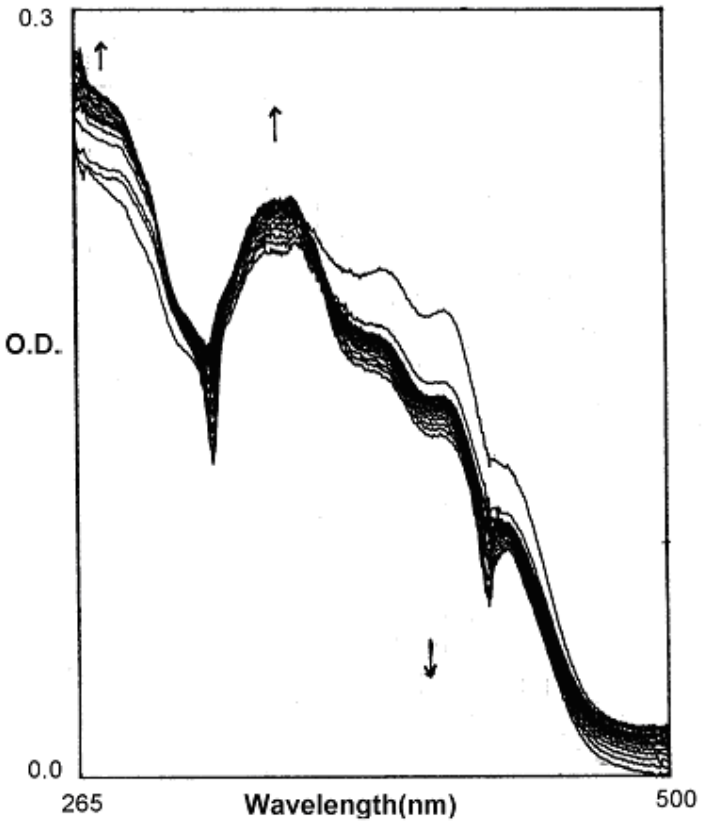

Fig. (III-67): Absorption spectral changes recorded at 10 min interval during the reaction of compound **(4)** (6.0×10^{-5} mol) with $Me_3N{\rightarrow}O$ (3.2×10^{-3} mol) in CH_3OH at 318K.

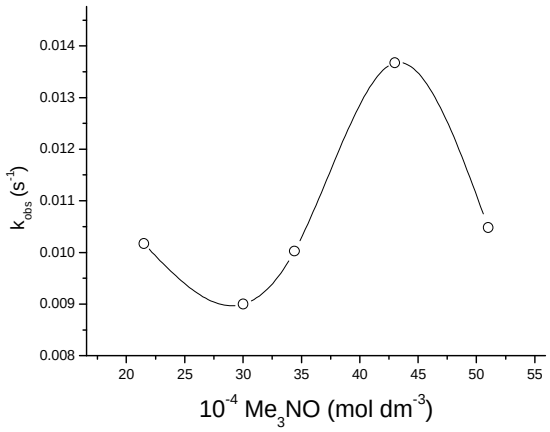

Fig. (III-68): Plot of k_{obs} (s^{-1}) at different concentrations of $Me_3N{\rightarrow}O$ at 318K, for the reactivity stated in Fig. (III-67).

The k_{obs} (s^{-1}) values of this reaction are also determined at different temperature (313-328K) to obtain the activation parameters. From Eyring plot [ln(k/T) versus 1/T] $\Delta S^{\neq}$ value was calculated and found to be - 196.70 J K^{-1} mol^{-1}. The negative value of $\Delta S^{\neq}$ indicates associative nature of the reaction. The rate constants are plotted against the different $Me_3N\rightarrow O$ concentration [Fig. (III-68)].

Fig. (III-69) represents the spectrophotometric monitoring of the reaction between compound **(5)** and $Me_3N\rightarrow O$, in CH_3OH at 319K. Here it may be noted that a continuous decrease of optical density from 280 nm to 500 nm without any definite isosbestic point.

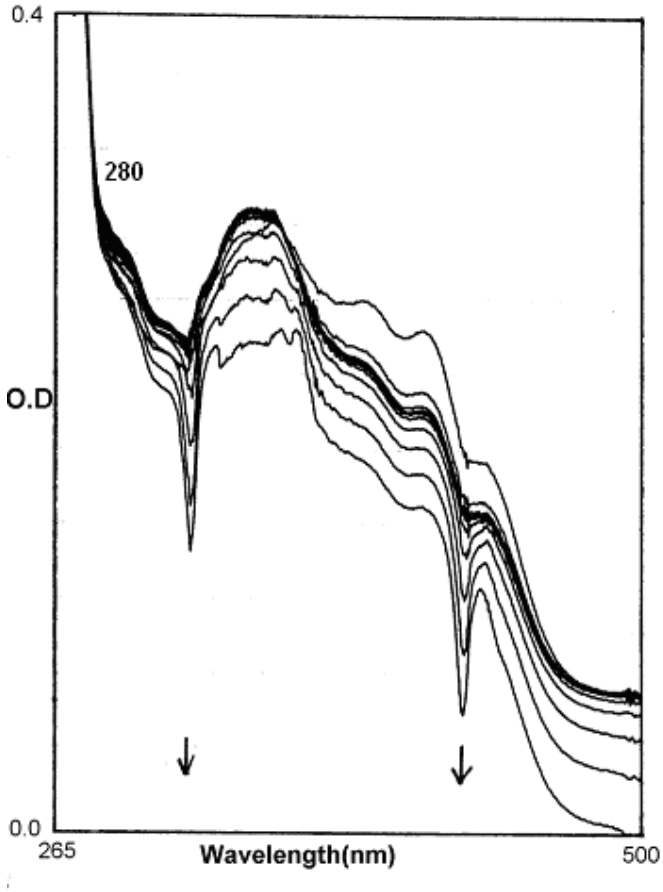

Fig. (III-69): Absorption spectral changes recorded at 10 min interval during the reaction of compound **(5)** (2.30 x 10^{-5} mol) with $Me_3N\rightarrow O$ (3.46 x 10^{-3} mol) in CH_3OH at 319K.

The rate constants (k_{obs}, s^{-1}) of this reaction are determined under pseudo first order condition by least-square method by plotting log (A_t-A_∞) versus time maintaining 16-114 times excess of $Me_3N\rightarrow O$ concentration at 319K. A plotting of k_{obs} (s^{-1}) versus concentration of $Me_3N\rightarrow O$ is illustrated in the Fig. (III-70). First the rate constants decreases with increase in concentration of $Me_3N\rightarrow O$ then again increase to reach a saturation level. The values of k_{obs} obtained are within the range of other oxygen atom transfer reaction by Mo(IV) complexes. The rate constants are also determined at four different temperatures (314 - 329K) maintaining sixteen fold excess concentration of $Me_3N\rightarrow O$ to obtain activation parameter ($\Delta S^{\neq}$ = - 196.77 J K^{-1} mol^{-1}) from Eyring plot [ln(k/T) versus 1/T]. The negative $\Delta S^{\neq}$ value indicates the associative nature of reaction.

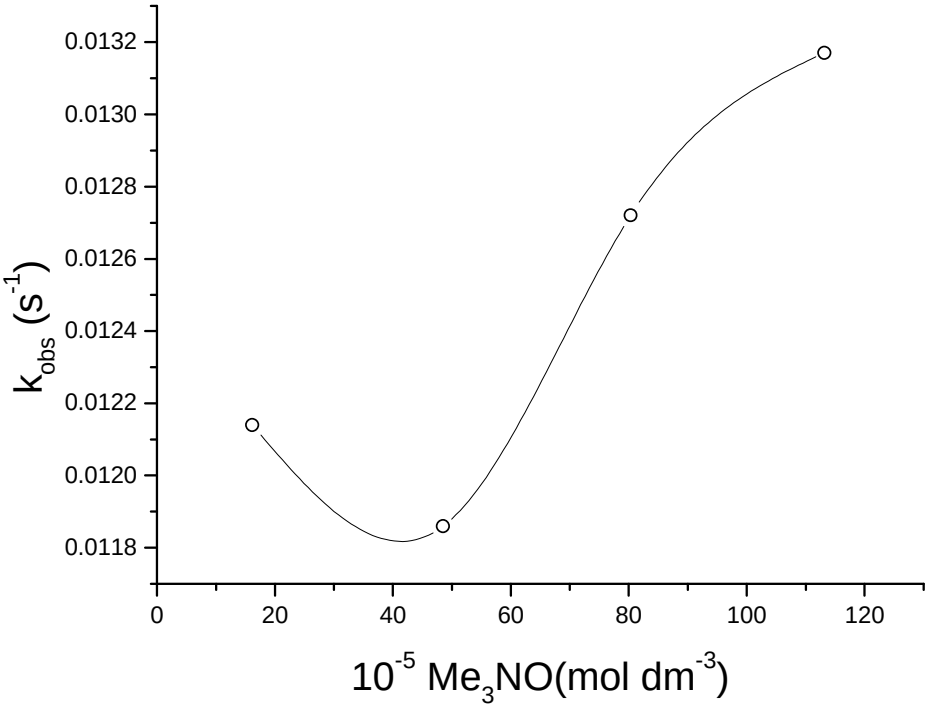

Fig. (III-70): Plot of k_{obs} (s^{-1}) at different concentrations of $Me_3N\rightarrow O$ at 318K, for the reactivity stated in Fig. (III-69).

In case of compound **(6)**, it has been found to be reactive towards PPh_3. A spectroscopic monitoring of this reaction is represented in the Fig. (III-71). Here a continuous decrease in optical density from 320 nm to 500 nm is observed. This reactivity

can be outlined in Scheme (III-11). Nucleophilic attack by PPh_3 on the di-μ-oxo center leads to oxygen atom transfer and concomitant oxidation of phosphorous as well as reduction of the Mo(V) center. The exceptionally low band gap between the HOMO and HOMO-1 levels [$\Delta(E_4 - E_3)$], may have special significance here.

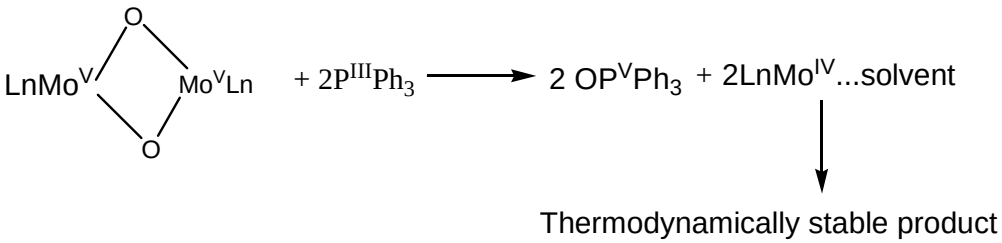

Scheme (III-11)

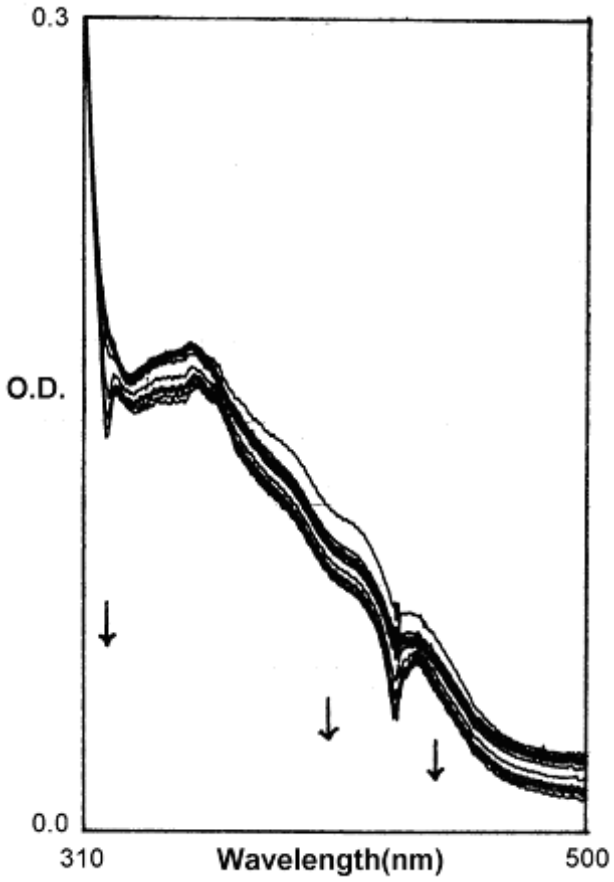

Fig. (III-71): Absorption spectral changes recorded at 10 min interval during the reaction of compound **(6)** (2.5×10^{-5} mol) with PPh_3 (1.13×10^{-3} mol) in CH_3OH at 316K.

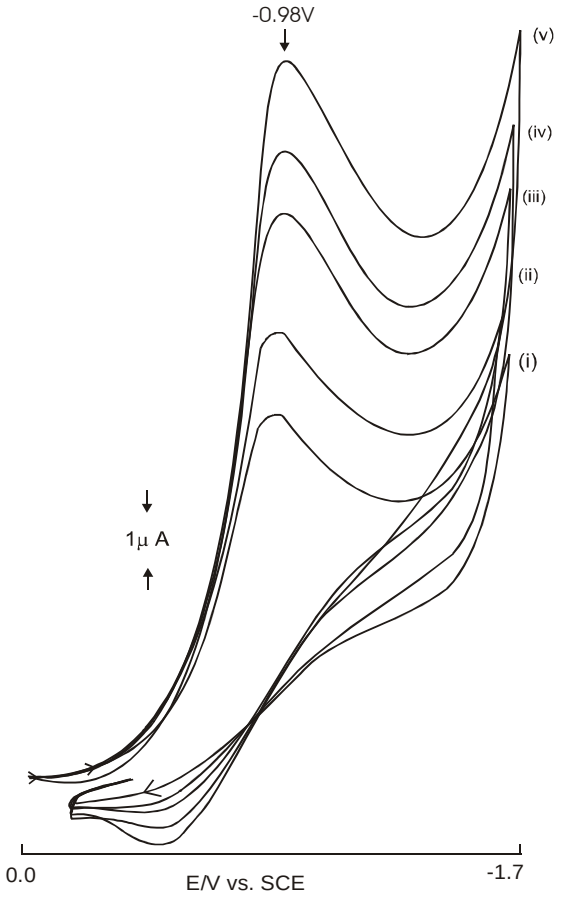

Fig. (III-72): Cyclic voltammograms of the compound **(1)** (1.38 x 10^{-3} mol) in DMF (0.1 mol TBAP) at (i) 50 mVs^{-1}, (III) 100 mVs^{-1}, (III) 150 mVs^{-1}, (iv) 200 mVs^{-1} and (v) 250 mVs^{-1}.

Cyclic voltammetry

Cyclic voltammetry was performed in DMF solutions (3 x 10^{-3} - 1 x 10^{-3} M complex) over a potential range of 0.0 to -1.7 V vs SCE with 0.1 M tetra-*n*-butylammonium perchlorate [*n*-Bu_4N][ClO_4] (TBAP) as the supporting electrolyte. The DMF was triply distilled. Background scans of deoxygenated DMF with 0.09 M [*n*-Bu_4N][ClO_4] exhibited no impurities or solvent degradation in the potential window observed. The electrochemical cell consisted of a platinum disk (1.6 mm) working electrode (Bioanalytical Systems, BAS), platinum wire counter electrode (BAS), and KCl saturated Ag/Ag+ reference electrode

(BAS). The platinum disk electrode was polished using alumina (BAS). Prior to each experiment, the electrode was cleaned.

Usually in CV studies, the Mo(IV)→Mo(III) reduction occurs around -0.9 to -1.0 volt (versus SCE) in different ligand systems. The free pterin ligand (H_2L^2) also undergoes reduction in the same region, e.g., E_{pc} at -0.93 volt. Only a simple irreversible reduction peak (E_{pc}) at -0.98 volt characterizes [Fig. (III-72)] compound **(1)** and no separate reduction peaks (E_{pc}) are observed for the metal and ligand centres. The reduced species is decomposed through solvent attack; only at fast scan rates (250 mVs^{-1}), the reoxidation peak (E_{pc} at -0.47 V) of the reduced species can be identified.

The above observation can be rationalized in terms of extensive electron exchange between the molybdenum atom and the pterin ligand, as indicated below.

Burgmayer and coworkers represented the electron exchange interaction between different oxidation states of molybdenum (e.g., VI, V, IV) and the tetrahydro as well as dihydro forms of the pterin ligand in the following way:

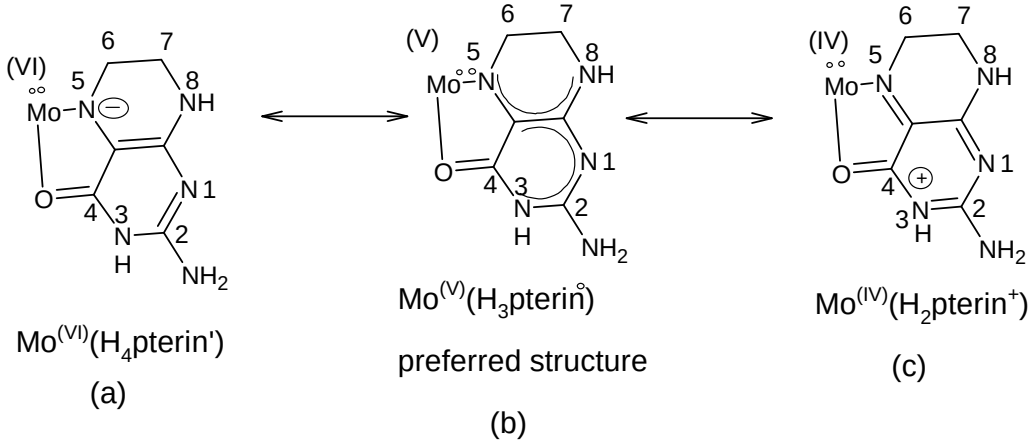

The explicitly drawn lone pair of electrons in the above schematic structures can be considered to originate from the deprotonation of the tetrahydropterin at N(5). The shift of this pair to reduce Mo to +4 oxidation state in (c) would result in a net two-electron redox reaction. The variable reactivity can be understood as the shifting of this electron pair to either the Mo or to the pterin depending on the environment presented by the ancillary ligands [12].

Of the three chemically relevant oxidation states of molybdenum [e.g., Mo(VI), Mo(V) and Mo(IV)], during catalysis only the Mo(V)(d^1) state could be detected as a

transient species by EPR spectroscopy in oxomolybdoenzyme; the Mo(IV)(d^2) state is consistently diamagnetic in such cases [13]. Almost all the synthetic molybdenum-pterin complexes reported so far are diamagnetic, including the Mo(IV) complexes (d^2) as well as complex formulated as containing a Mo(V) centre [12]; diamagnetic behaviour of this system is explained by invoking a strong antiferromagnetic coupling between d^1[Mo(V)] electron and the delocalized electron system of the redox "non-innocent" pterin ligand [12]. This unique nature of the pterin ligand is responsible for the observed diamagnetism of compound **(1)** [a Mo(IV)-d^2 system] and its high resolution ^{1}H-NMR data. This is true for the other Mo(IV)(d^2) compounds reported in this chapter (i.e., compounds **(1)** to compound **(5)** in giving high resolution ^{1}H-NMR spectra as well as possessing diamagnetic property. Another factor, i.e., distorted octahedral geometry (as evident from bond angle data of optimized structures of the above compounds indicated in Tables (III-3, 6, 8,10, 12 and 14) leads to splitting of e_g and t_{2g} levels of O_h symmetry and favours spin pairing in the $(4d_{xy})^2[(b_2)^2]$ levels of the $Mo^{(IV)}$-d^2 system [14]. Basu and coworker from calculations of frontier orbital energies of molybdenum complexes inferred that the distinguishing electron occupancy (e.g., d^1/d^2) occurs in the predominantly molybdenum $4d_{xy}$ type orbital; this is in good agreement with experimental data as well as ligand-field theory [15].

Compounds **(6)** is also diamagnetic and provides with a good ^{1}H-NMR spectrum; in this bi-μ-oxo bridged binuclear Mo(V) complex, the spins of the two Mo(V)(d^1) centers coupled involving the 2p orbital of the bridging oxygen atom [14]. Participation of the pterin ligand electrons in this process, in the foregoing manner cannot be ruled out [12].

Kirk and coworkers interpreted active-site stereochemical control of oxygen atom transfer reacting in sulfite oxidase on the basis of electronic structure (e.g., characteristic features of HOMO and LUMO) obtained using a optimized computational model [16].

The cyclic voltammetric diagram of compound **(2)** (Fig. (III-73) reflects two reduction peaks (E_{pc}) at -1.0 V and -1.36 V corresponding to reductions of this complex and its ancillary sulphur donor ligand residue $(atp)^{1-}$ respectively. A Mo(IV) → Mo(III) reduction takes place at -1.0V, followed by decomposition of the reduced species through solvent attack. The free pterin ligand is characterized by a single irreversible peak at -0.93V. On complex formation with the Mo(IV) enter in three complexes, it is shifted to more negative potential range.

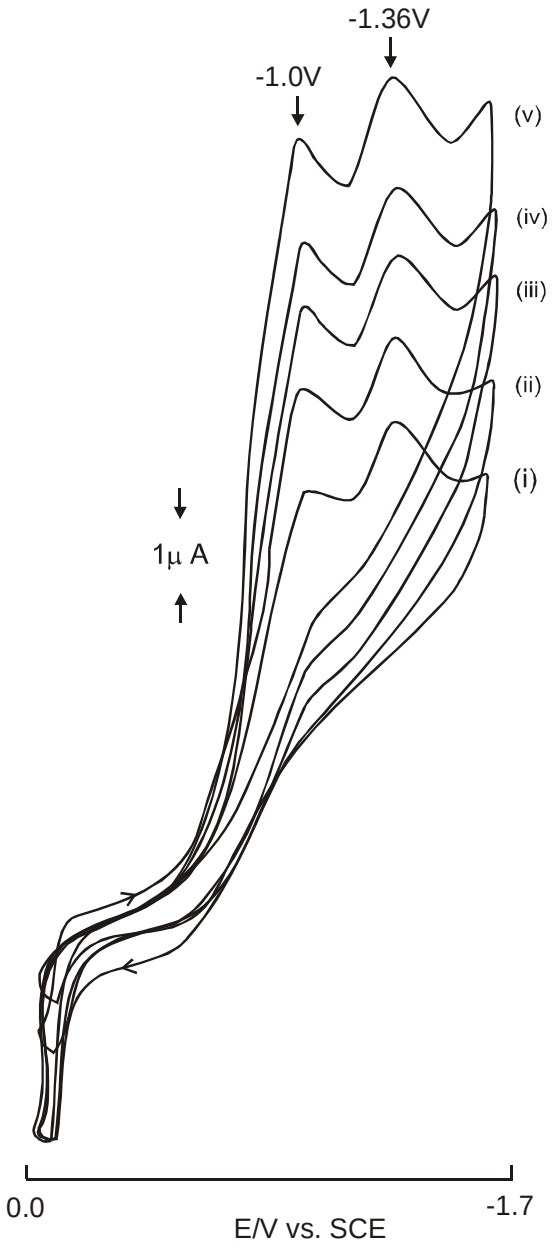

Fig. (III-73): Cyclic voltammograms of the compound **(2)** (1.02 x 10^{-3} mol) in DMF (0.1 mol TBAP) at (i) 50 mVs^{-1}, (III) 100 mVs^{-1}, (III) 150 mVs^{-1}, (iv) 200 mVs^{-1} and (v) 250 mVs^{-1}.

In the cyclic voltammetric data of compound **(3)** [Fig. (III-74)] the Mo(IV) → Mo(III) reduction peak appears at -0.91V.

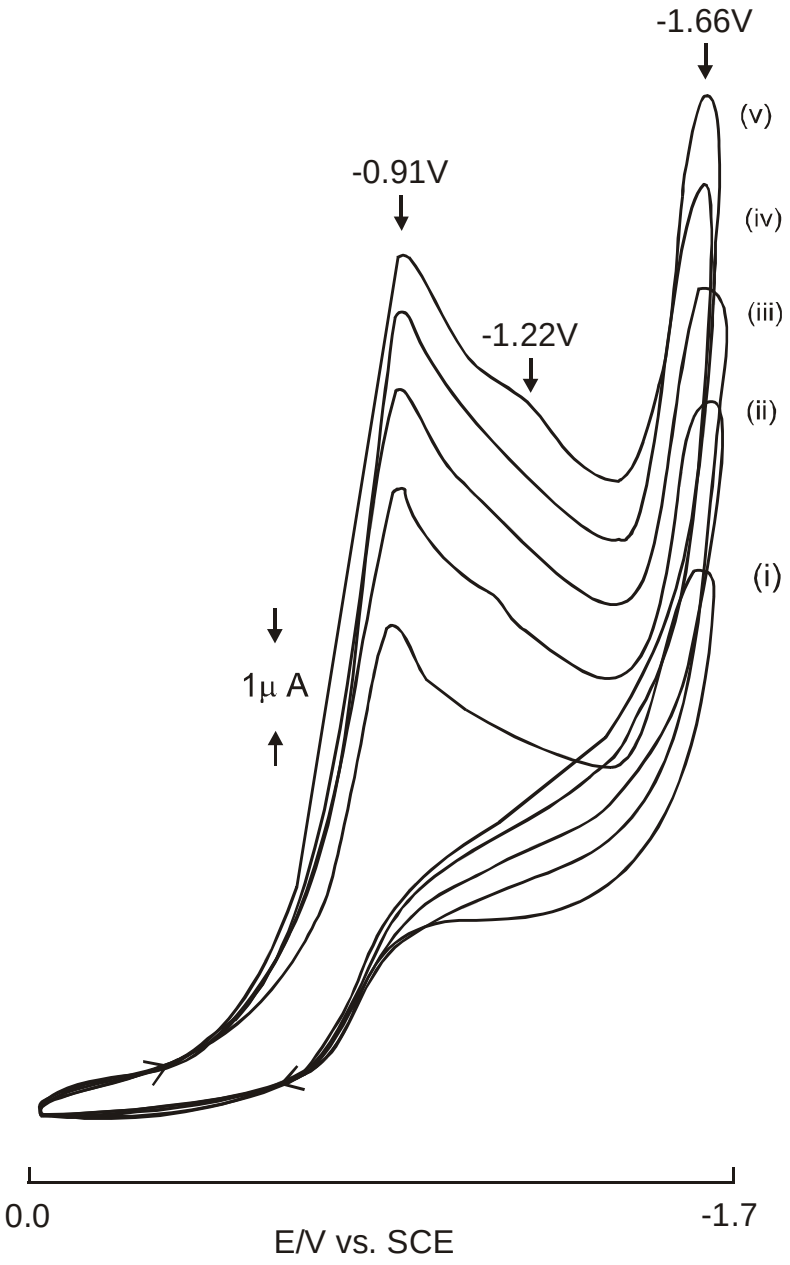

Fig. (III-74): Cyclic voltammograms of the compound **(3)** (1.14×10^{-3} mol) in DMF (0.1 mol TBAP) at (i) 50 mVs^{-1}, (III) 100 mVs^{-1}, (III) 150 mVs^{-1}, (iv) 200 mVs^{-1} and (v) 250 mVs^{-1}.

For compound **(4)** [Fig. (III-75)], the ligand reduction peak appears at -1.12V. The Mo(IV)→Mo(III) reduction occurs at -0.74V whereby the reduced species is decomposed through solvent attack. At faster scan rate this metal-centered reduction is not visible.

The cyclic voltammetric reduction peak at -0.88V [Fig. (III-76)] for compound **(5)** corresponds to reduction Mo(IV)→Mo(III). Only at fast scan speed (250 mVs^{-1}) the reoxidation of the reduced species could be visualized at -0.52 V (E_a).

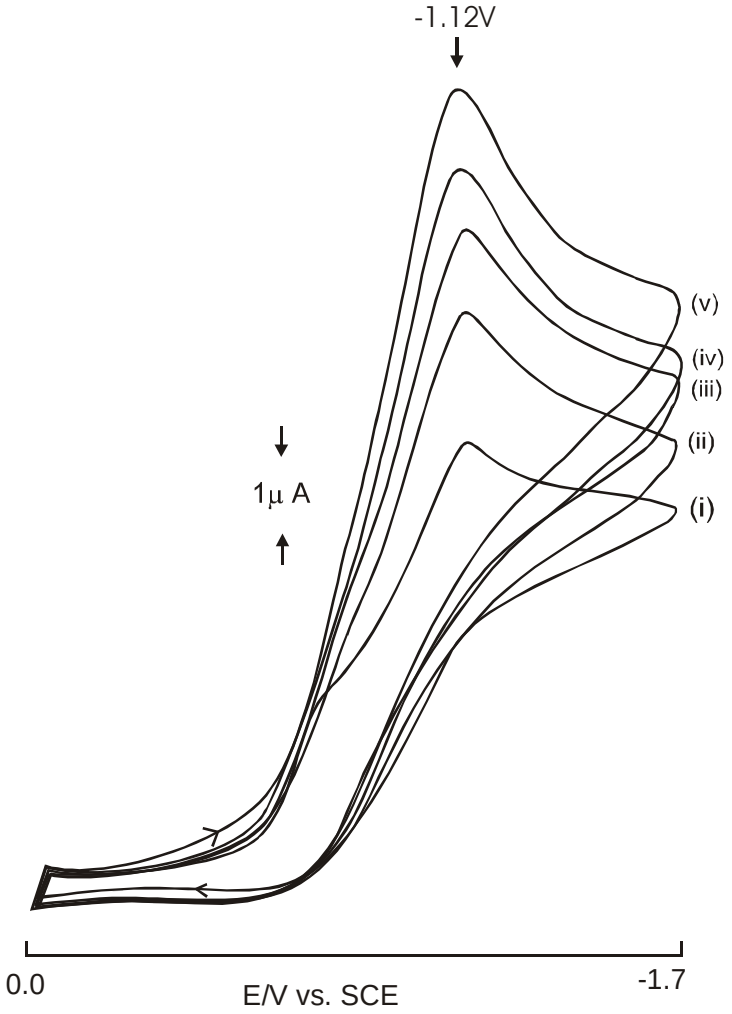

Fig. (III-75): Cyclic voltammograms of the compound **(4)** (1.94 x 10^{-3} mol) in DMF (0.1 mol TBAP) at (i) 50 mVs^{-1}, (III) 100 mVs^{-1}, (III) 150 mVs^{-1}, (iv) 200 mVs^{-1} and (v) 250 mVs^{-1}.

In the cyclic voltammogram of compound **(6)** [Fig. (III-77)] it may be noted that the metal and ligand-centered reduction peaks appear at -0.86V and -1.54V respectively.

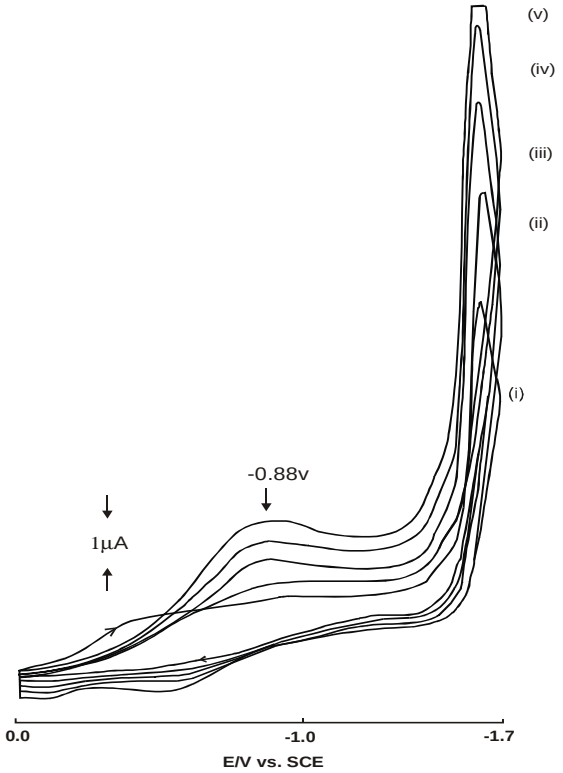

Fig. (III-76): Cyclic voltammograms of the compound **(5)** (1.07×10^{-3} mol) in DMF (0.1 mol TBAP) at (i) 50 mVs^{-1}, (III) 100 mVs^{-1}, (III) 150 mVs^{-1}, (iv) 200 mVs^{-1} and (v) 250 mVs^{-1}.

Conclusion

The different physic-chemical parameters of all the six new compounds discussed in this chapter are summarized in Table (III-16). They have been synthesized under carefully controlled conditions including dinitrogen atmosphere/darkness/paraffin oil bath heating as well as purification through flash chromatography under dinitrogen flow. Compounds **(4)** and **(5)** have been obtained as shining microcrystals. Conditions beyond control prevented their x-ray characterization. They have been characterized through elemental analysis, mass spectrometry, UV-VIS, IR, ^{1}H-NMR and fluorescence spectral data. Their CHEM3D models have been obtained through MM2 calculations and the corresponding frontier – orbital energies have been obtained (extended Huckel surfaces). Some of the spectral data have been interpreted in terms of the geometric parameters obtained from the CHEM3D models. The

frontier – orbital energy data assist in rationalizing their reactivity aspect. For example, the large HOMO – LUMO band gap [$\Delta(E_3 - E_2)$] is consistent with relative aerial stability of these complexes (after drying in vaccuo). However, the smaller ΔE values for the other frontier – orbital energies [Fig. (III-58) and (III-59) help in throwing light on their reactivities, e.g., kinetic studies with Me_3NO as the substrate as well as cyclic voltammetric data. The stoichiometric aspets these reactions has been established through the isolation of the product in one case, e.g., compound **(6)** from compound **(5)**. The sulfur donor ancillary ligands confer a special meaning to the relevant ^{1}H-NMR spectral data. For example, the suitable orbitals on the sulfur atom can interact with the t_{2g} type (d_{xy}, d_{yx}, d_{zx}) orbitals on the Mo(IV) center and ultimately electron density is transmitted to the pterin ring through the suitable pπ orbitals (of the pterin ring).

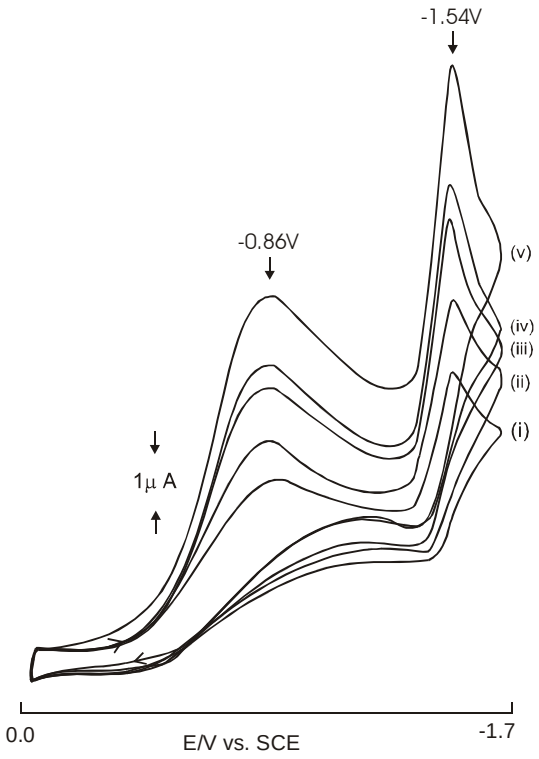

Fig. (III-77): Cyclic voltammograms of the compound **(6)** (1.09×10^{-3} mol) in DMF (0.1 mol TBAP) at (i) 50 mVs^{-1}, (III) 100 mVs^{-1}, (III) 150 mVs^{-1}, (iv) 200 mVs^{-1} and (v) 250 mVs^{-1}.

Table (III-16): Comparison of different physic-chemical parameters of the molybdenum compounds of the pterin ligand (H_2L^2) with selected sulfur and nitrogen donor as ancillary ligands.

Compounds → / Parameters ↓	Compound **(1)**	Compound **(2)**	Compound **(3)**	Compound **(4)**	Compound **(5)**	Compound **(6)**
1. Colours	deep brown	snuff red	yellow-brown	dark brown	reddish brown	dark brown
2.UV-VIS data	280(4.38), 346(4.69), 376sh (4.58) 415(4.48), 450sh (4.21).	347(4.84), 373.5sh (4.63) 414.5(4.54) 446.5sh(4.33)	220(4.93), 239(5.51), 331(4.55), 348(4.56), 410(4.26), 445sh(4.01)	218(4.40), 269sh(3.96) 309(3.86), 347(4.08), 377sh (3.89), 414sh (3.87), 442sh(3.66)	254(4.48), 268(4.57), 275sh (4.54),347 (4.46) 416sh (4.10) 456sh (3.77).	252sh (4.20), 270 (4.26), 308sh (3.70), 350 (4.10), 410sh (3.80)
3.Floures cense data (λ_{max}/ nm)	402	410	400.5	473.0	368	419
3. Steric energy (Kcal/mol)	69.37	15.85	20.14	17.17	16.28	24.81
4. Cyclic Voltammetry data [E_{pc}(V) of Mo(IV) →Mo(III)]	-0.98	-1.0	-0.91	-1.12	-0.88	-0.86
5. Substrate for reactivity study	$Me_3N\rightarrow O$	$Me_3N\rightarrow O$	$Me_3N\rightarrow O$	$Me_3N\rightarrow O$	$Me_3N\rightarrow O$	PPh_3
6. k_{obs}, s^{-1}	1.23×10^{-2}	1.21×10^{-2}	*	1.05×10^{-2}	1.30×10^{-2}	-
7. $\Delta S^{\neq}$ ($J\ K^{-1}\ mol^{-1}$)	- 197.52	- 197.51	*	- 196.70	- 196.77	-
8.ΔE (HOMO-LUMO) eV	5.66	4.92	0.98	4.63	4.66	4.66

* Cannot be determined due to nonavailability of the compound **(3)**.

Shielding of the ^{1}H-NMR signal of the NH(2) group from the free ligand position of δ4.30 to δ3.45 – 3.48 [Δδ = -0.85 – (-0.82)] in some of these complexes, highlights this aspect. X-ray structural data of the Zn(II)-pterin complex reported in Chapter II support this view. Here also in the chelated pterin ligand, the C(2) – NH_2(2) bond acquires a double bond character, i.e., increasing electron density around the NH(2) group; this is reflected by the shielding of the corresponding NH(2) signal from the free ligand and position. Appearance of the almost intact molecular ion peaks in the ESIMS data for compounds **(1)**, **(2)** and **(4)** point to the stability of the coordination environment in these cases; even the substituents at the 2- and 6- positions remaining intact due to the multiple nature of their bonds to the pterin ring [Scheme (III-9)]; ^{1}H-NMR data point towards a multiple nature of NH(2) – C(2) bond.

The above discussion highlights the redox non-innocent behaviours of the pterin ligand as well as enhancement of this aspect in presence of supporting sulfur donor ligands. Possibly, this aspect is needed by the Mo center in oxomolybdoenzymes for the performing the essential biological role.